MReadings: MSK

Contributions from our MAGNETOM users

SIEMENS

Ignacio Vallines, PhD
Global Segment Manager
Orthopedic MRI

Dear Reader,

Musculoskeletal imaging is routine to the vast majority of MAGNETOM users because MR has a lot to offer in this field: exquisite soft tissue contrast and great spatial detail not only for bone lesions but also for the evaluation of pathology in ligament, muscle and cartilage. Siemens has been pushing the boundaries of MR diagnostic imaging by closely working with our customers on the optimization and further product implementation of techniques, which go way beyond standard imaging: from fast high-resolution isotropic 3D imaging to biochemical tissue evaluation. Some of those efforts in the field of musculoskeletal imaging are best portrayed by recent contributions from our customers to our customer magazine, the MAGNETOM Flash, which we are proud to offer you with this compilation.

We would like to take this opportunity to thank the authors of these articles and those who continuously support the development of MR by sharing their experiences and expertise with other MAGNETOM users worldwide.

Ignacio Vallines
Global Segment Manager Orthopedic MRI

Content

Biochemical Imaging

Besides improvements in morphological imaging, the ability to assess and quantify biomarkers is increasingly important in MSK imaging. The use of biochemical imaging instead of morphological imaging is gaining importance as a means of both improving accuracy of diagnosis and of planning and monitoring the effectiveness of therapy.

Based on the different biomarkers, there are several approaches to biochemical imaging described and used for clinical imaging. The different biomarkers can be obtained by contrast and non-contrast examination techniques resulting in T1-, T2- and T2*-maps. Thanks to *syngo* MapIt today it is possible to obtain parametric mapping results automatically. *syngo* MapIt can be used fro all joints in the body (Figs. 1–5). All of the images were prepared within the *syngo* environment from maps which were created automatically, using Inline Technology. These maps can then be retrieved and post-processed using any of the standard *syngo* tools, such as Region of Interest (ROI), pixel lens, etc. Furthermore, it is possible to use *syngo* Fusion to overlay these maps with their corresponding anatomical image and to conduct manual carti-

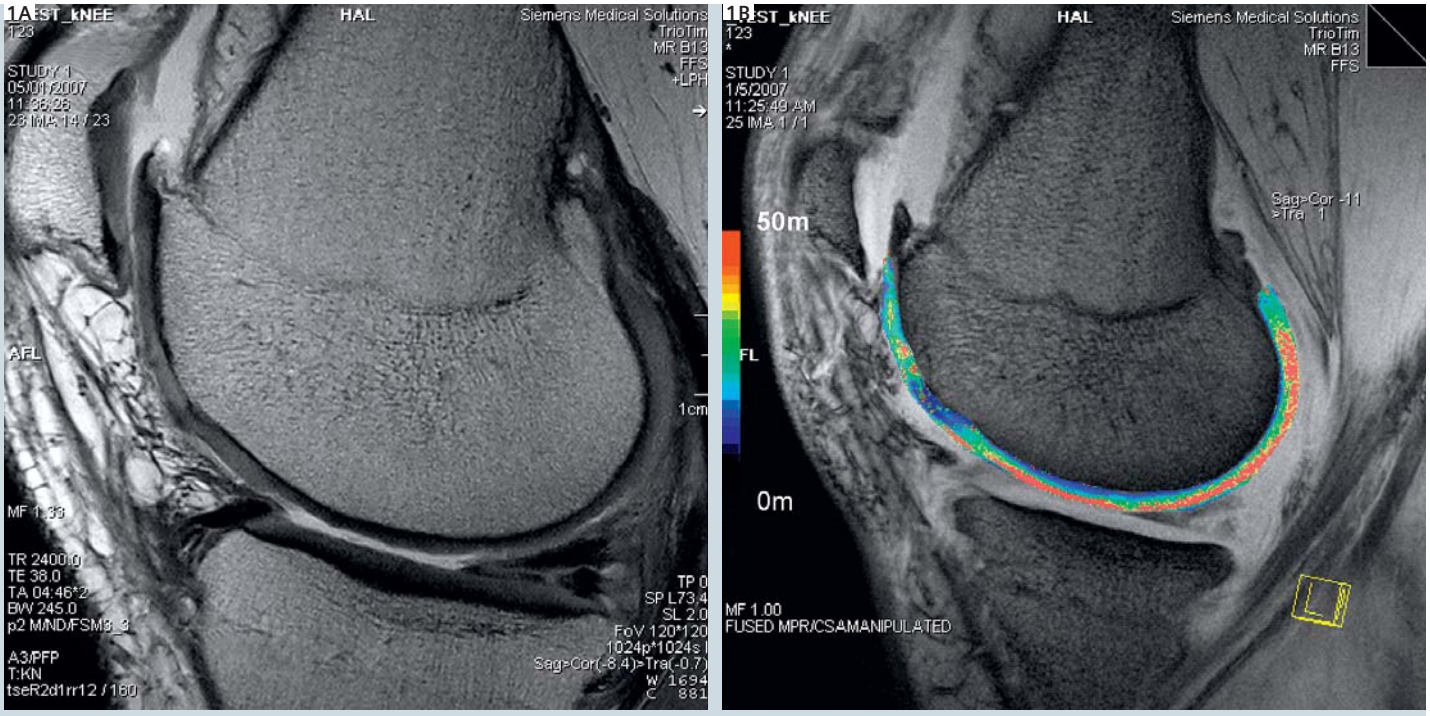

1 **Example of a high in-plane resolution (0.3 x 0.3 x 2 mm) protondensity-weighted (PD) TSE image and the corresponding biochemical (T2*) high-resolution image in a patient with cartilage lesion.**

lage segmentation. There is now no need to transfer any data offline, as everything can be accomplished on the measurement console.
It is also necessary to expand the biochemical imaging capabilities. To this end new sequence techniques are being examined to evaluate the cartilage. One of the most promising candidates for this is Steady State Free Procession (SSFP) diffusion imaging using a PSIF sequence, with of course Inline mapping. An alternative approach is to use Echo Planar Imaging (EPI) diffusion which has also delivered good results making advanced techniques such as tensor imaging possible. First examples of the use of SSFP diffusion are shown in Fig. 5 in a patient with cartilage degeneration in comparison to a T2-mapping.

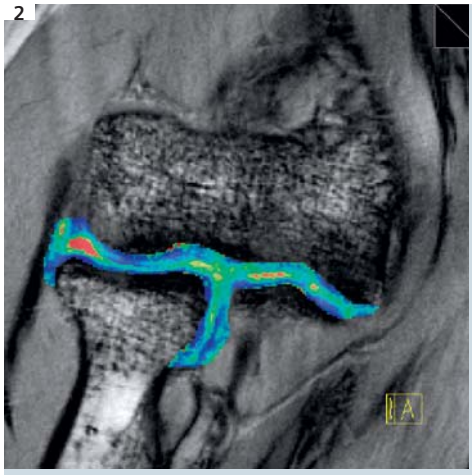

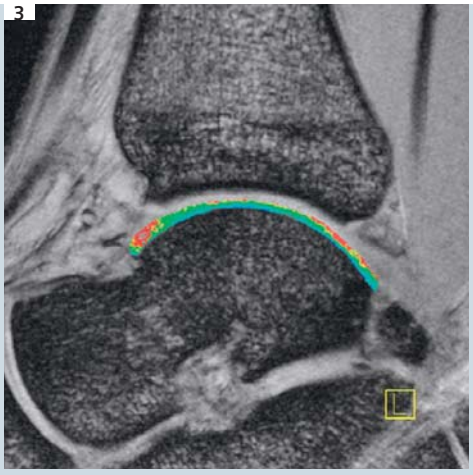

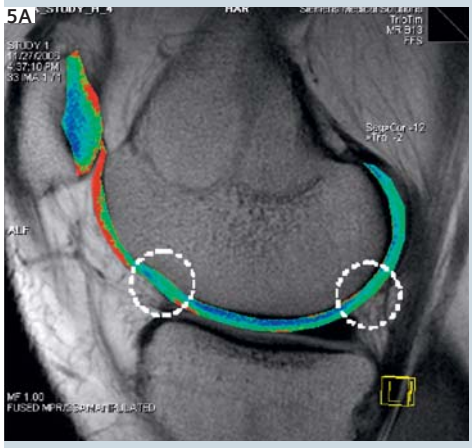

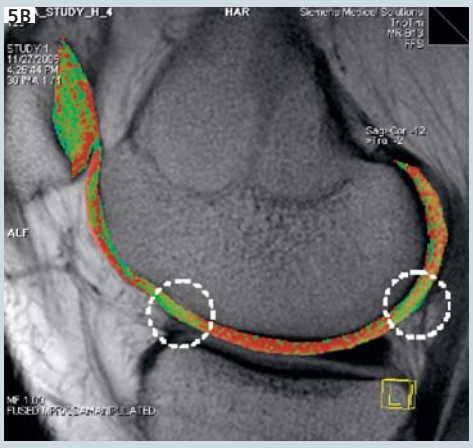

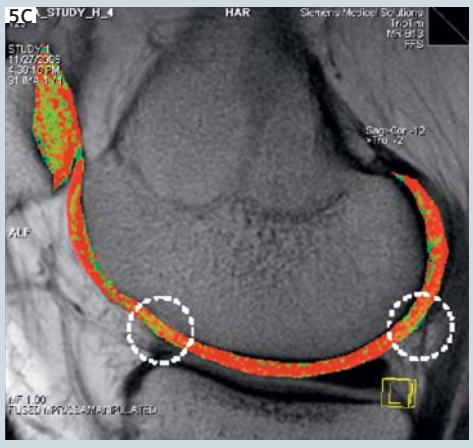

2 **Elbow imaging with the small flex coil. High-resolution T2*-map.**

3 **The 8-channel foot-ankle coil is used to produce high-resolution T2* cartilage mapping at 3T (0.3 x 0.2 x 2 mm) under load restriction over time.**

Courtesy of Prof. Siegfried Trattnig, Medical University Vienna, Austria

4 **T1-mapping in the carpometacarpal (CMC) joint for diagnosis of rheumatoid arthritis.**

5 **A–C: Comparison of a T2-mapping (4A) with the diffusion map in read (4C) and phase (4B) direction (qualitative mapping based on SSFP diffusion sequence).**

High-Resolution (Fast-) Imaging

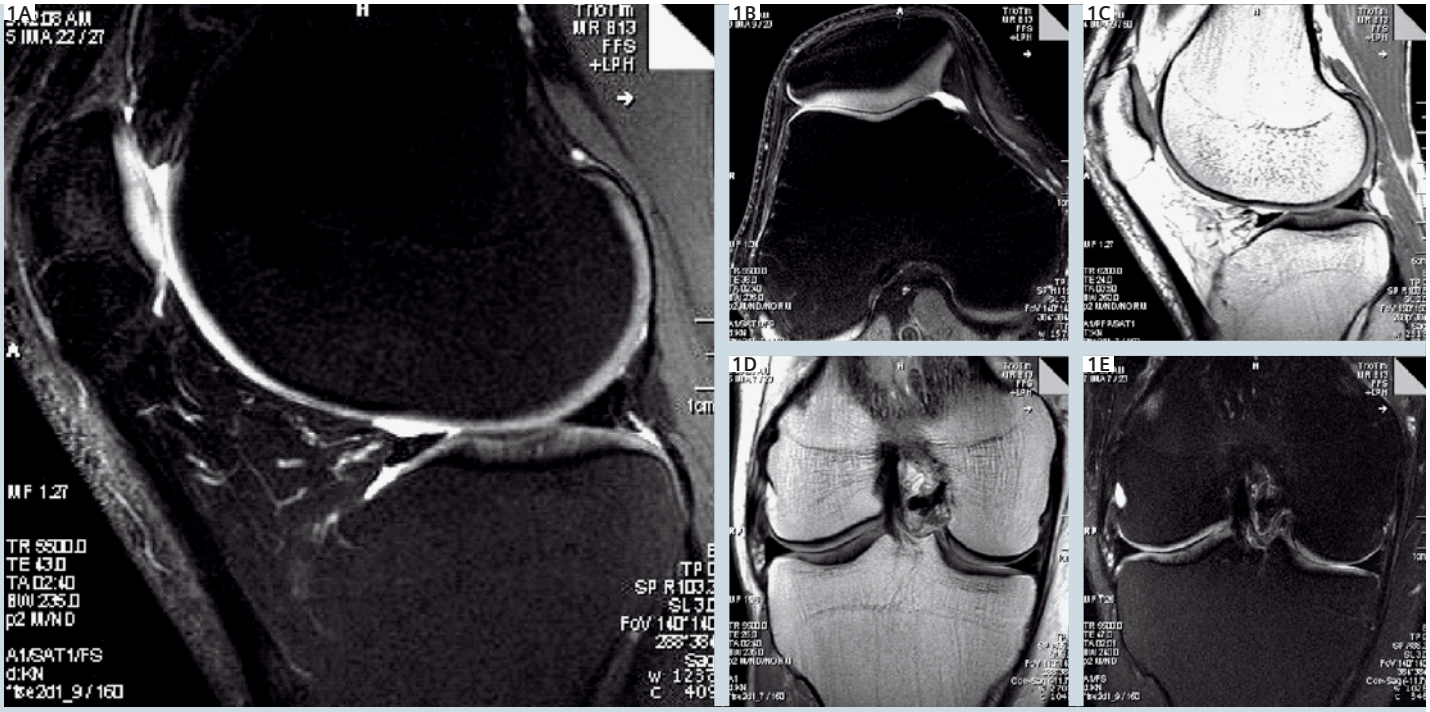

1 **A series of five high-resolution examinations of the knee completed in under 15 minutes. Sequences used:**
A: Sagittal protondensity-weighted Turbo Spin Echo (TSE) image with fat saturation (fatsat), 512 matrix.
B: Axial T2-weighted image with fatsat, 512 matrix.
C: Sagittal T1-weighted image, 512 matrix.
D: Coronal T1-weighted image, 512 matrix.
E: Coronal protondensity-weighted TSE image with fatsat, 512 matrix.

The first goal to achieve in musculoskeletal (MSK) imaging is a high resolution with the necessary contrast for precise detection of the small and complex structures of the MSK system. This requirement leads to the use of Turbo Spin Echo (TSE) sequences optimized for maximum matrix size and small FoV.
Beside more accurate diagnosis there is also a competing requirement for increased throughput. Due to lower reimbursements, a study must be optimized to allow for a total MSK joint study within 15 to 30 minutes. Fig. 1 shows an example of a standard knee study consisting of 5 series using an 8-channel knee coil (Invivo, Latham, NY, USA) and integrated Parallel Imaging Technique (iPAT), with a PAT factor of 2. Total scan time is just under 15 minutes for these high-resolution images.
This optimization has taken the form of more efficient utilization of the imaging gradients coupled with a flexible reordering scheme and parallel imaging techniques.
The new reordering techniques for TSE sequences allow a more flexible choice of TE to allow better optimization of protocols so as to maintain image contrast whilst using longer echo train lengths.
The advantages of this new sequence are shown in Fig. 2. In (A–D) the length of the echo train is increased thus decreasing the scan time from 4 min to 80 s and with the new enhanced sequence the TE can be kept constant resulting in similar contrast properties between the 4 images. Furthermore even numbered Echo Train Lengths (ETLs) are now possible. In (E–H) the TE has been varied to allow for different contrasts. As can be seen, the TSE sequence is now completely flexible and can be configured in any manner.
By using these new sequences coupled with clinical 3T machines and dedicated MSK coils, it is possible to achieve a new level in accurate clinical diagnosis as demonstrated in Fig. 3 where a cartilage delamination in a patient with femoro-acetabular impingement is diagnosed with the help of a non-contrast protondensity (PD)-weighted TSE high-resolution scan (0.3 x 0.3 x 3 mm) with fat suppression.

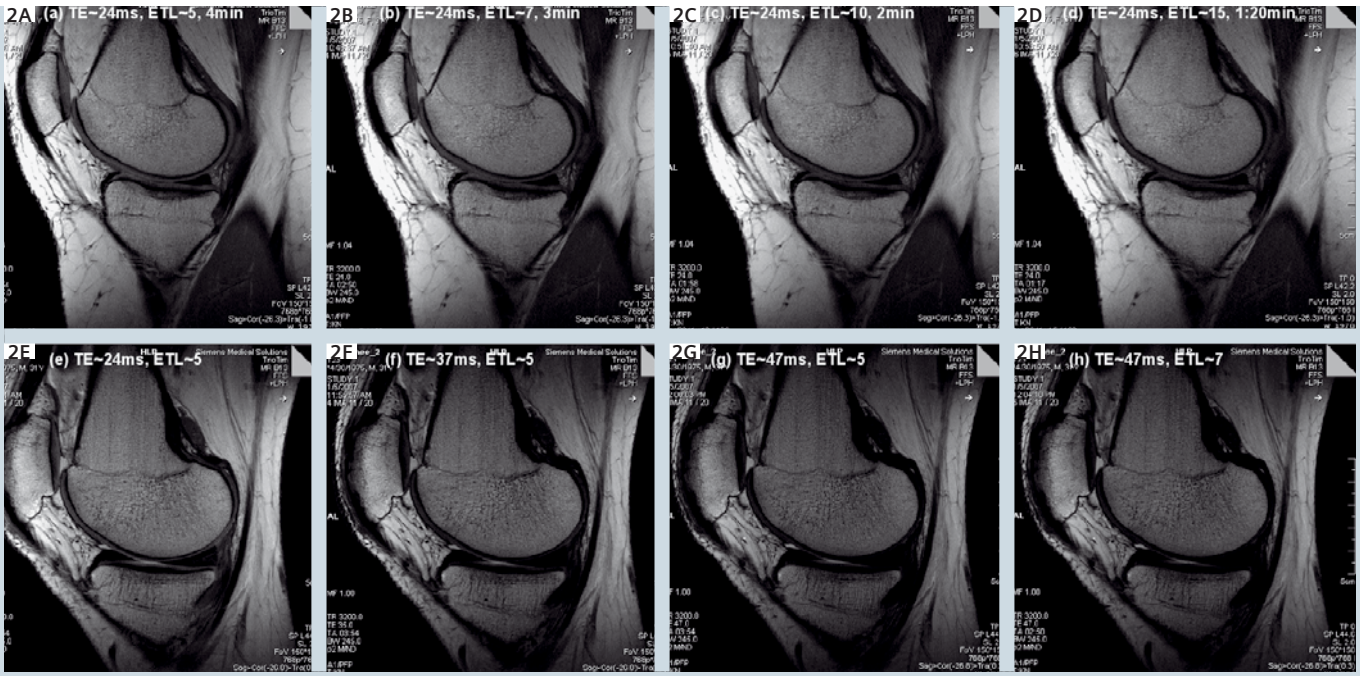

2 The enhanced flexibility of the TSE sequence is demonstrated within this series where in (A–D) scan time has been reduced from 4 min to 80 s. In the second row (E–H) the ability to select intermediate echo times is shown.

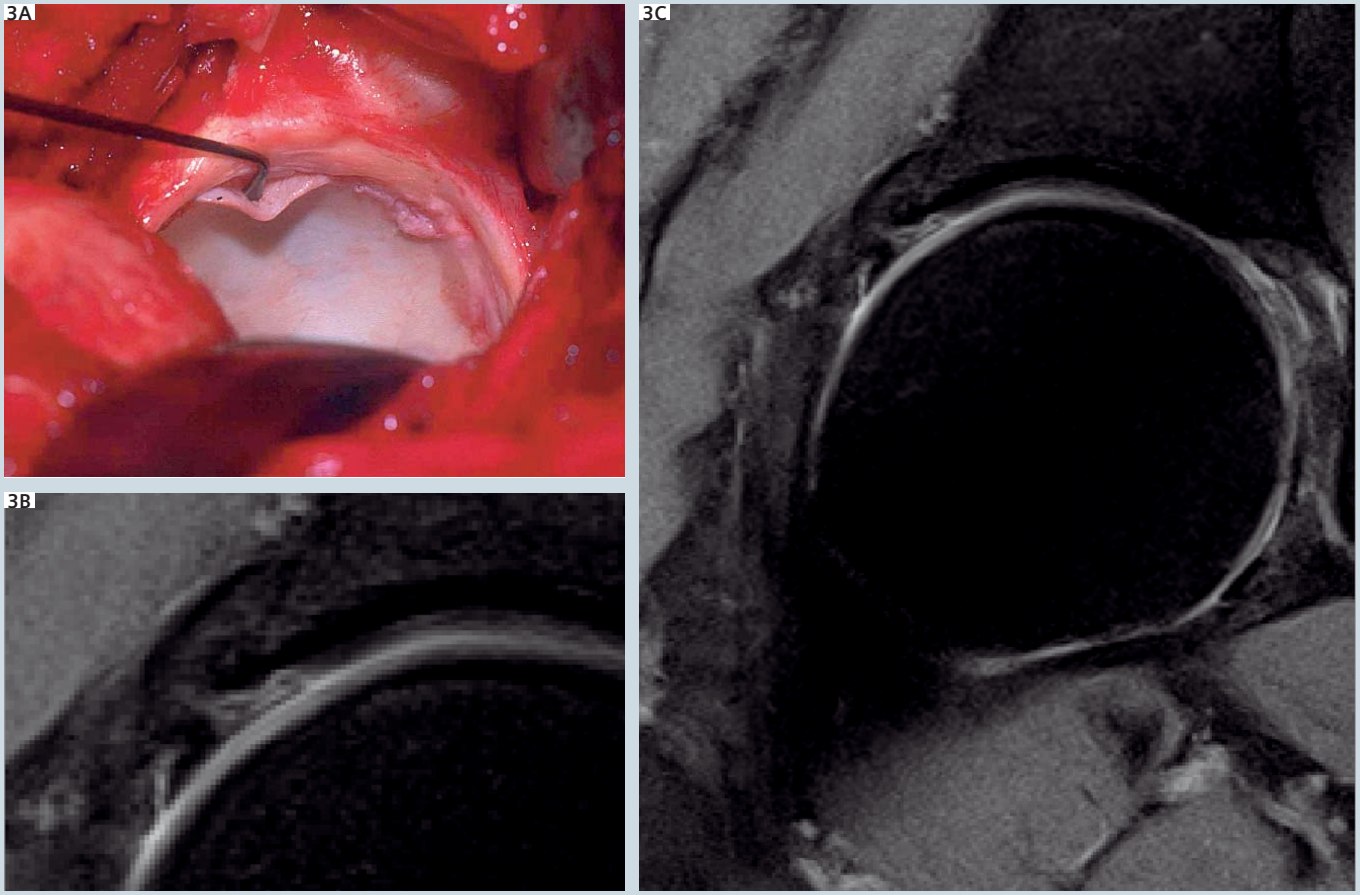

3 **A–C High in-plane resolution (0.3 x 0.3 x 3 mm) image (fat suppressed PD-weighted TSE) of a cartilage flap in the hip joint. Patient with femoro-acetabular impingement.**

Courtesy of T. C. Mamisch, University Bern, Switzerland.

Isotropic 3D Imaging

High-resolution, sub-millimeter, fast 3D isotropic imaging is becoming increasingly important as a means of enhancing workflow and providing more accurate diagnosis.

The philosophy behind this innovation is that 3D imaging allows total flexibility of examination i.e. by reformatting the joint can be examined in any plane.

The advantages associated with this new philosophy can be summarized as follows:

- Spatial localized diagnosis of the meniscus. Current research emphasizes the role of a more precise diagnosis of the localization of the meniscal injury for the possibility of applying different therapy concepts. In addition, in terms of monitoring of the meniscus after injury and therapy a reproducible localization is necessary.
- Accurate diagnosis of the cruciate ligaments requires angulations of the diagnostic plane to the position of the ligament within the joint. This can be done in a reproducible manner using the isotropic sequence as shown in Fig. 2.
- Diagnosis of cartilage damage or monitoring of cartilage therapy requires accurate determination of the spatial extent of the cartilage lesion or repair tissue. Using International Clinical Scoring Systems for accurate diagnosis requires reproducible and spatially accurate imaging data. This can be achieved with isotropic sequences which allow flexible and accurate reformatting along well defined diagnostic planes.

These examples summarize how isotropic sequences enable the accurate diagnosis of internal structures such as cartilage, meniscus and ligaments based on free angulations reconstruction. Through the use of an isotropic 3D sequence these areas can be reformatted in a reproducible way with a high resolution. This provides further workflow improvements by acquiring one 3D sequence that can be reformatted in the different planes needed for precise diagnosis.

Another example is an anatomical complex situation such as in the hip joint, where different angulations based on anatomical landmarks are necessary for precise diagnosis. By using an isotropic sequence as shown in Figure 5, these reconstructions can be done within one scan.

Recent developments in 3D sequences allow different contrasts to be achieved i.e. using DESS (Dual Echo Steady State), MEDIC (Multi-Echo Data Image Combination), VIBE (Volume Interpolated Breath-hold Examination) and TrueFISP. Most interesting is the capability now to achieve 3D TSE contrast with high signal-to-noise ratio using SPACE (Sampling Perfection with Application optimized Contrasts using different flip angle Evolutions) with long echo trains within a reasonable imaging time.

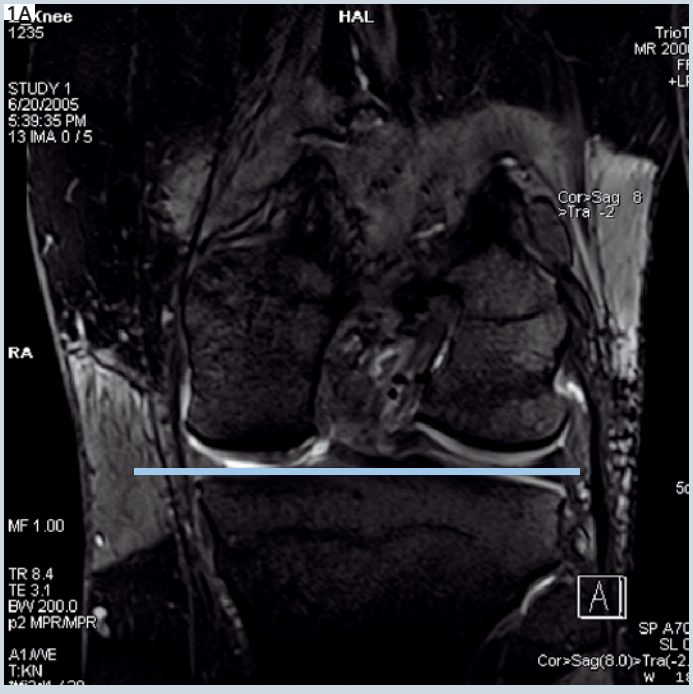

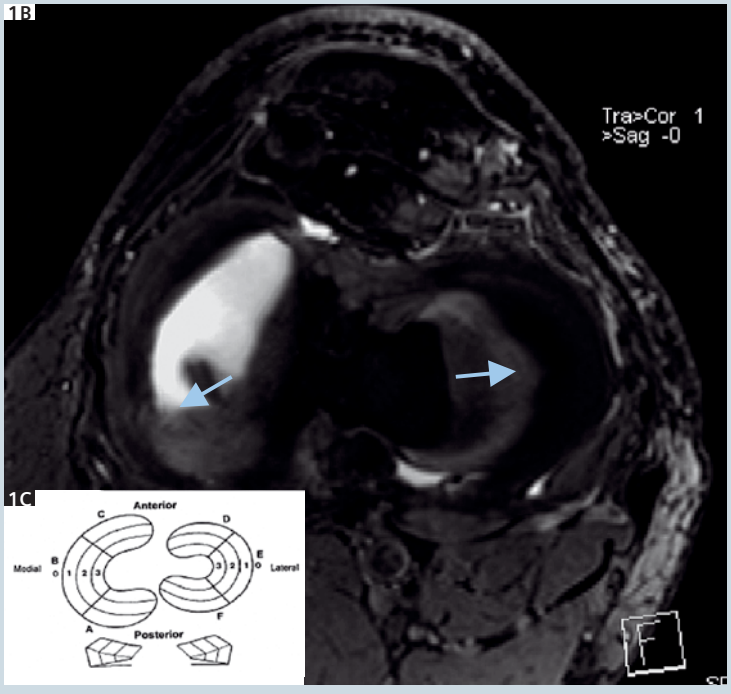

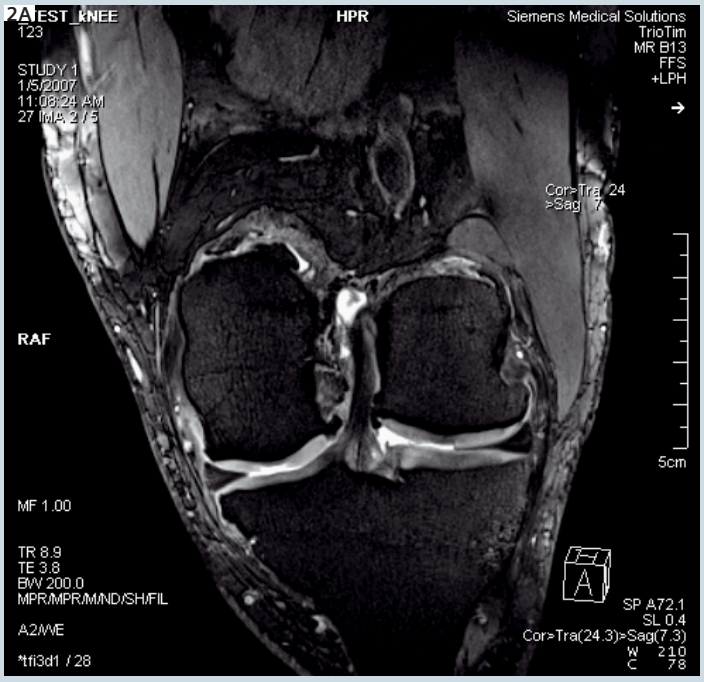

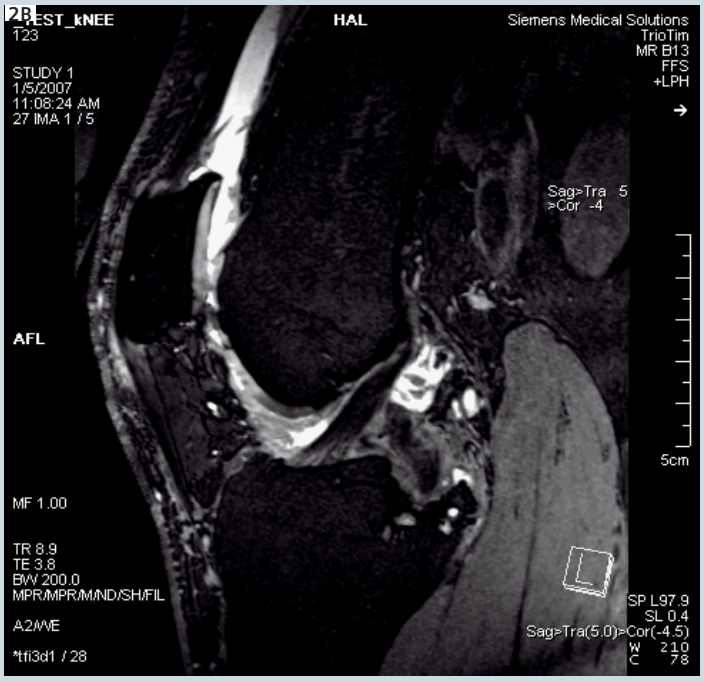

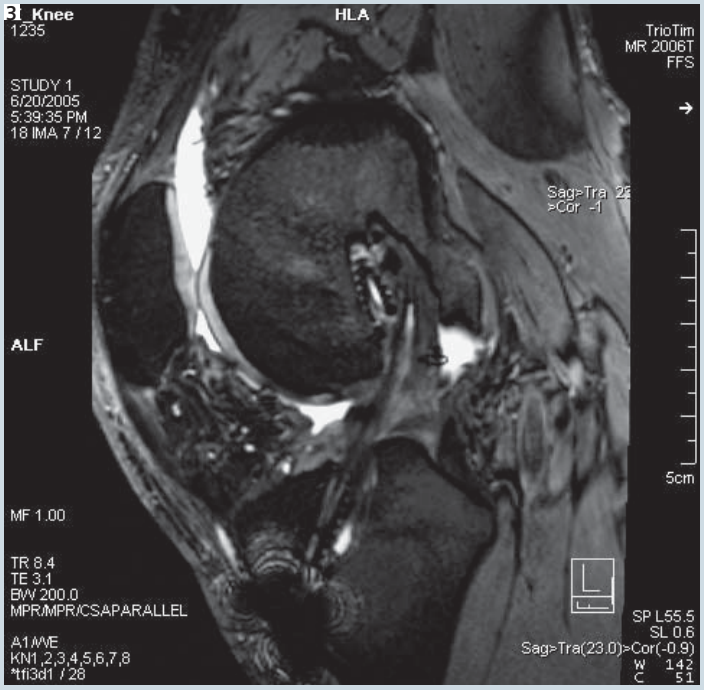

1 **A–C: Example of patient after partial lateral meniscal resection after trauma. Oblique axial plane reconstruction of the meniscus for precise localization for follow up and diagnosis.**

2 **A, B: Visualization of the anterior cruciate ligament oblique coronal and sagittal based on a 3D TrueFISP (isotropic resolution 0.4 x 0.4 x 0.4 mm).**

3 **Visualization after replacement of anterior cruciate ligament for monitoring of therapy.**

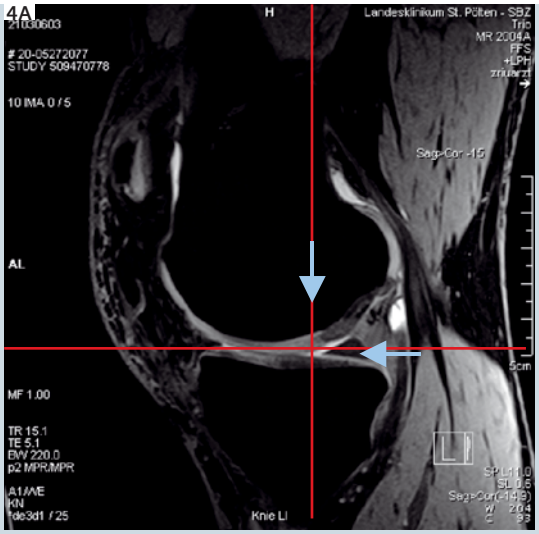

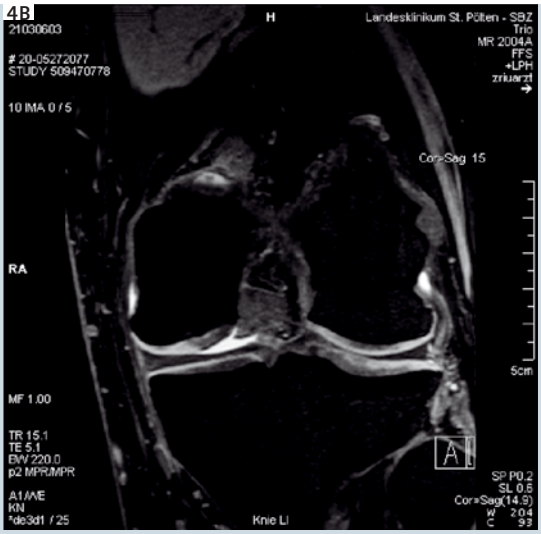

4 **A–D: 3D TrueFISP of patient with cartilage repair procedure (matrix-associated autologous chondrocyte transplantation – MACT technique). Reconstruction of anatomical image planes for localization of the damaged tissue based on classification cartilage repair society scheme (Fig. 4D).**

Courtesy: Siegfried Trattnig M.D., Medical University of Vienna, Austria

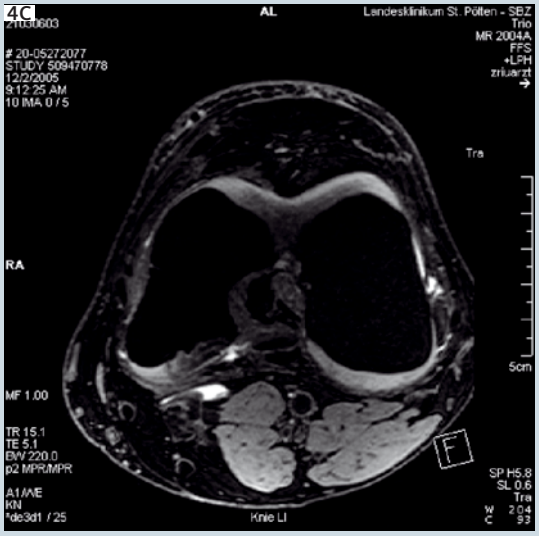

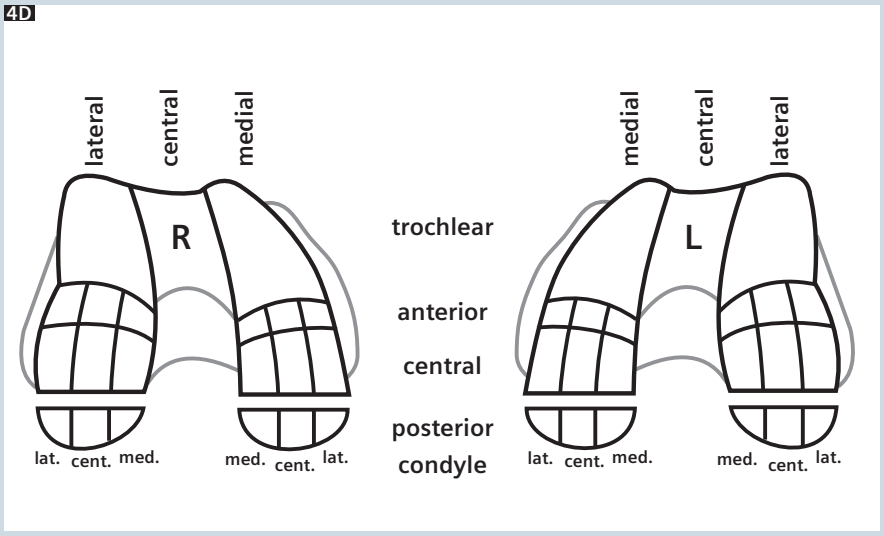

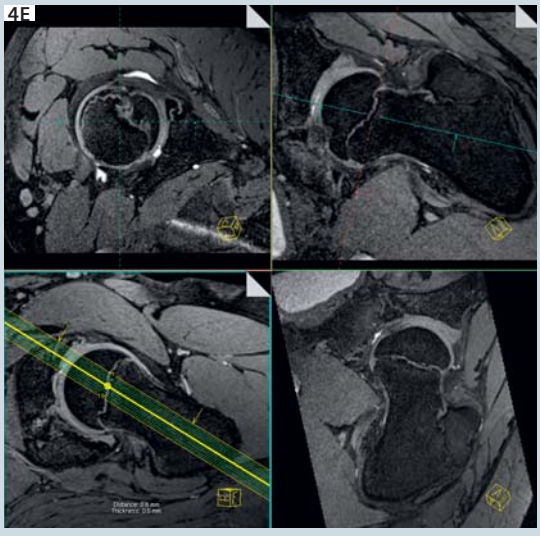

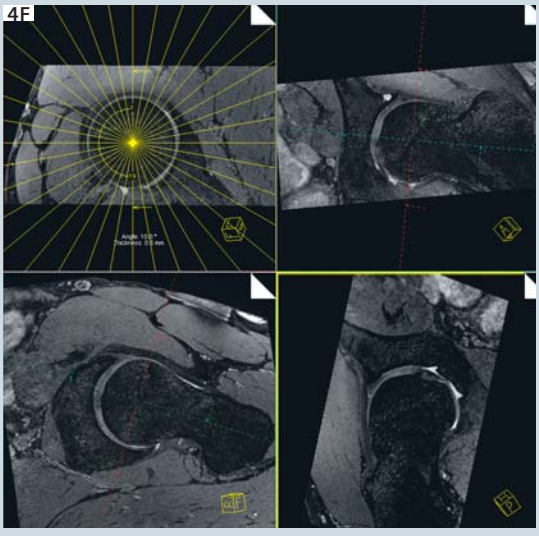

4 **E–F: Hip joint evaluated from different angles with the help of isotropic imaging.**
E: Oblique coronal.
F: Radial reconstruction for the assessment of labrum and cartilage morphology.

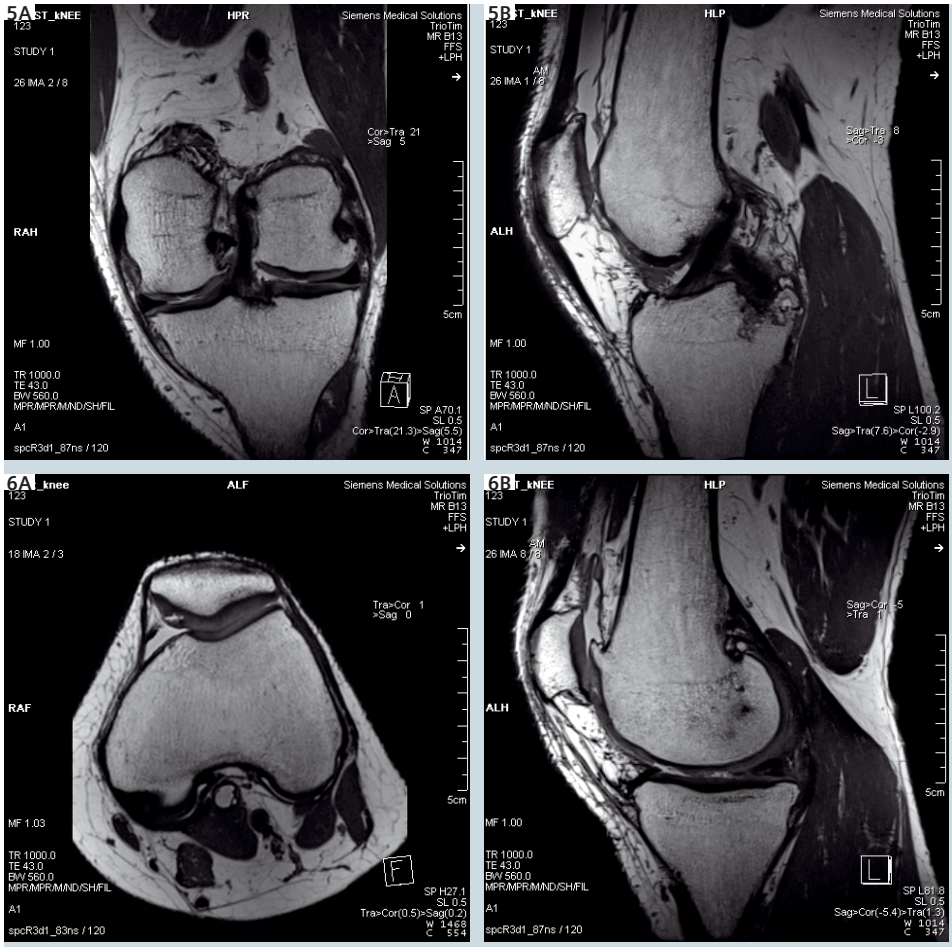

5 **6** **Figures 5 and 6 show the cruciate ligament and a cartilage diagnostic view angulated based on a 3D PD-weighted SPACE sequence (0.6 x 0.6 x 0.6 mm isotropic resolution).**

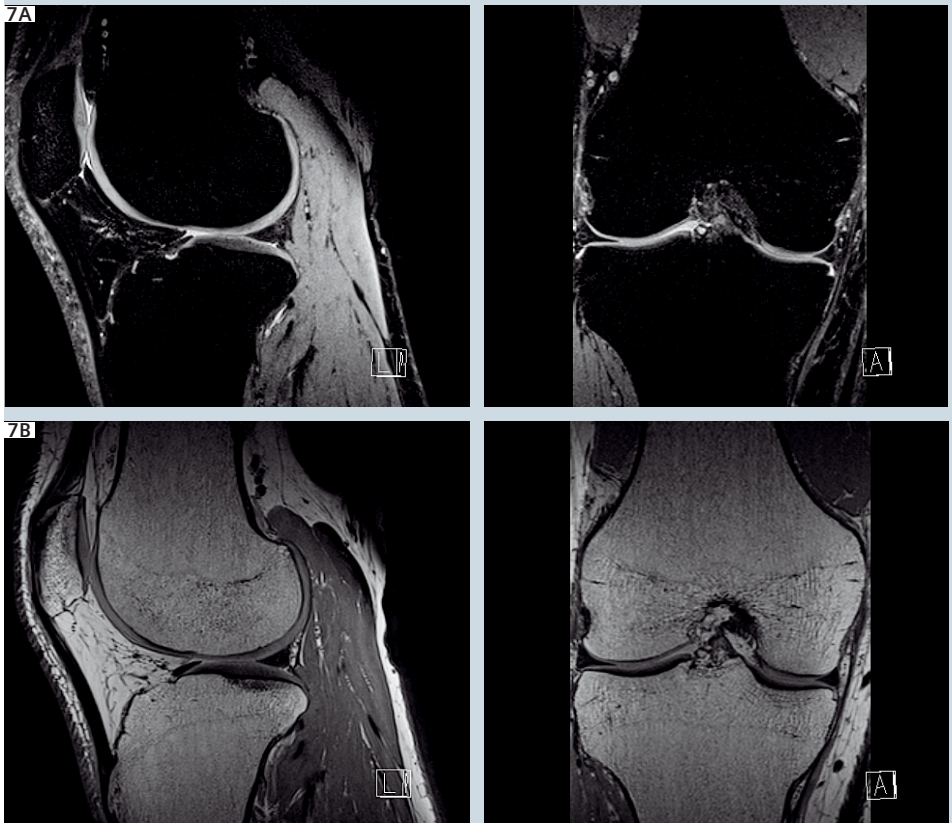

7 **A–B: Protondensity-weighted SPACE sequence with (A) and without (B) SPAIR fat suppression.**

Molecular Imaging of Articular Cartilage and Cartilage Repair

Siegfried Trattnig, M.D.[1]; Götz Welsch, M.D.[2]; Stefan Marlovits, M.D.[3]; Tallal Charles Mamisch, M.D.[4]

[1]*Department of Radiology, Medical University of Vienna, Austria*
[2]*Department of Radiology, AKH Vienna, Austria*
[3]*Department of Trauma Surgery, AKH Vienna, Austria*
[4]*Inselspital, University Bern, Switzerland*

MR imaging of the morphology of cartilage and cartilage repair tissue has significantly improved in recent years due to the development of clinical high-field MR systems operating at 3 Tesla. The improved performance has also been achieved as a result of the higher gradient strengths and the application of dedicated coils with modern configuration, such as phased array coils. The combination of these technological advances now allows high-resolution imaging of cartilage within reasonable scan times. In addition to the evaluation of gross cartilage morphology by MRI, there is growing interest in the visualization of ultra small structural components of cartilage by MR in two fields:

1. Osteoarthritis is manifested by significant changes in biochemical composition of articular cartilage. Loss of glycosaminoglycans (GAG) and increased water content represent the earliest stage of cartilage degeneration, while the collagenous component of the extracellular matrix remains mainly intact during this early phase of cartilage degeneration [1].

2. During recent years many new cartilage surgical techniques have been developed based on tissue engineering techniques such as autologous chondrocyte implantation (ACI) and matrix-associated autologous chondrocyte transplantation (MACT).

In addition to morphological MR imaging of cartilage repair tissue, an advanced method for non-invasively and quantitatively monitoring parameters reflecting the biochemical status of cartilage repair tissue is a necessity for studies which seek to elucidate the natural maturation of MACT grafts and the efficacy of the technique. Therefore, several MR techniques have been developed which allow detection of biochemical changes that precede the morphological degeneration in cartilage:

Delayed gadolinium-enhanced MRI of cartilage (dGEMRIC) [2]

Based on the fact that GAG molecules contain negatively charged side chains which lead an inverse proportionality in the distribution of the negatively charged contrast agent molecules. Consequently, T1 which is determined by the Gd-DTPA2-concentration becomes a specific measure of tissue GAG concentration. The dGEMRIC technique has provided valuable results in studies on hip dysplasia, in comparative studies with arthroscopically determined cartilage softening in early osteoarthritis, and demonstrated the positive effects of moderate exercise on glycosaminoglycan content in knee cartilage [3]. However there are two main problems, firstly the standard dGEMRIC technique is either limited to single slices in 2D acquisition or is time consuming in 3D sequences such as 3D inversion recovery prepared fast spoiled gradient recalled acquisition in the steady state. This therefore limits the attractiveness of dGEMRIC for clinical use. The second problem with dGEMRIC is more specific to cartilage repair tissue. Previous clinical studies of early cartilage degeneration showed that the differences in the pre-contrast T1 values between degenerative cartilage and normal cartilage were so small that they could be ignored [4]; however, this is not true for cartilage repair tissue. For a correct evaluation of glycosaminoglycan concentration in cartilage repair tissue, the pre-contrast T1 values also have to be calculated [4]. If a quantitative T1 analysis is also performed prior to contrast administration, it is possible to calculate the concentration of Gd-DTPA in the cartilage. The concentration is represented by Δ R1, the difference in relaxation rate (R1 = 1/T1) between T1 pre-contrast and T1 post-contrast. This places time limitation problems on the patient evaluation since both pre-contrast MR imaging and delayed post-contrast MR imaging must be performed in cartilage repair patients. To overcome these problems we used fast T1 determination by using different excitation flip angle values in gradient echo based sequences. For the follow-up of cartilage implants, quantitative T1-mapping based on a 3D GRE sequence, Volume Interpolated Breath-hold Examination (VIBE), with a TR 50 ms, TE 3.67 ms, flip angle 35/10°, a field of view (FoV) of 183 x 200 mm and a matrix size of 317 x 384 was performed, resulting in a resolution in plane of 0.6 x 0.5 mm with an effective slice thickness of 1 mm. The scan time was 6 min 53 s. The repetition time of 50 ms was chosen as a compromise between signal-to-noise ratio (SNR) and the reduction of any slice profile effects. The flip angle combination of 35°–10° proved to be the best compromise for obtaining reliable T1 values in the long range of T1 values present in the pre-contrast repair tissue (800–1200 ms) as well as in the short range of T1 values seen in post-contrast repair tissue (300–500 ms) as demonstrated by a good correlation with inversion recovery sequence in both T1 value ranges in the phantom study. In the in vivo part of this study we have shown that it is feasible to apply this 3D variable flip angle dGEMRIC technique in patients following MACT surgery in clinically acceptable scan times as a way to obtain information related to the long-term development and maturation of

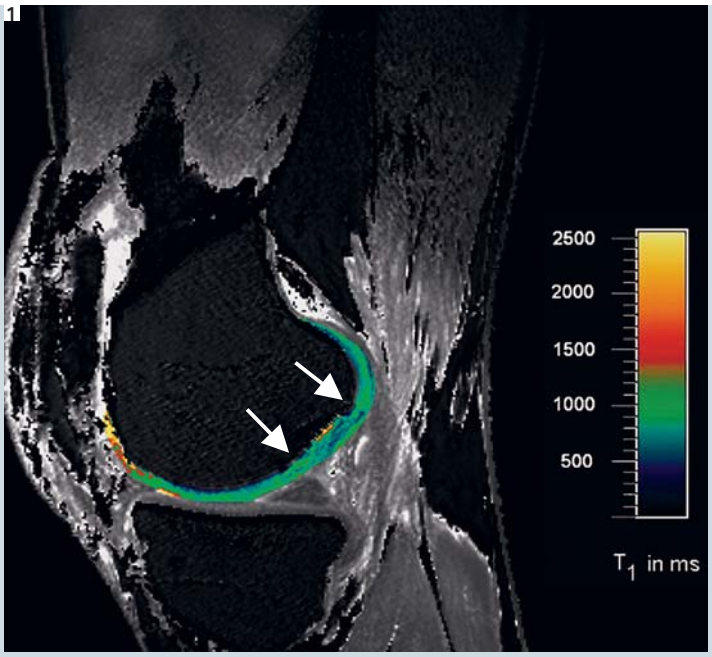

1 **Pre-contrast.** **Image of T2-map shows the pseudo-colour T2 values distribution within MACT. Corresponding T2 values are shown in the color-bar. Transplant cartilage shows higher T2 values, compared to the hyaline cartilage reference. The MR measurement was conducted 5 months after the surgery. White arrows mark the borders of the cartilage transplant.**

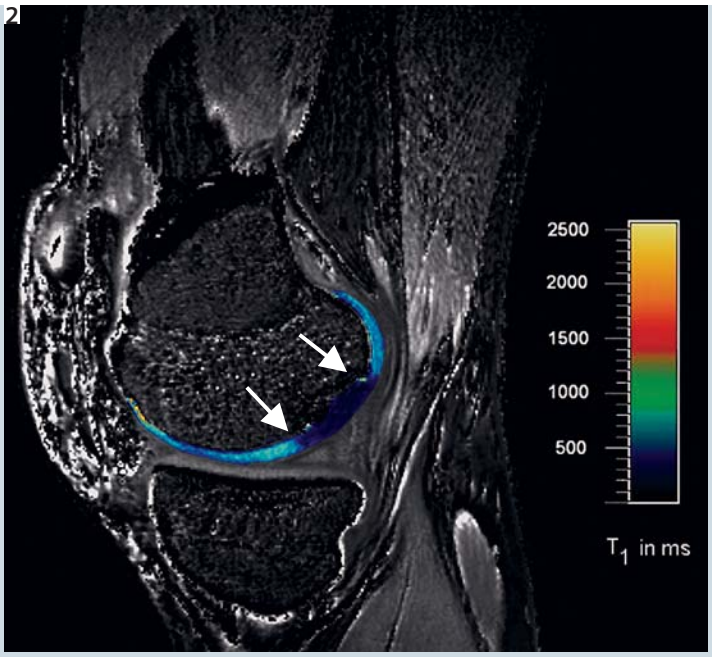

2 **Post-contrast.** **Figure shows color coded cartilage transplant post-contrast T1-map. This figure shows contrast enhancement of cartilage transplant after i.v. administration of contrast agent. White arrows mark the borders of the transplant.**

grafts. Thus, we found that the GAG content is significantly lower in repair tissue than in normal hyaline cartilage and does not change even after 3 to 4 years.
While GAG content reflects stiffness properties of repair tissue, the organisation of the collagen matrix in repair tissue over time is important too, as failure within the collageneous fibre network is considered to entail further cartilage breakdown.

Quantitative T2-mapping

Reported to be sensitive to collagen content and organization. In our examinations the T2 relaxation times were obtained from T2-maps reconstructed using a multi-echo spin echo (SE) measurement with a repetition time (TR) of 1.650 s and six echo times (TE) of 12.9 ms, 25.8 ms, 38.7 ms, 51.6 ms, 65.5 ms and 77.4 ms. Field of View (FoV) was 200 x 200 mm, pixel matrix 320 x 320 and voxel size of 0.63 x 0.63 x 1 mm. Using quantitative T2-mapping of patients at different post operative intervals after MACT surgery, we found significantly higher T2 values in cartilage repair tissue in the early stage (3–6 months) compared to native hyaline cartilage. Furthermore, we found a decrease in repair tissue T2 values over time with the T2 values becoming similar to native healthy cartilage by approximately one year. One encouraging alternative to these sequence modalities for the evaluation of cartilage microstructure is the use of DWI.

DWI: Diffusion-weighted sequences [8]

Diffusion-Weighted Imaging (DWI) is based on molecular motion that is influenced by intra- and extra-cellular barriers. Consequently, it is possible, by measuring the molecular movement, to reflect biochemical structure and architecture of the tissue. Conventional DWI based on spin-echo (SE) sequences is relatively insensitive to susceptibility effects, but diffusion-weighted SE sequences require a long acquisition time which, for practical reasons, in a clinical examination is inapplicable. Echo planar imaging (EPI)-based diffusion sequences, the gold standard of DWI in neuro applications, suffer from image distortions due to susceptibility changes as well as from limitations in contrast due to the rather long echo times needed. Both render them impracticable for low T2 tissues like cartilage and muscles. Alternatively, diffusion imaging can be based on steady state free precession sequences (SSFP) which realize a diffusion weighting in relatively short echo times. This is achieved by the application of a mono-polar diffusion sensitizing gradient which, under steady state conditions, leads to a diffusion weighting of consecutive echoes (spin

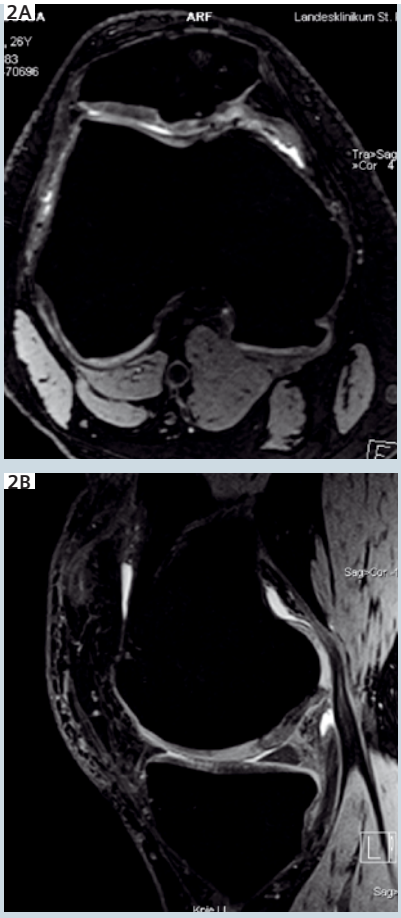

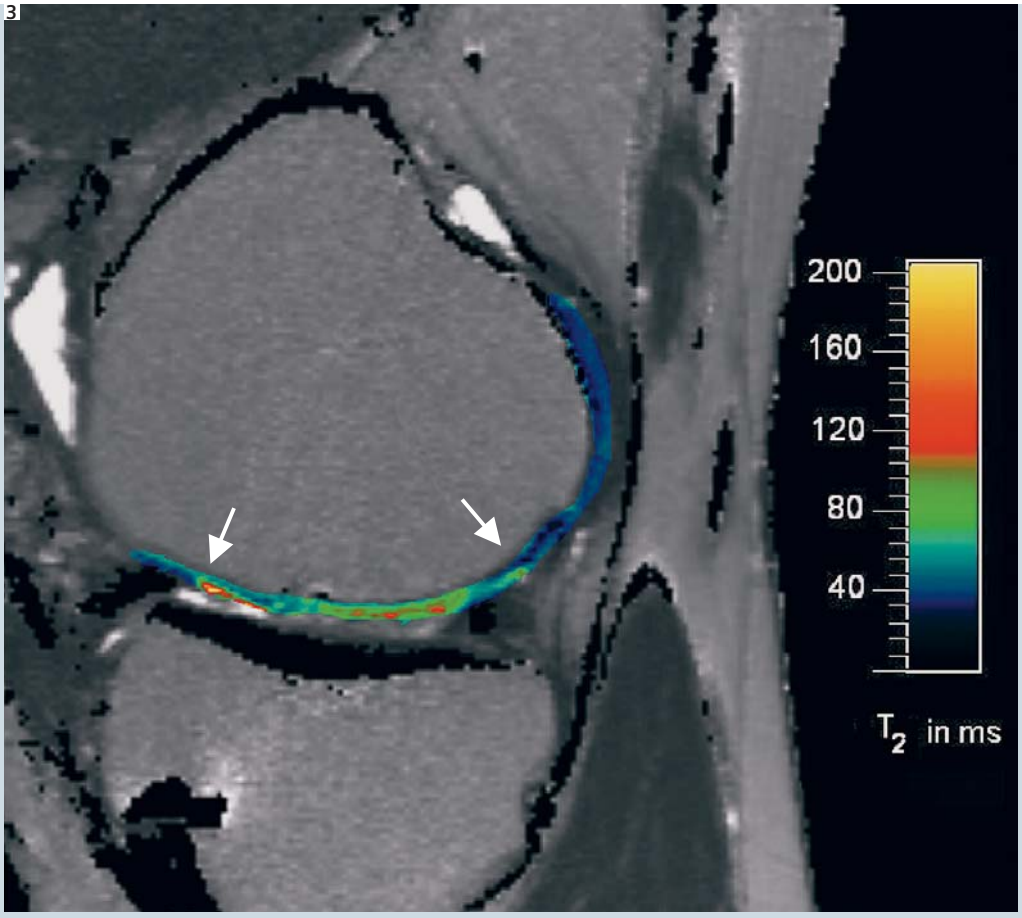

2 A, B: 3D Morphological imaging: 3D DESS sequence for assessment of cartilage repair axial (top) and sagittal (bottom).

3 **T2: Post-contrast.** Pseudo-color image of T2-map of the measurement after the surgery shows lower T2 values presented in cartilage transplant, compared to the normal hyaline cartilage reference. White arrows mark the borders of the cartilage transplant. Corresponding T2 values are shown in the color-bar.

echoes and stimulated echoes). For the assessment of diffusion-weighted images, a three-dimensional steady state diffusion technique, called PSIF (which is a time reversed FISP (Fast Imaging by Steady State Precession) sequence), has been used [9]. Imaging parameters of the DW-PSIF acquisition for cartilage were as follows: TR 16.3 ms, TE 6.1 ms, flip angle 30°, 48 sagittal slices, 170 x 170 mm FoV, 256 x 256 matrix size, slice thickness 1.5 mm, voxel size 0.6 x 0.6 x 1.5 mm^3. Scan time for each diffusion-weighted sequence was 4:40 min. In order to allow a semi-quantitative assessment of the diffusional behaviour in the cartilage, the diffusion sequence protocol consisted of 2 separate but immediately consecutive measurements using none (0), and 75 mT*ms*m-1 monopolar diffusion gradient moments for Diffusion-Weighted Imaging (DWI) and otherwise identical imaging parameters. For evaluation, the quotient image (non-diffusion-weighted /diffusion-weighted image) was calculated on a pixel-by-pixel basis. In a series of 15 patients after MACT we could demonstrate the feasibility of diffusion-weighted PSIF imaging with high resolution in vivo. The results show that in the follow up at different time points after MACT the diffusion behaviour of the transplants is changing. In the earlier period after MACT the diffusion was higher restricted which declined in the later follow up, but even after a period of up to 42 months there was still a difference in diffusion values between repair tissue and normal hyaline cartilage. With imaging techniques such as DW PSIF and a semi-quantitative evaluation forming the quotient, functional analysis of cartilage and cartilage repair with high SNR and high resolution can be achieved within comparably short acquisition times. In this context, diffusion-weighted imaging can practicably complement the information obtained from approaches which rely on relaxation properties such as dGEMRIC or T2-mapping. In comparison to dGEMRIC imaging of cartilage and cartilage repair procedures, no contrast medium is needed, coverage and resolution is improved and scan times reduced. It may be another tool of biochemical evaluation of cartilage transplants in the near future and could be added in a clinical setting to dGEMRIC and T2-mapping for evaluation of cartilage repair outcomes.

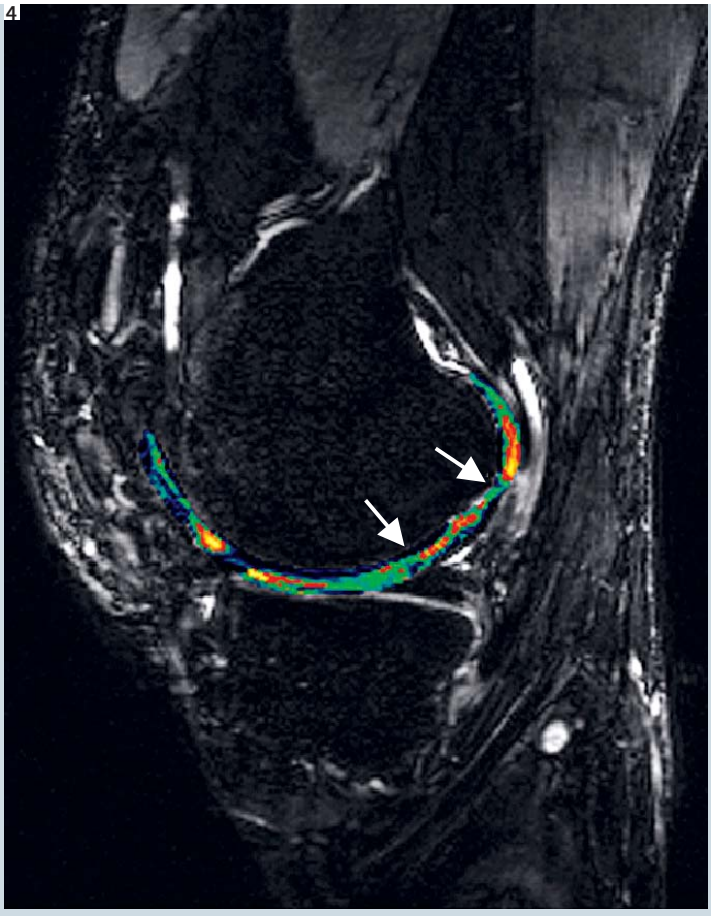

4 **DIFF: None.** **This is not a diffusion-weighted image. The intensity of the greyscaled part of the image was modified for better representation. The intensity of the pseudo-colored cartilage part was not modified and can be evaluated using the colorbar.**

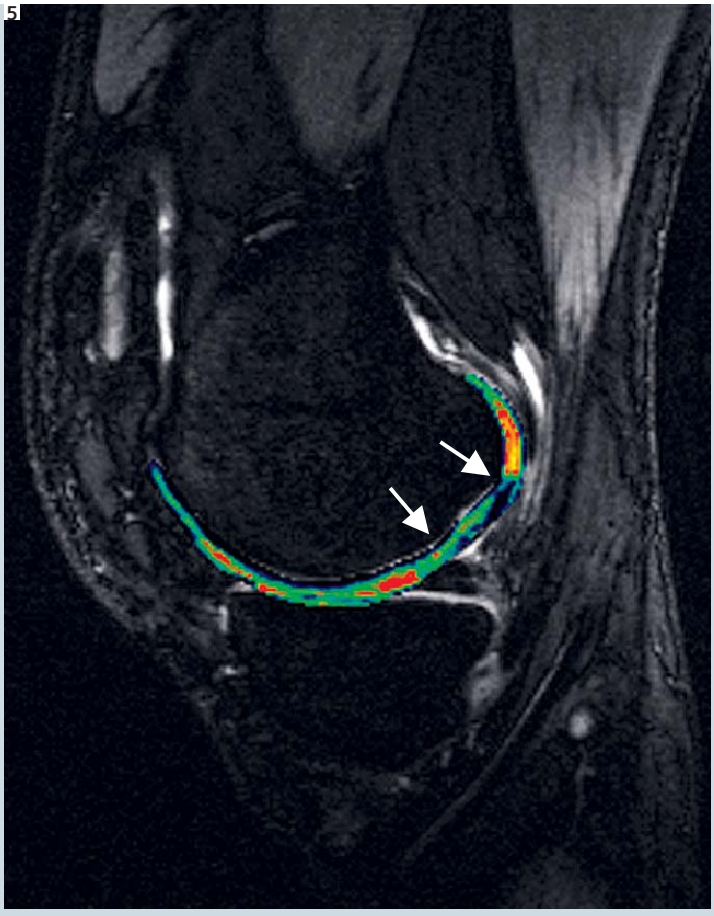

5 **DIFF: 75.** **The colored diffusion image in a medial condyle from central weight bearing zone aspects. The cartilage transplant is visible (arrows). Whereas in the central aspects the diffusivity is a little higher, it reduces to the more peripheral areas.**

References

1 Grushko G, Schneiderman R, Maroudas A. Some biochemical and biophysical parameters for the study of the pathogenesis of osteoarthritis: a comparison between the processes of aging and degeneration in human hip cartilage Connect Tissue Res 1989; 19: 149–76.

2 Brittberg M, Lindahl A, Nilsson A, Ohlsson C, Isaksson O, Peterson L. Treatment of Deep Cartilage Defects in the Knee with Autologous Chondrocyte Transplantation. New Engl J Med 1994; 331(14): 889–895.

3 Bashir A, Gray ML, Burstein D. Gd-DTPA2- as a measure of cartilage degradation. Magn Reson Med 1996; 36: 665–73.

4 Burstein D, Velyvis J, Scott KT et al. Protocol issues for delayed Gd(DTPA) (2-) enhanced MRI (dGEMRIC) for clinical evaluation of articular cartilage. Magn Reson Med 2001; 45: 36–41.

5 Watanabe A, Wada Y, Obata T, et al. Delayed gadolinium-enhanced MR to determine glycosaminoglycan concentration in reparative cartilage after autologous chondrocyte implantation: Preliminary results. Radiology 2006; 239(1): 201–208.

6 Miller KL, Hargreaves BA, Gold GE, et al. Steady-state diffusion-weighted imaging of in vivo knee cartilage. *Magn Reson Med.* Feb 2004; 51(2): 394–398.

T2 Mapping of Articular Cartilage in Hip Joint

Atsuya Watanabe, M.D.[1, 2]; Chris Boesch, M.D.[1]; Tallal C. Mamisch, M.D.[3]; Suzanne E. Anderson, M.D.[1, 2]

[1]Department of Clinical Research, Unit for MR Spectroscopy and Methodology, University of Bern, Switzerland
[2]Department of Diagnostic, Interventional and Pediatric Radiology, Inselspital, University of Bern, Switzerland
[3]University Hospital Bochum, Bergmannsheil Clinics, Department of Trauma Surgery, Bochum, Germany

Introduction

T2 (transverse relaxation time) mapping is an MR imaging technique which is able to evaluate the cartilage matrix status, such as collagen fiber integrity and hydration in cartilage [1]. As early degeneration of cartilage is characterized by deterioration of the extracellular matrix components, T2 mapping has the potential to identify cartilage degeneration in an early stage.
It has been known that there is a variation of cartilage matrix composition in the joint, and that T2 of cartilage is sensitive to the relationship between the collagen network and orientation of the static magnetic field (B_0) due to the orientation dependent dipolar interaction [2, 3]. To inspect the cartilage degeneration, it is important to understand the regional differences of T2 in a specific joint. There have been several clinical studies of T2 mapping in knee joints; however, few studies of T2 mapping have involved the hip joint.
The aim of this study is to demonstrate the ability of T2 mapping in detecting early degeneration of cartilage in the hip joint.

Examination and Analysis

Healthy volunteers and patients with femoro-acetabular impingement (FAI) syndrome diagnosed by previous examinations were evaluated.
MR imaging was performed with a 3.0 Tesla system (MAGNETOM Trio, A Tim System; Siemens, Erlangen, Germany). A dedicated Body Matrix coil (Tim system) was used to image both hip joints.
T2 measurement was performed at an oblique coronal plane, which was parallel to the femoral neck and passed through the center of the femoral head. A multi-spin-echo sequence was used for T2 measurements. The scanning parameters were 1500 msec repetition time, 10 echo times of 10.3–103 msec, 150×150 mm field of view, 4.0 mm slice thickness, 512×512 matrix, and 1 excitation. Color-coded T2-calculated maps were generated using MATLAB software (Mathworks, Natick, MA, USA) with a mono-exponential curve fit. The appearance of cartilage T2 maps in healthy hip joints were compared with that in hips with FAI syndrome.

Findings

T2 maps of acetabular and femoral cartilage in healthy hips for a representative case are shown in figures 1A and 1B respectively. The T2 in cartilage was slightly longer in the superficial layer than in the deep layer. In addition, slightly high T2 was observed in the lateral areas of femoral cartilage located symmetrically with each other.
The main cause of the high T2 observed at these areas might be the orientation dependent dipolar interaction, as magic angle effect is supposed to be observed when the collagen network structure is oriented 54.7° relative to B_0.
T2 map and T1- and T2-weighted MR images of acetabular cartilage in the same slice position of the hip for a representative patient with early stage of FAI syndrome are shown in figures 2A, 2B, and 2C respectively.
In the conventional T2-weighted MR

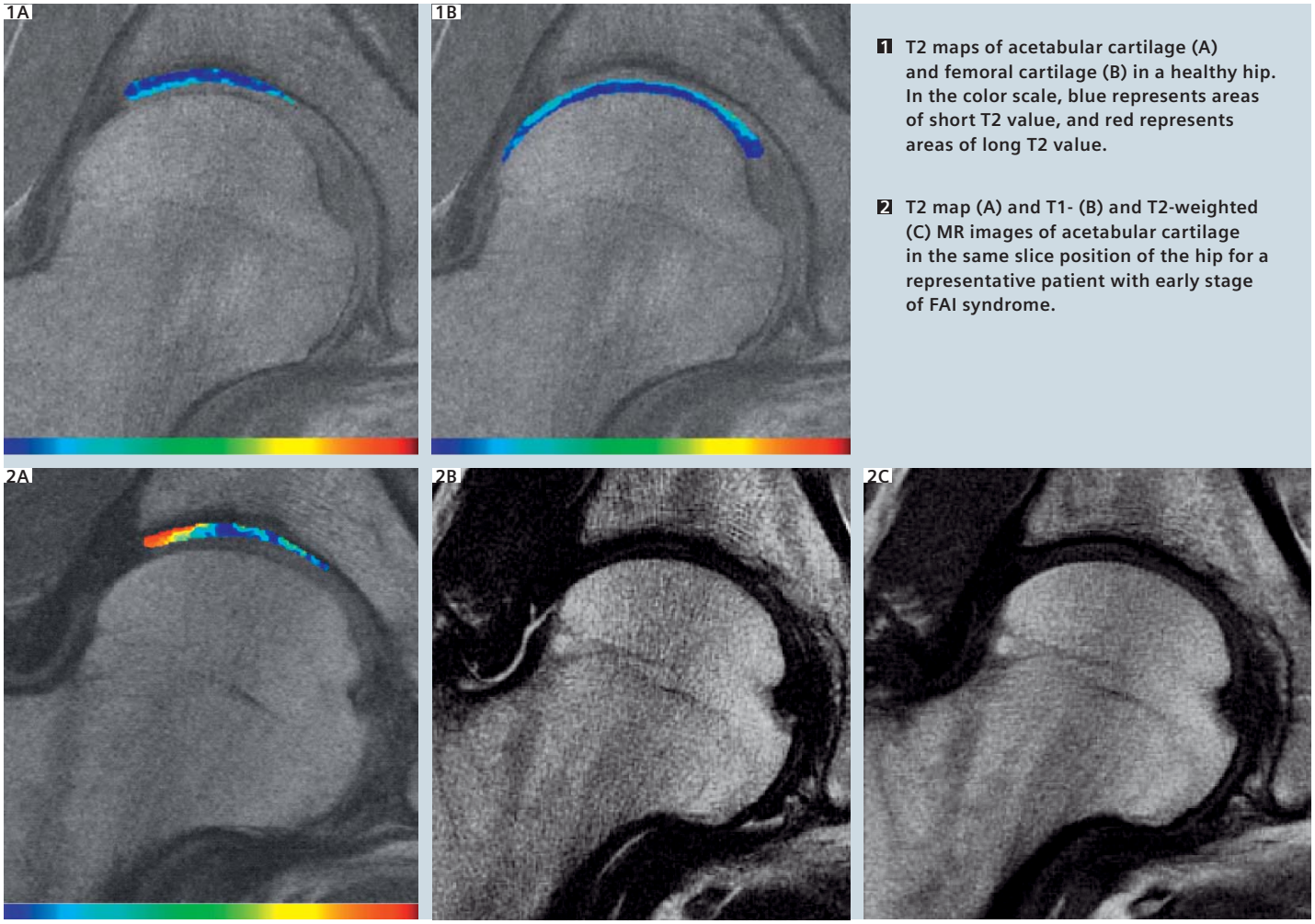

1 T2 maps of acetabular cartilage (A) and femoral cartilage (B) in a healthy hip. In the color scale, blue represents areas of short T2 value, and red represents areas of long T2 value.

2 T2 map (A) and T1- (B) and T2-weighted (C) MR images of acetabular cartilage in the same slice position of the hip for a representative patient with early stage of FAI syndrome.

image, degeneration of acetabular cartilage was not clearly evident. However, high T2 in the lateral acetabular cartilage was observed with the T2 map, indicating the presence of degeneration within this area.

Discussion

T2 mapping may be able to detect early degeneration better than the conventional MR imaging techniques. The ability to detect early degeneration of hip articular cartilage may contribute to better understanding of the progression of degeneration seen with degenerative hip disease. It has been shown that the outcome of joint-preserving operations in hip joints correlates with the initial joint condition [4], the ability to evaluate cartilage status prior to operation could improve the predictability of post-operative outcomes. In this study, relatively large topographic variation of hip cartilage T2 in young healthy volunteers was observed. As this variation of T2 can lead to possible misinterpretation regarding cartilage degeneration, special attention should be paid when T2 mapping is applied to patients with degenerative cartilage of the hip joint.

References

1 Nieminen MT, Rieppo J, Toyras J, et al. T2 relaxation reveals spatial collagen architecture in articular cartilage: a comparative quantitative MRI and polarized light microscopic study. Magn Reson Med 2001; 46: 487–493.

2 Goodwin DW, Zhu H, Dunn JF. In vitro MR imaging of hyaline cartilage: correlation with scanning electron microscopy. Am J Roentgenol 2000; 174: 405–409.

3 Mosher TJ, Smith H, Dardzinski BJ, Schmithorst VJ, Smith MB. MR imaging and T2 mapping of femoral cartilage: in vivo determination of the magic angle effect. AJR Am J Roentgenol. 2001; 177: 665–669.

4 Trousdale RT, Ekkenkamp A, Ganz R, Wallrichs SL. Periacetabular and intertrochanteric osteotomy for the treatment of osteoarthrosis in dysplastic hips. J Bone Joint Surg 1995; 77A: 73–85.

3D-$T_{1\rho}$-Mapping of Cartilage at 3T with integrated Parallel Imaging Technique (*syngo* GRAPPA)

Ravinder R. Regatte, Ph.D.; Mark E. Schweitzer, M.D.

Center for Biomedical Imaging, Department of Radiology, New York University School of Medicine, New York, USA

Introduction

Osteoarthritis (OA) affects over 50 million Americans and has a substantial impact on the economy and the health care system. Currently, there is no cure for this debilitating chronic disease and the effective treatment is, at best, focused on symptomatic relief. The conventional imaging techniques have shown promise for the identification of more subtle morphologic alterations as determined by cartilage thickness, volume, or surface fibrillation. However, even the more innovative of these conventional techniques have not been consistent in detecting the earliest stages (biochemical/functional integrity) of cartilage degeneration.

The loss of proteoglycan content (PG) is an initiating event in the early stages of OA. Currently, the loss of PG can be measured via contrast enhanced MRI of cartilage (dGEMRIC) or $T_{1\rho}$-MRI (spin-lattice relaxation time in the rotating frame) or ^{23}Na-MRI. For clinical applications, dGEMRIC requires an exogenous contrast agent ($Gd\text{-}DTPA^{2-}$) with long temporal delay after intravenous injection (~90 minutes). However, sodium MRI is highly specific to PG but it requires RF hardware modification and high static magnetic fields (B_o) and has inherently low sensitivity, all of which limit this techniques clinical utility. Alternatively, $T_{1\rho}$ relaxation mapping has been shown to be sensitive to early biochemical changes in cartilage especially PG. It is well suited for probing low-frequency interactions between macro molecular protons (e.g. –NH and –OH sites) and bulk water protons. In cartilage, $T_{1\rho}$ is strongly correlated with PG content and is being studied for its potential as a biochemical marker of early OA. However, the clinical applications of 3D-$T_{1\rho}$ -relaxation mapping at high field systems (e.g. 3T and above) are currently limited due to the long imaging times as well as significant radio-frequency (RF) energy deposition. The combination of 3D-$T_{1\rho}$-weighted MRI with multi-coil RF technology and parallel imaging (GRAPPA) should be able to address both of these problems (total imaging time and RF energy deposition). The main purpose of the article is to demonstrate the feasibility of rapid $T_{1\rho}$- relaxation mapping of cartilage in early OA subjects at 3T clinical scanner with parallel imaging.

Examination and Data Analysis

Osteoarthritis subjects were recruited based on clinical symptoms and Kellgren-Lawrence grades. 3D-$T_{1\rho}$-relaxation mapping with parallel imaging was performed employing 3.0 Tesla clinical MRI system (MAGNETOM Trio, A Tim System; Siemens Medical Solutions, Erlangen, Germany). All the MRI experiments were performed employing a phased-array (PA) RF coil (18 cm diameter, 8-channel transmit-receive). We utilized a 3D-FLASH sequence in combination with parallel imaging (GRAPPA with 24 reference k-space lines) to acquire 3D-$T_{1\rho}$-weighted images. In order to achieve $T_{1\rho}$ magnetization preparation, we used a "self-compensating" spin-lock pulse cluster (duration of each 90° pulse = 200 µs). Four 3D- $T_{1\rho}$-weighted images with varying spin-lock pulse lengths (TSL = 2, 10, 20 and 30 ms) were acquired in order to construct $T_{1\rho}$ maps. Color coded $T_{1\rho}$-maps were generated using MATLAB software (Mathworks, Natick, MA, USA).

Results and Discussion

Representative $T_{1\rho}$ maps from a data set of 16 slices obtained with parallel imaging (PAT factor = 2) from two osteoarthritis subjects are shown in Fig. 1 (early OA, 35-year-old female volunteer) and Fig. 2 (moderate OA, 45-year-old male volunteer). In the group of early OA subjects studied, there is an approximately 15–20% elevation in $T_{1\rho}$ relaxation times (shown by white arrows) when compared to age-matched asymptomatic subjects. However in the case of moderate OA (Fig. 2), there is ~20–45% increase in $T_{1\rho}$ numbers as well as more compartments are involved in the progression of OA (shown by white arrows). The 3D-$T_{1\rho}$ in combination with parallel imaging (PAT factor = 2) show excellent *in-vivo* reproducibility for cartilage imaging (data not shown). Therefore, these preliminary studies clearly demonstrate the potential of rapid $T_{1\rho}$ with parallel imaging as a non-invasive biochemical marker of proteoglycan loss as well as early degeneration at high field systems (3T) without exceeding the RF energy deposition.

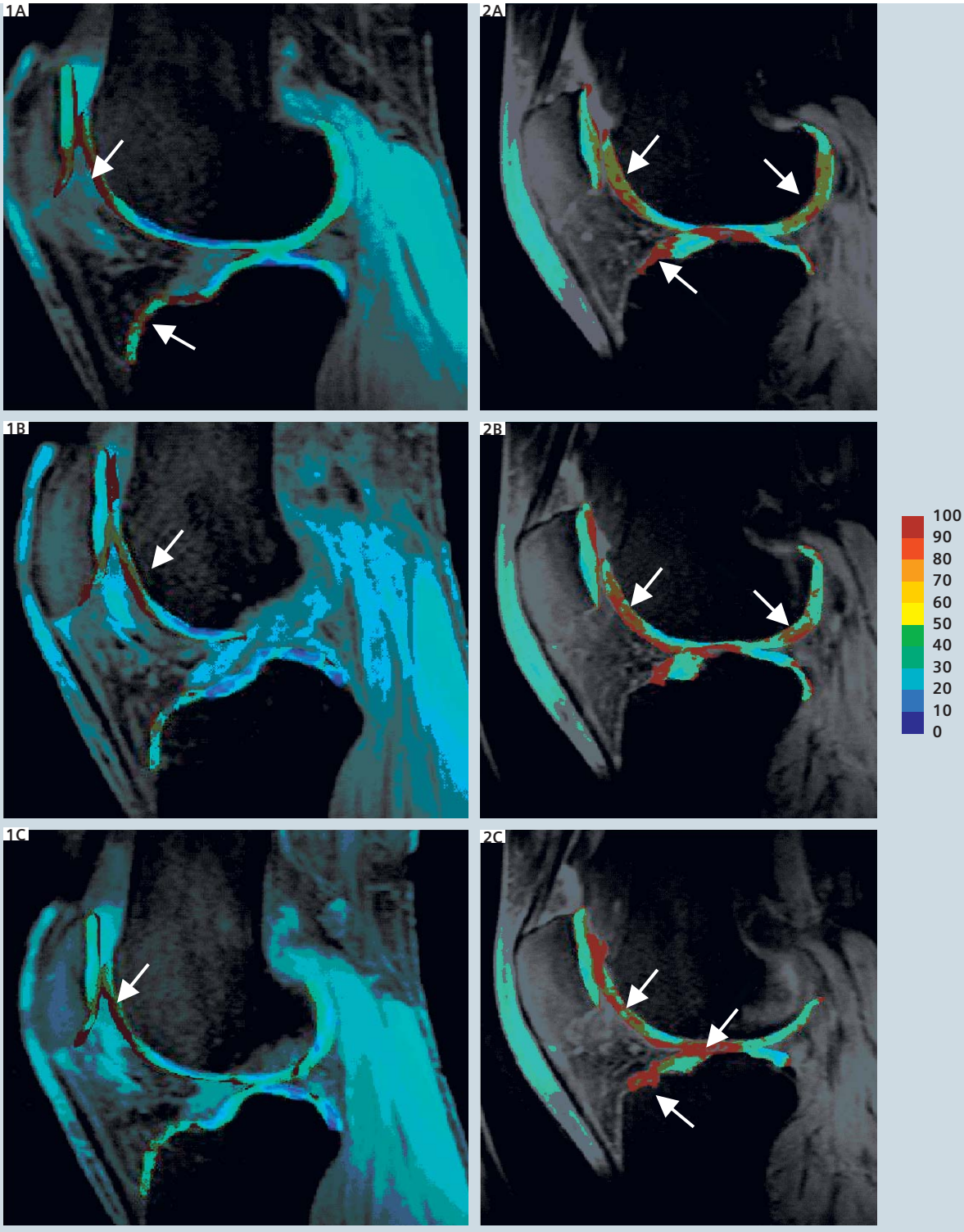

1 2 Representative $T_{1\rho}$-maps computed from two OA subjects are shown in Fig. 1 (early OA) and 2 (moderate OA) respectively. The 3D- $T_{1\rho}$-weighted imaging (GRAPPA with PAT factor = 2) was performed using $T_{1\rho}$ preparation pulse cluster and 3D-FLASH as a readout. The imaging parameters are TR 175ms; TE 3 ms; flip angle 25; slices 16; matrix 256 x 256; bandwidth 130 Hz/pixel, spin-lock amplitude 250 Hz. The color bar scale at the right indicates the $T_{1\rho}$-relaxation times in the cartilage (0–100 ms).
The elevated pixels in both OA subjects are shown by white arrows.

MR-Arthrography of the Hip

Stefan F. Werlen, M.D.

Klinik Sonnenhof, Radiology Dept., Bern, Switzerland

Introduction

This article describes the technique and findings of MR-Arthrography (MRA) of the hip joint, with special regard to the clinical setting of femoro-acetabular impingement.
MRA of the hip joint is a technique that uses intra-articular contrast medium, high field scanners and dedicated coils and sequences. With this technique only, one is able to detect subtle, but important changes of labrum, cartilage and bone of the hip joint. Today the direct MRA technique is widely used among musculoskeletal radiologists.

Examination Technique

Under fluoroscopic control, a 22-gauge spinal needle is introduced from ventral into the joint in the outer third of the head/neck-junction. Then 10 to 20 cc of diluted Gadolinium is injected.
All examinations are performed with a 1.5T Magnet (MAGNETOM Avanto, Siemens Medical Solutions, Erlangen, Germany). On the MR table a flex coil is positioned over the joint. After a short localizer in three planes the following sequences are used:
1. Axial T1-weighted sequence to assess bony structures and pathologies and also capsule configuration and thickness, as well as periarticular soft tissue changes (TR 650, TE 20, 200 mm field of view, 224 x 512 matrix, 4 mm slice thickness section thickness with a 0.2 mm section gap, 17 slices, 3 min).
2. Axial FLASH-sequence with a few thin slices, centered on the upper joint-space. This sequence is used to evaluate the version of the acetabulum and subcortical hypersclerosis and cystic changes of the acetabular rim (TR 550, TE 10, Flip angle 90°, 120 mm field of view, 256 x 256 matrix, 2 mm section thickness with a 0.1 mm section gap, 11 slices, 3:06 min).
3. Coronal-oblique protondensity-weighted (PDW) thin-slice sequence especially for the evaluation of the cartilage and its damages (TR 3200, TE 15, 120 mm field of view, 256 x 256 matrix, 2 mm section thickness with a 0.1 mm section gap, 23 slices, 5 min). This sequence is aligned perpendicular to the femoral neck and is marked on the axial T1-weighted sequence.
4. PDW sequence in sagittal direction also for cartilage assessment (TR 3200, TE 196 15, 120 mm field of view, 256 x 256 matrix, 2 mm section thickness with a 0.2 mm section gap, 23 slices, 5:37 min).
5. Radial PDW sequence is used in which all slices are oriented basically orthogonal to the acetabular rim and labrum. This sequence is based on a sagittal oblique localizer, which is marked on the PDW coronal sequence, and runs parallel to the sagittal oblique course of the acetabulum (TR 2000, TE 15, 260 mm field of view, 266 x 512 matrix, 4 mm section thickness, 16 slices, 4:43 min). In the center of the radial sequence, where the slices cross over, the signal wipes out. This produces a broad line without signal on the image, which affects the quality of the image. The more slices cross over, the broader the no signal line becomes. To reduce this artifact, this sequence is split into two sequences with 8 slices each. The whole examination, including the hip injection, lasts approximately 50 to 60 min.

Findings

In the impingement patients we found osseous changes, like retroversion of acetabulum and acetabular cysts. Osseous bumps and deformation of the femoral head/neck junction.
Often labral tears and ganglions are detected.
The PDW sequences showed nicely various cartilage defects and capsular thickening or scarring after surgical procedures.

References

1 Leunig M, Podeszwa D, Beck M, Werlen S, Ganz R, Magnetic resonance arthrography of labral disorders in hips with dysplasia and impingement., Clin Orthop 418, 74–80, Jan, 2004.

2 Locher S, Werlen S, Leunig M, Ganz R, [MR-Arthrography with radial sequences for visualization of early hip pathology not visible on plain radiographs], (Arthro-MRI mit radiarer Schnittsequenz zur Darstellung der praradiologischen Huftpathologie.), Z Orthop Ihre Grenzgeb 140: 1, 52–7, Jan–Feb 2002.

3 Magnetic Resonance Arthrography of the Hip in Femoroacetabular Impingement: Technique and Findings Stefan Werlen MD, Michael Leunig MD†, and Reinhold Ganz MD† Operative Techniques in Orthopaedics Volume 15, Issue 3 , July 2005, pages 191–203.

4 Werlen S, Porcellini B, Ungersböck A, Magnetic resonance Imaging of the hip joint. Seminars in Arthroplasty, Vol 8, Jan 1997.

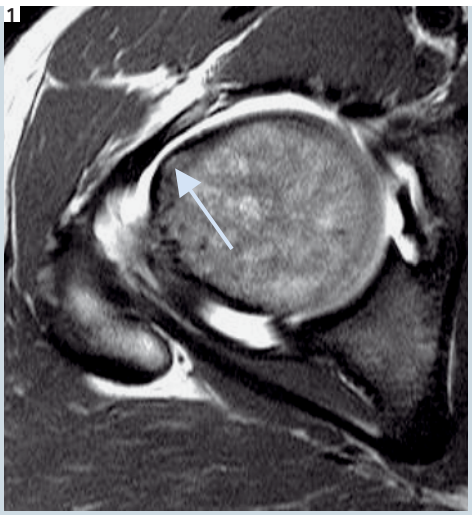

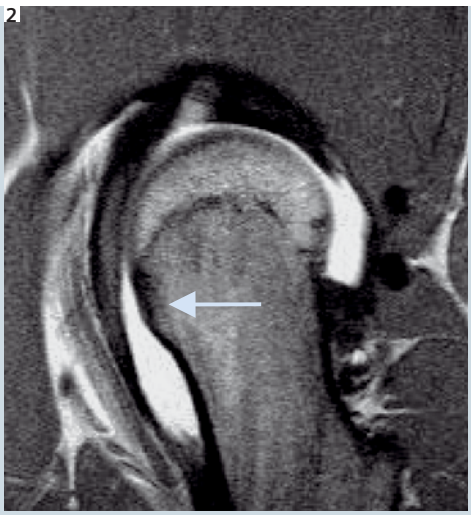

1 2 Osseus bump at the anterosuperior femoral neck, causing Cam Impingement.

3 Impingement cyst at the anterosuperior femoral neck.

4 White arrow indicating rupture of labral base.

5 Huge intra- and extracapsular labral ganglion.

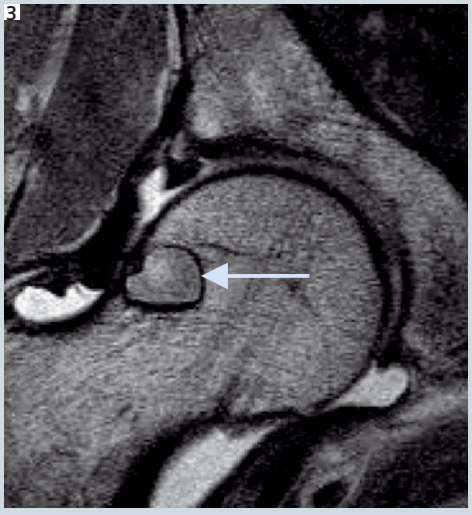

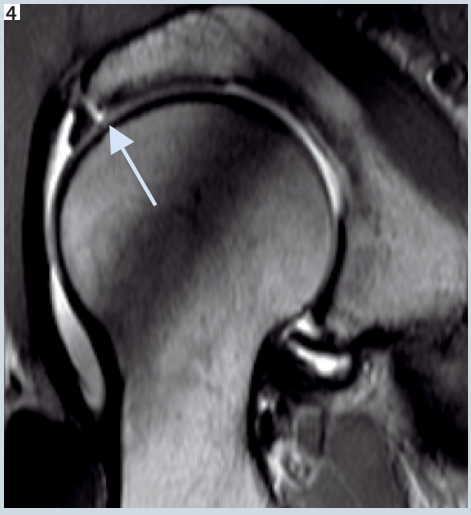

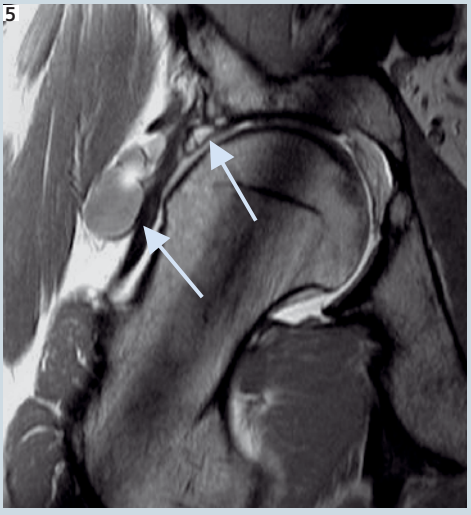

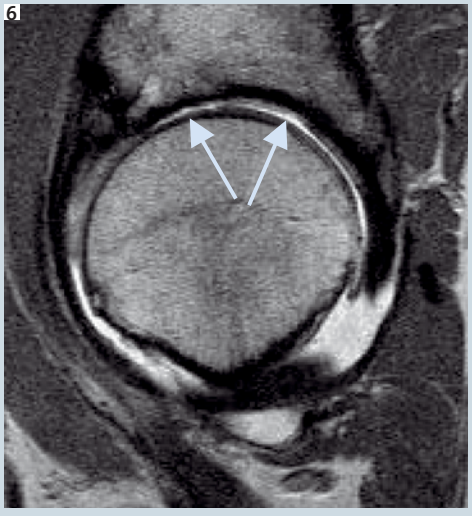

6 Focal cartilage ulcers at the acetabular joint surface.

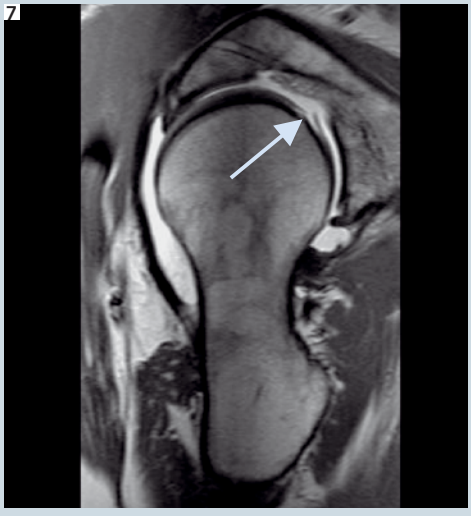

7 Cartilage rupture and flap formation at the femoral head in pincer type impingement.

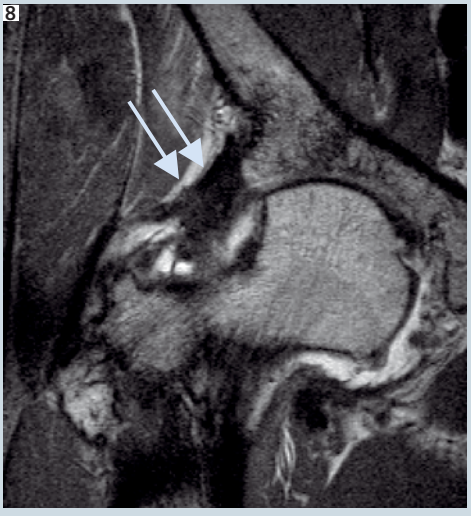

8 Extensive postoperative thickening and scarring of joint capsule.

Application Hints for MR Orthopedic Imaging: The Knee Examination

Steve Rigsby, MR Internal Education Specialist

Siemens Medical Solutions USA

Introduction

Advancements in coil technology, sequences, and optimization of the spectral fat saturation process have improved MR image quality of the knee.

Coils

Depending upon the Siemens MAGNETOM system and configuration used, there are a variety of coils available. These include both radio frequency (RF) receive (Rx) only and RF transmit (Tx) and receive coils. These two RF options offer circular polarized (CP), multiple element array and Tim Matrix coils. All of these coil options have advantages for improving image quality in knee imaging, but we will focus on the use of *syngo* GRAPPA (iPAT) and its benefits. *syngo* GRAPPA uses multi-element coils, aligned in the phase encoding direction, which combines under-sampled phase encoding data from each coil's raw data before Fourier-Transform to produce the final reconstructed image. iPAT is utilized to optimize some of the sequences being discussed in the next section. It reduces scan time without loss of image resolution which increases exam throughput.

Table 1: iPAT Compatibility Chart

Coil Name	# of Channels	Sagittal iPAT	Coronal iPAT	Transverse iPAT
CP Extremity	1	no	no	no
Tim Body Matrix	6	yes	yes	yes
8-Channel knee coil (1.5T)	8	Yes (R to L only)	Yes (R to L only)	yes
3T CP Tx/Rx	1	no	no	no
8-Channel knee coil (3T)	8	Yes (R to L only)	Yes (R to L only)	yes

Application Hint: In order to use the iPAT (integrated Parallel Acquisition Technique) option a multi-element coil must be utilized. If you only have a CP coil and want to utilize this option, the Tim Body Matrix coil is a good alternative. There are simple rules to follow if using this option: Do not overlap the coil ends as stronger bending can result in damage to the coil electronics. Do not bend the coil crosswise. Use fixation material and cushions to avoid patient motion during the examination.

Coil examples for current MAGNETOM systems:
1. CP extremity coil,
2. Tim Body Matrix coil,
3. 1.5T 8-channel Rx Coil,
4. 3T CP Tx/Rx Coil,
5. 3T 8-channel Tx/Rx coil

Sequences

Aside from the standard T1, T2, GRE and TIRM sequences, two sequences useful for orthopedic imaging are *syngo* SPACE (Sampling Perfection with Application optimized Contrasts using different flip angle Evolutions), and *syngo* BLADE. The first is a three dimensional scan allowing for very thin slice partitions. If isotropic resolution is used MPR (multi-planar reconstruction) can be performed to generate images of equal resolution in alternate image planes. The second is two-dimensional imaging but is used to compensate for patient motion and vascular flow motion related artifacts. *syngo* SPACE is a single slab 3D-TSE with variable flip angle over the echo train, using non-selective refocusing pulses, which allows for short echo spacing and ultra-high turbo factors. This sequence can be combined with an inversion recovery and restore pulses to offer T1, T2, PD, DarkFluid and Fluid contrast. Using iPAT with this sequence reduces the scan time and specific absorption rate (SAR) without loss of image resolution.
syngo BLADE is a motion insensitive multi-shot Turbo Spin Echo (TSE) se-

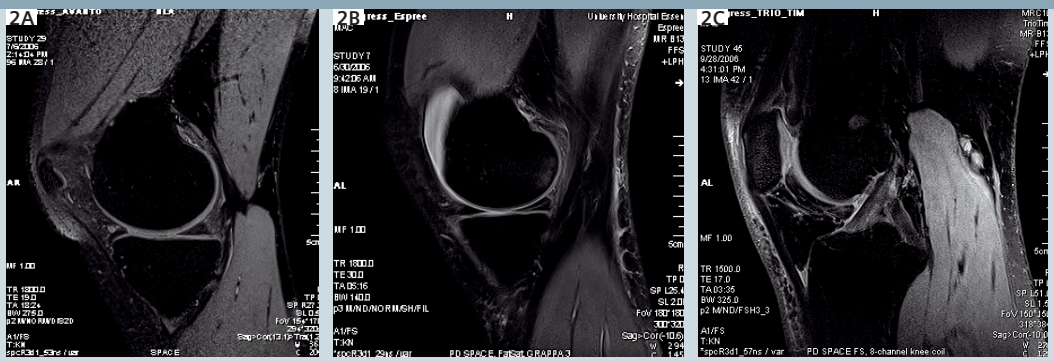

2 Examples of *syngo* SPACE (protondensity-weighted sagittal image with fat suppression) from
A: MAGNETOM Espree,
B: MAGNETOM Avanto
C: MAGNETOM Trio, A Tim System.
Each of these scans has 2 mm or less in-plane resolution.

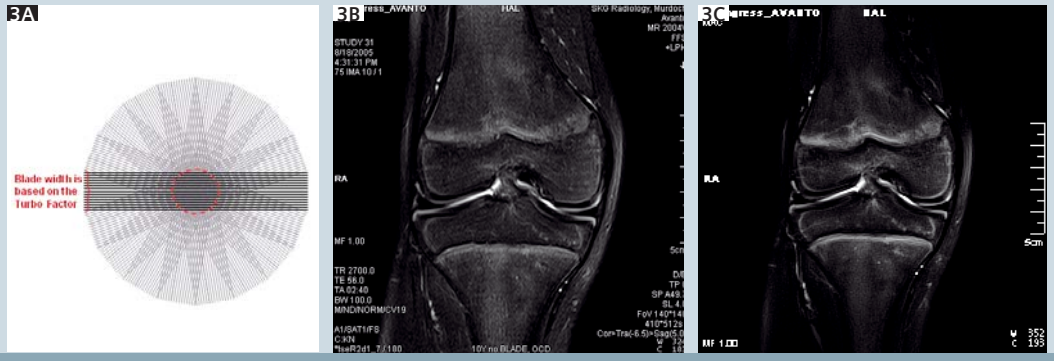

3 For *syngo* BLADE k-space is filled in a radial fashion.
B: Without motion correction.
C: With *syngo* BLADE.

quence with inter-shot motion correction for in-plane motion. K-space is filled in a radial fashion (see Fig. 3A). It can be used in any image plane. iPAT can be used to increase the accuracy of the motion correction due to broader blades, reduce SAR, and generate faster acquisitions.

Application Hint:
1. When using *syngo* BLADE with a CP or single channel coil ensure the "coil combine mode" within the protocol has the "sum of squares" option selected.
2. Since a radial filling is used with *syngo* BLADE, the phase encoding direction changes with every projection of this BLADE, and therefore wrap is a concern in the sagittal and coronal plane. To correct for this, use a slightly larger FoV as well as sat bands to minimize aliasing.

Optimization of Fat Saturation Process

When performing spectral fat saturation techniques with automatic frequency adjustments the results are not always optimal. This could be a result of the anatomy positioned far from iso-center. To correct or confirm the accuracy of the fat and water peak adjustments there is a simple pre-scan procedure to follow. On the selected protocol, choose the "confirm frequency adjustment" option on the "system>adjustment" tab. When the automatic adjustments are completed a pop-up will appear on the screen. This will give a graphic display of the water peak (default on the right) and the fat peak (default on the left).
The next step is to "float" the curser over the fat peak on the graphic display. If the number displayed in Hertz is the separation of fat from water for the field strength of the scanner, based on the chart (Table 2), the adjustment is correct. The scan can be started by selecting the continue icon. If the number displayed is not correct, for example 235 H difference on a 1.5T system, a manual adjustment of the frequency can be performed.
To perform this manual adjustment from this same graphical display, select the fat peak (left click). The system frequency will temporarily adjust to the center of the fat peak (a red line will display on the fat peak). The next step is to add the appropriate Hertz value (from chart above) to this temporary value. This will re-adjust the frequency to allow the spectral fat saturation RF pulse to suppress the fat peak. For example, based on the values seen in the graphical display above, the system frequency is 63.659134: Adding 220 H would now change the frequency to 63.659354. Select the "apply" icon and then the "continue" icon to start the scan. This process can be used for fat saturation throughout the body to improve this technique.
These application hints provided for coil selection, iPAT use, sequences and optimization of fat saturation can help to improve the knee examination image quality.

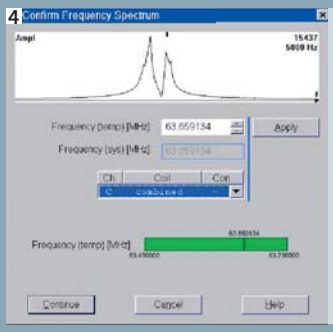

4 Graphical display of confirm frequency.

Table 2: Fat/Water separation

Field Strength	Freq. separation of fat and water
1.0T	145 H
1.5T	220 H
3.0T	440 H

Fat/water separation in Hertz per field strength.

Clinical Application of delayed Gadolinium Enhanded MRI of Cartilage (dGEMRIC)

Young-Jo Kim, M.D., Ph.D.[1]; Tallal Charles Mamisch, M.D.[2]

[1]Children's Hospital-Boston, Harvard Medical School, Boston, MA, USA
[2]University of Bern, Switzerland

Introduction

Joint preservation surgery of the hip for young patients with early osteoarthritis (OA) is increasingly recognized as an important therapeutic option. One of the underlying conditions that leads to joint injury is femoroacetabular impingement (FAI) due to decreased head-neck offset. In this condition, the aspherical femoral head causes mechanical damage to the articular cartilage, leading to pain and stiffness, and eventual osteoarthritis. Various surgical treatments exist to successfully treat the underlying bony abnormality of this condition. However, in all cases, the ultimate outcome is highly dependent on the amount of pre-existing articular cartilage damage [1].
Advances in MRI techniques for cartilage imaging have occurred in recent years. Hip imaging is particularly demanding because of the spherical nature of joint, deep anatomical position and the thin articular cartilage. However, advances in coil design and incorporation of parallel imaging has allowed practical application of not only high-resolution morphologic imaging but also some of the newer biochemical imaging techniques for early osteoarthritis.
Due to the importance of the extent of

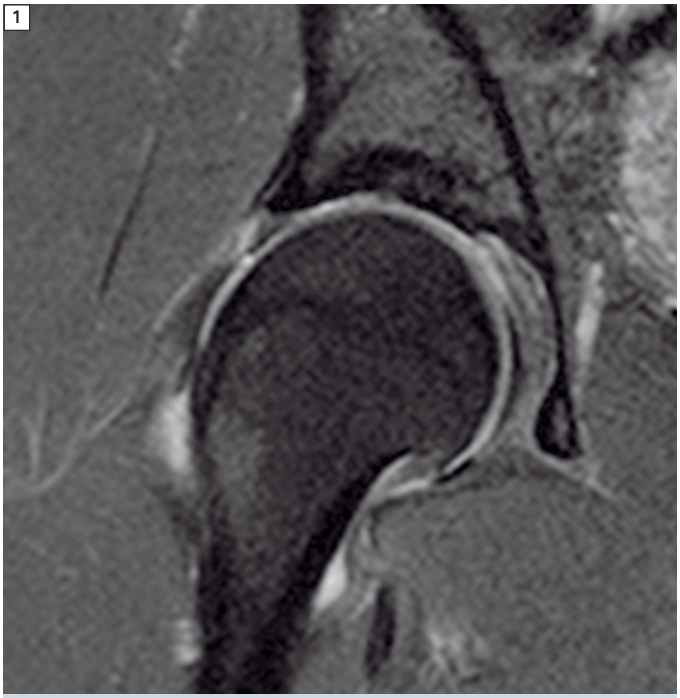

1 Clinical example of the routinely used T1-weighted 2D coronal Turbo Spin Echo acquisition; images were acquired with the standard surface coil. Resulting voxel size is 0.3 x 0.3 x 3.0 mm³.

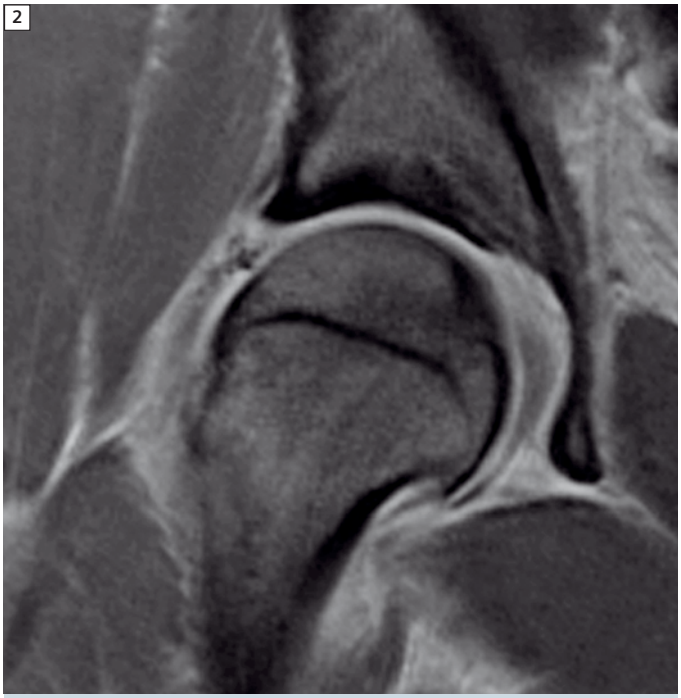

2 In this figure, the corresponding image to figure 1 of one of the two corresponding T1-weighted VIBE measurements is shown; this sequence is used for the dual flip angle fast T1 mapping. Resulting voxel size is 0.6 x 0.6 x 4.0 mm³.

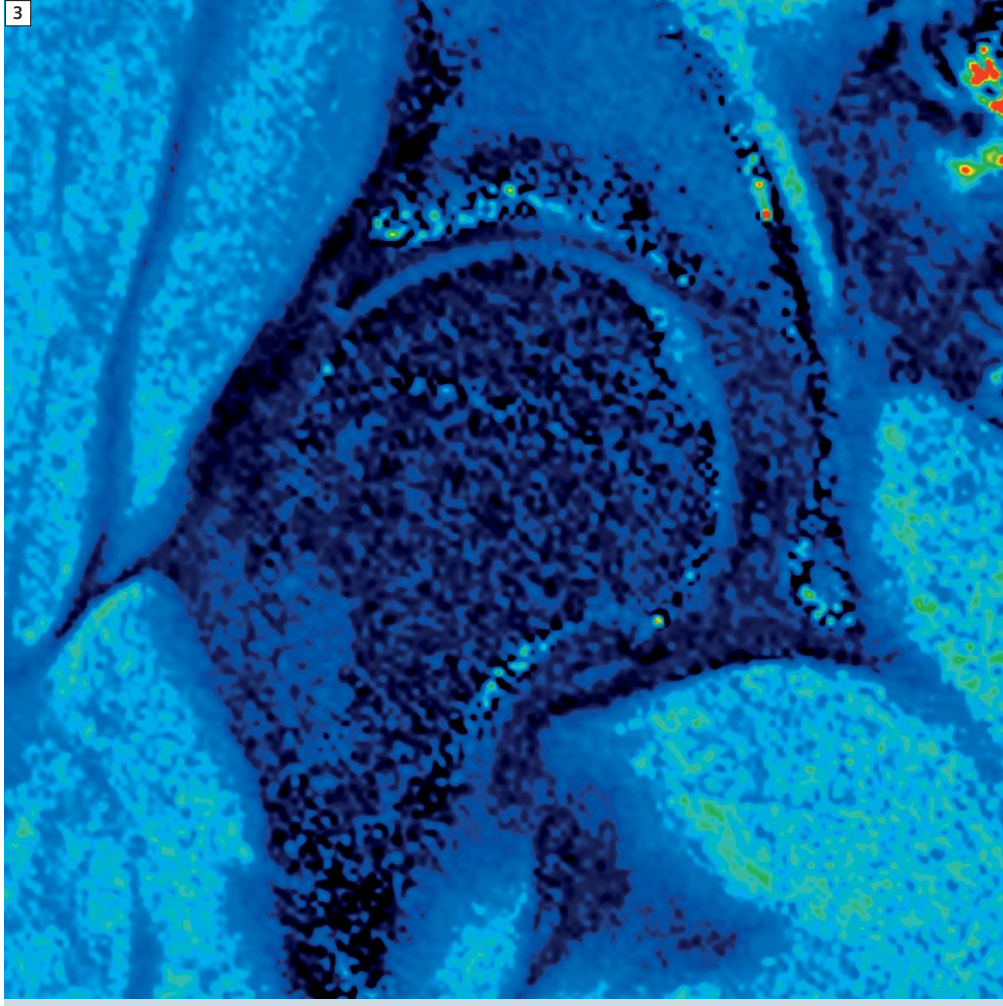

3 The resulting T1 map for the dGEMRIC imaging is shown in this figure. This map is calculated Inline using *syngo* Mapit. The blue color code shows different T1-times (the darker blue the color, the shorter the T1-time). The cartilage is well delineated and structural changes can be easily obviated or visualized.

the pre-existing articular cartilage damage in our clinical outcome after joint preserving procedures, we have incorporated the delayed Gadolinium Enhanced MRI of Cartilage (dGEMRIC) technique [2, 3] into our routine clinical imaging protocol. We have previously shown that dGEMRIC technique for the hip correlates with clinical symptoms [4] and is the best predictor of outcome after joint preservation surgery [5]. This technique takes advantage of the fact that in early OA, the negatively charged extracellular matrix is lost [6]. Using the dGEMRIC technique, the charge density is measured by the change in T1 relaxation times of the articular cartilage after penetration of gadopentetate-DTPA(2-) into the tissue. Intravenous injection of gadolinium allows the most rapid penetration of contrast agent into the articular cartilage due to penetration both from the synovial fluid as well as the subchondral bone. The patient needs to move the joint after injection and the dGEMRIC imaging needs to occur within a 30–100 minute time window after injection for a reliable biochemical assessment of the articular cartilage [7, 8].

Clinical imaging protocol

In our current clinical routine scan, we use a 1.5T Siemens MAGNETOM Avanto scanner with a surface coil for hip imaging. The patients are injected with Gadopentetate dimeglumine (Magnevist; Berlex Laboratories, Wayne, NJ). They are then asked to walk for 15 minutes. The imaging is started 30 min after contrast injection and the imaging protocol includes sequences for morphologic and biochemical imaging. The intra-venous gadolinium injection provides an indirect arthrogram and is much better tolerated by the patients than a direct injection arthography, which in many centers is the standard. Our imaging protocol consists of the following sequences:

1) coronal and sagittal oblique Turbo Spin Echo (TSE) acquisition with fat saturation (Fig 1.) (TR 530 msec, TE 11 msec, FOV 160 mm, matrix 512 x 512, slice thickness 3 mm),
2) 3D isotropic TrueFISP acquisition with water excitation (TR 12.6 msec, TE 5.5 msec, flip angle 30, FOV 160 mm, matrix 256 x 256 x 256, 0.63 mm voxel size),
3) Dual flip angle fast T1 mapping using two VIBE acquisitions for dGEMRIC imaging (Fig 2.), (TR 20 msec, TE 4.8 msec, flip angle 4.8/26.9, FOV 160 mm, matrix 256 x 256, slice thickness 4 mm).

The total scan time for this protocol is under 30 minutes and the *syngo* MapIt software performs the Inline T1 map calculations for the dGEMRIC imaging obviating the need for post-processing of imaging data (Fig. 3). Additionally, the 3D isotropic TrueFISP imaging data set is reconstructed in a rotating imaging plane around the femoral neck axis for accurate femoral head-neck junction and articular cartilage and labral characterization.

In order to obtain an accurate and reliable dGEMRIC imaging, the need for the patient to move the joint and delay the imaging for the appropriate amount of time is critical since the imaging technique relies on penetration of the contrast agent into the articular cartilage. Additionally, it is the anionic form of gadolinium that provides specificity to the imaging technique, hence, care must be taken to use the appropriate contrast agent. The dual flip angle fast T1 mapping technique with Inline map calculation makes this technique practical by decreasing the imaging time to practical levels and eliminating the

need for post-processing of the imaging data. The dual flip angle technique has been validated against the traditional inversion recovery technique. With this gradient echo based technique, it is important to center the hip in the middle of the imaging matrix since the T1 mapping data is inaccurate at the periphery of the imaging matrix. Additionally, the choice of flip angles are critical for this fast T1 mapping technique since the range of T1 in which this technique will be accurate is limited [9].

Clinical case example

The utility of this technique is illustrated in this case of a 19-year-old college hockey player suffering severe right hip pain that initially limited her playing. Eventually, the pain increased to the point where even every day activity became limited. The plain radiographs show intact joint space with no obvious evidence of osteoarthritis (Fig. 4). The lateral radiograph shows the prominence in the anterior head-neck junction consistent with a Cam type femoro-acetabular impingement (Fig. 5). The surgical treatment options range from a limited anterior open arthrotomy and osteochondroplasty to a full surgical dislocation with trimming of the damaged acetabular rim and femoral head-neck junction osteochondroplasty. Advanced imaging is critical in proper patient selection for each surgical technique as well as predicting the prognosis of this patient after surgery.

The standard morphologic imaging shows some heterogeneity in the acetabular articular cartilage (Fig. 6 A). The femoral head cartilage appeared intact and the labrum appeared intact. However, on the dGEMRIC scan, the entire acetabular cartilage showed markedly lower T1 values, demonstrating increased enhancement of the extracellular matrix by the gadopentetate-DTPA(2-), suggesting lower inherent negative charge in the matrix and hence significant articular cartilage damage in the acetabulum (Fig. 6 B). Based on this information, the patient was scheduled for an open surgical dislocation and osteoplasty rather than the more limited surgery. At time of surgery, the extent of articular cartilage damage in the acetabulum is verified (Fig. 6 C). The addition of the dGEMRIC imaging technique to our clinical hip imaging protocol allows us to improve patient selection and therefore improve the ultimate outcome of our surgical procedure. It also allows us to avoid unnecessary surgery with improved staging of the articular cartilage damage at time of initial assessment. Additionally, the indirect arthrogram is much better tolerated by the patients than a direct injection arthography and the imaging technique is sufficiently fast and easy to use to allow the full complement of diagnostic imaging sequences to run within a 30 min scan time as part of a routine clinical imaging protocol.

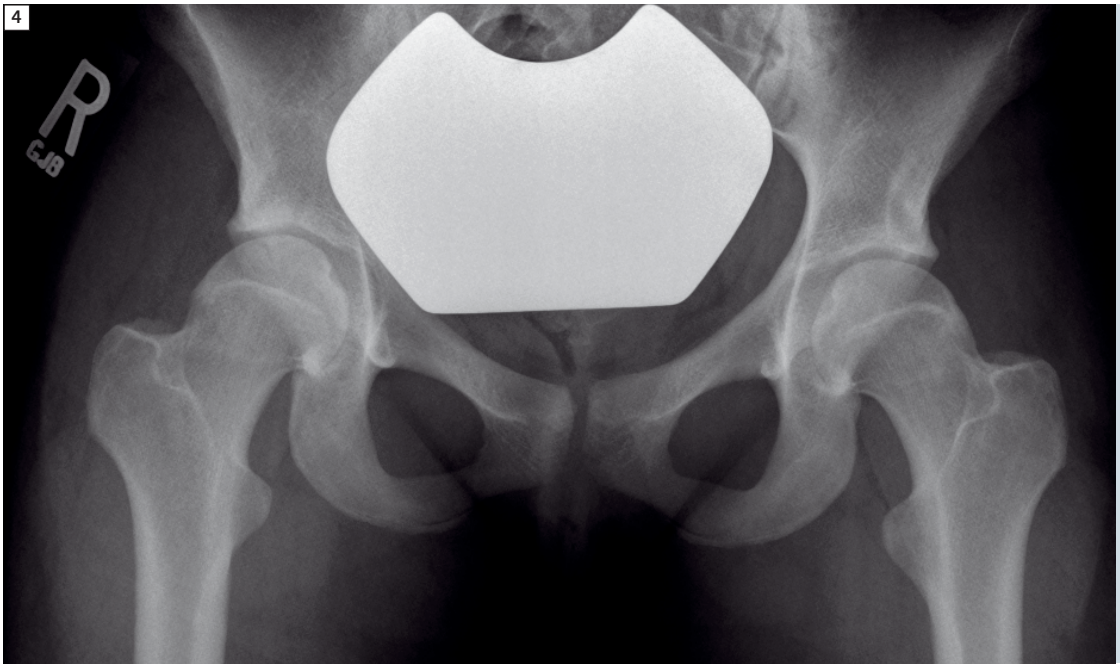

4 Pelvic radiograph of a 19-year-old woman with right hip pain. Minimal radiograph evidence of osteoarthritis is present. Some asphericity of femoral head suggesting possible impingement.

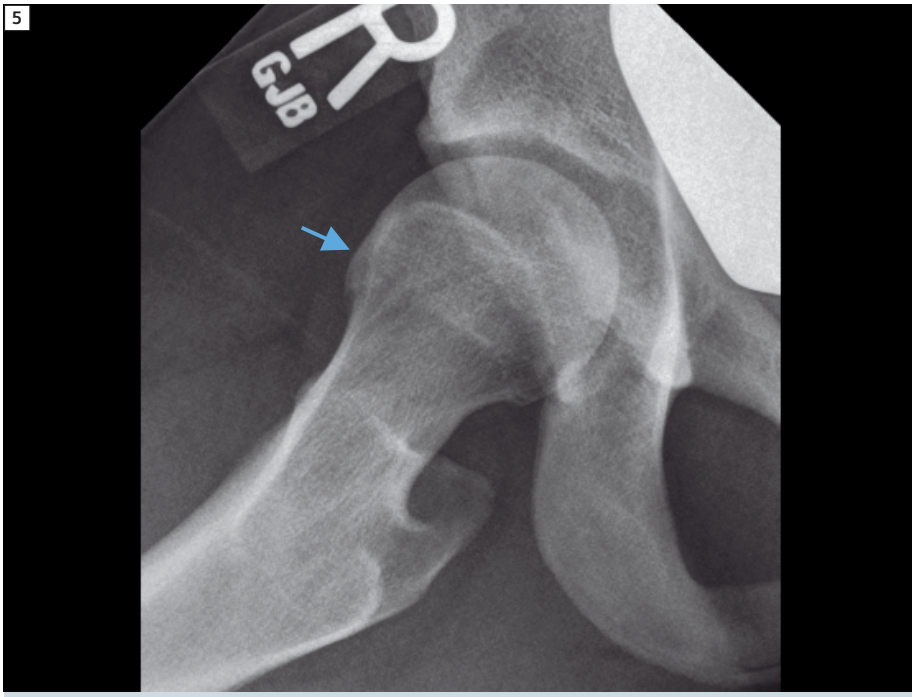

5 Lateral radiograph of the right hip shows a prominence in the anterior head-neck junction which could lead to Cam type femoroacetabular impingement.

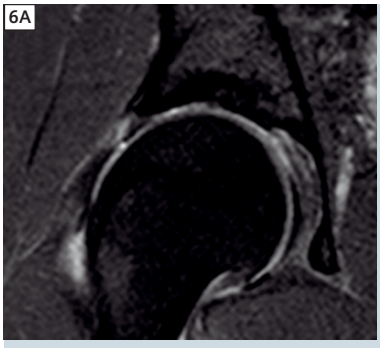

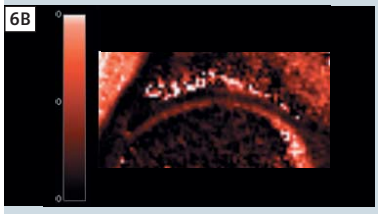

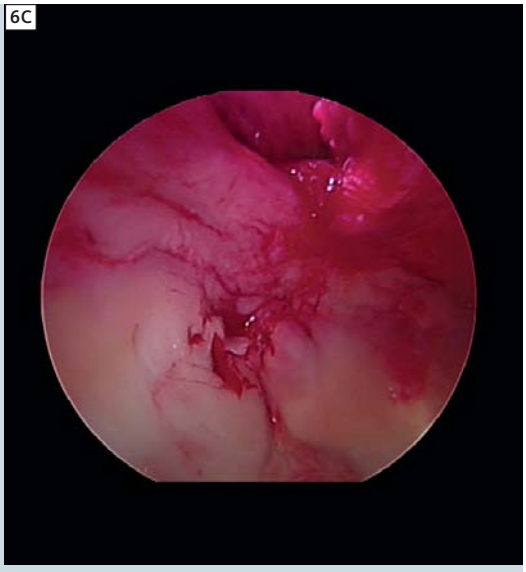

6A Coronal TSE image shows some focal signal change in the acetabular articular cartilage. **6B** The corresponding section on the dGEMRIC scan shows extensive articular cartilage change in the acetabular side but the femoral head cartilage appears intact. The lower T1 values (dark red and black areas) on the dGEMRIC scan corresponds to more cartilage degeneration. **6C** The intraoperative view shows intact labrum but deep fissuring of the acetabular articular cartilage.

References

1 Kim, Y.J., et al., Hip joint-preserving surgery: beyond the classic osteotomy. Instr Course Lect, 2006. 55: p. 145–58.
2 Bashir, A., et al., Glycosaminoglycan in articular cartilage: in vivo assessment with delayed Gd(DTPA)(2-)-enhanced MR imaging. Radiology, 1997. 205(2): p. 551–558.
3 Bashir, A., et al., Nondestructive imaging of human cartilage glycosaminoglycan concentration by MRI. Magn Reson Med, 1999. 41(5): p. 857–65.
4 Kim, Y.J., et al., Assessment of early osteoarthritis in hip dysplasia with delayed gadolinium-enhanced magnetic resonance imaging of cartilage. J Bone Joint Surg Am, 2003. 85–A(10): p. 1987–92.
5 Cunningham, T., et al., Delayed gadolinium-enhanced magnetic resonance imaging of cartilage to predict early failure of Bernese periacetabular osteotomy for hip dysplasia. J Bone Joint Surg Am, 2006. 88(7): p. 1540–8.
6 Venn, M. and A. Maroudas, Chemical composition and swelling of normal and osteoarthrotic femoral head cartilage. I. Chemical composition. Ann Rheum Dis, 1977. 36(2): p. 121–9.
7 Burstein, D., et al., Protocol issues for delayed Gd(DTPA)(2-)-enhanced MRI (dGEMRIC) for clinical evaluation of articular cartilage. Magn Reson Med, 2001. 45(1): p. 36–41.
8 Tiderius, C.J., et al., Hip dGEMRIC in asymptomatic volunteers and patients with early osteoarthritis: the influence of timing after contrast injection. Magn Reson Med, 2007. 57(4): p. 803–5.
9 Mamisch, T., et al., Comparison of delayed Gadolinium Enhanced MRI of Cartilage (dGEMRIC) using Inversion Recovery and Fast T1 Mapping Sequences. Mag Res Med, 2008. in press.

Contact
Young-Jo Kim, M.D., Ph.D.
Children's Hospital-Boston
300 Longwood Avenue
Boston, MA 02115
USA
young-jo.kim@childrens.harvard.edu

Case Report: Magnet Resonance Imaging in Inflammatory Arthritis

Marius Horger, M.D.

University Hospital Tübingen, Dept. of Diagnostic and Interventional Radiology, Tuebingen, Germany

Introduction

Magnetic Resonance Imaging (MRI) has advanced to the most accurate imaging modality in the diagnosis and response monitoring of inflammatory arthritis. Unlike conventional X-ray technique, MRI delivers information concerning both morphologic changes of the involved joint and pathophysiologic data with respect to the degree of synovial membrane and/or bone and juxta-articular inflammation. Furthermore, the excellent resolution and the high tissue contrast enable not only assessment of inflammatory activity, but also differentiation between the different types of arthritis disorders.

Hence, this short case series should help understand some of the most important benefits of the use of MRI. Early detection of inflammatory activity and onset of bone destruction, irrespective of the underlying arthritis type, remain major goals in the diagnosis. Established technologies (e.g. dynamic contrast enhanced MRI) and newer technologies (e.g. *syngo* ASL Arterial Spin Labeling) make even quantification of inflammation-related synovial perfusion practicable in the routine diagnosis. The latter delivers this information even without the use of intravenous contrast. Finally, MRI also helps to better understand the pathomechanisms responsible for disease progression.

Sequence details

The MR imaging protocol consisted of the following:

Axial T1-weighted 2D spin-echo sequence: Repetition time (TR) 863 ms; echo time (TE) 12 ms; slice thickness (SL) 2 mm; bandwidth (BW) 195 Hz/px; matrix 320 x 204; in-plane resolution (IPR) 0.4 x 0.3 mm; averages (AVR), 2; acquisition time (TA) 4:10 min, coronal T1-weighted 2D spin-echo sequence (TR, 570 ms; TE, 12 ms; SL, 1.5 mm; BW, 195Hz/px; matrix, 320x232; IPR, 0.4 x 0.3 mm; AVR, 2; TA, 5:11 min.)

Coronal T2-weighted 2D fast spin-echo sequence with spectral fat-saturation: TR 7210 ms; TE 81 ms; echo train length (ETL) 15; SL 1.5 mm; BW, 180 Hz/px; matrix 320 x 320; IPR 0.4 x 0.3 mm; AVR 4; TA 5:58 min.

3D DESS (dual-echo steady state): TR 21.6 ms; TE 6.8 ms; ETL 15; BW 180 Hz/px; matrix 256 x 256; resolution 0.6 x 0.6 x 0.6 mm; AVR 2; TA 7:12 min.

3D FLASH (fast low angle shot), a spoiled gradient-echo sequence with spectral fat saturation for dynamic MR imaging: TR 3.95 ms; TE 1.45 ms; resolution 0.6 x 0.6 x 0.8 mm; BW 350 Hz/px; 32 slices per slab; slice partial Fourier 6/8; flip angle 20°; IPR 0.4 x 0.3 mm; AVR 2; TA 13 s.

Axial T1-weighted spin-echo sequence with spectral fat saturation for post-contrast imaging: TR 798 ms; TE 12 ms; SL 1.5 mm; no gap; BW 195 Hz/px; matrix 320 x 2042; IPR 0.7 x 0.6 mm; AVR 2; TA 5:31min.

Case 1
Late rheumatoid arthritis (RA)

Patient history

A 48-year-old female patient with known rheumatoid arthritis presented with progressive swelling of the metacarpophalangeal joints. The patient was known to be incompliant and indolent and had discontinued therapy one year ago. On conventional radiographs of the hands (not shown), newly occurred intraosseous cysts were diagnosed, additionally to the typical erosions in the bare area of the metacarpal bones.

Image findings

High-resolution MRI of both hands using a dedicated hand coil and a 3T magnetic field (Siemens MAGNETOM Trio) revealed typical signs of elevated intraarticular pressure due to overproduction of joint effusion by the inflamed synovia. Due to the excellent image resolution (in plane resolution, 0.3 x 0.4 mm) and contrast and the use of a thin slice protocol (1.5 mm), interruption of cortical bone (arrow) along the metacarpal heads is well depicted on axial fat-saturated T1-weighted post-gadolinium image, demonstrating continuity of the joint cavity with the intraosseous cysts (Fig. 1A). Note enhancement of both articular synovia and metacarpal cystic

lesion representing extension of articular active pannus into the bony canal. There is only a small amount of effusion in the joint space and in the adjacent involved metacarpal bones II and III. Note also tenosynovitis of the flexor tendon sheaths.

In the other hand, coronal fat-saturated T2-weighted image (Fig. 1B) and coronal DESS image (Fig. 1C) both show the pathways of arousal of intraosseous cysts at sites where the cortical bone has become permeative. Note volar distension of articular synovial membrane in the interphalangeal joint of the 1st finger denoting overpressure and the accompanying intraosseous cysts (arrows). On the fat-saturated T2-weighted image, differentiation of articular fluid from

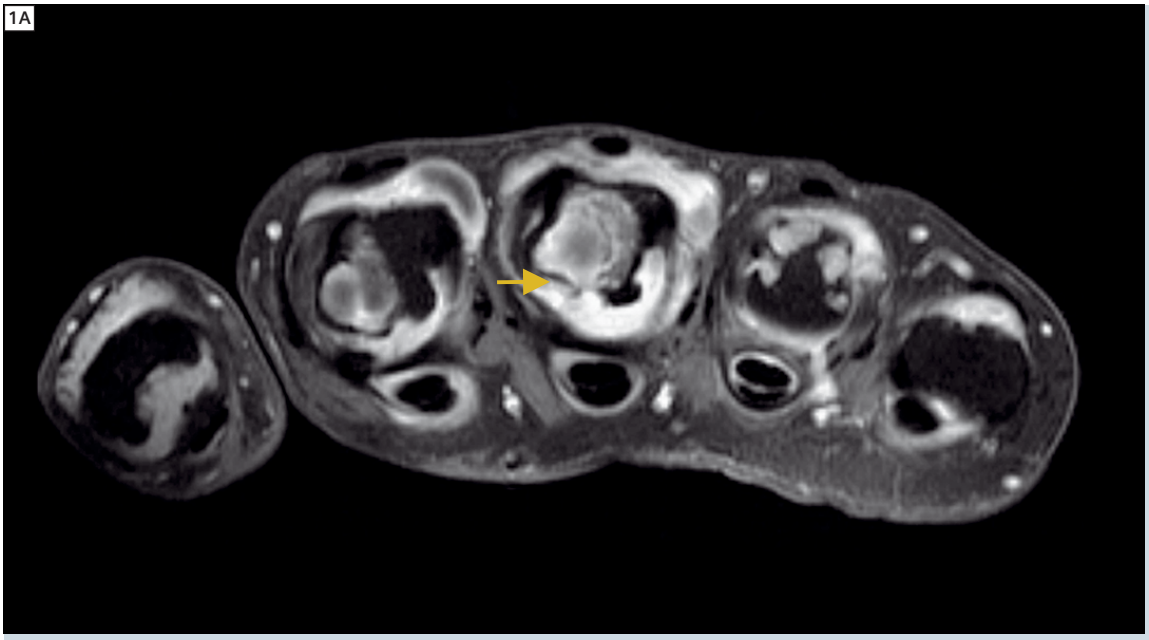

1A Axial fat-saturated T1-weighted post-gadolinium image, demonstrating continuity of the joint cavity with the intraosseous cysts.

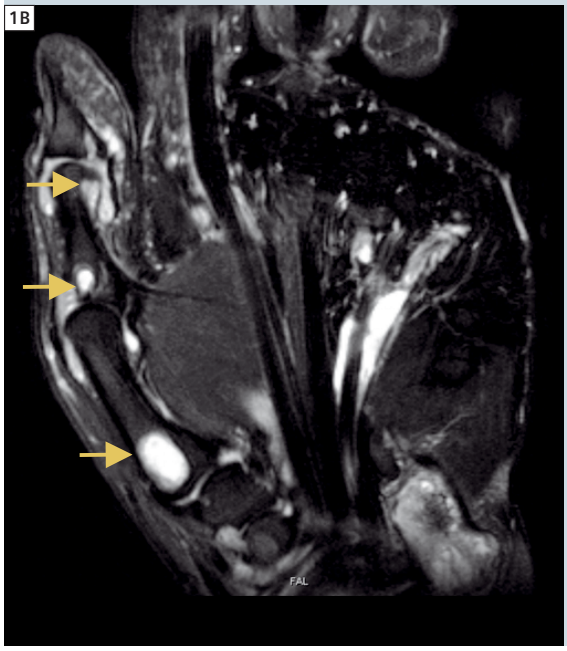

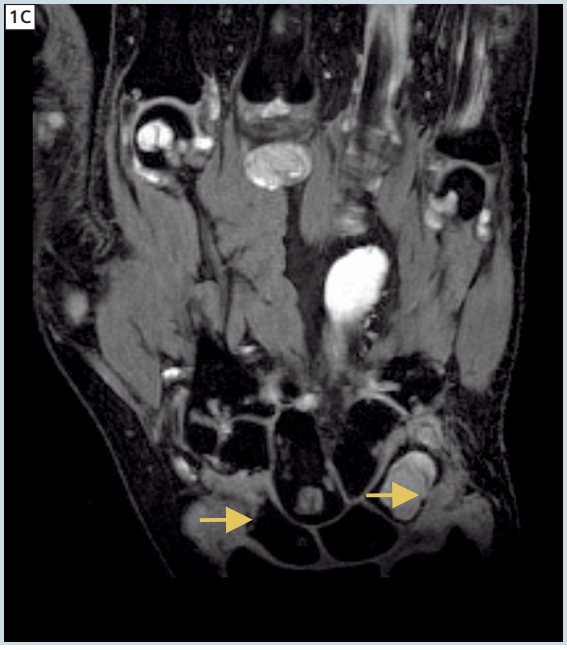

1B, C **B:** Contralateral hand to Fig. 1A, coronal fat-saturated T2-weighted image **C:** Contralateral hand to Fig. 1A, coronal DESS image.

active pannus is not possible. However, on the coronal DESS image synovial proliferation shows lower signal compared to intraarticular effusion. Fig. 1D shows extra-synovial inflammation on the dorsal side of the hand over the metacarpophalangeal joints. Note distension of articular capsule with disruption and formation of fistula (arrow, Fig. 1D) and pseudocyst, (Fig. 1E) both known decompression forms of inflamed joints occurring especially in untreated patients. Due to the high resolution synovial thickening can be delineated excellently also on the non-enhanced T1-weighted image (Fig. 1F).

Case 2
Psoriatic arthritis (PsA)

Patient history

A 64-year-old male patient with known psoriatic arthritis (PsA) presented with progressive exercise-induced joint pain and swelling involving all hand joints, despite ongoing immunosuppressive therapy.

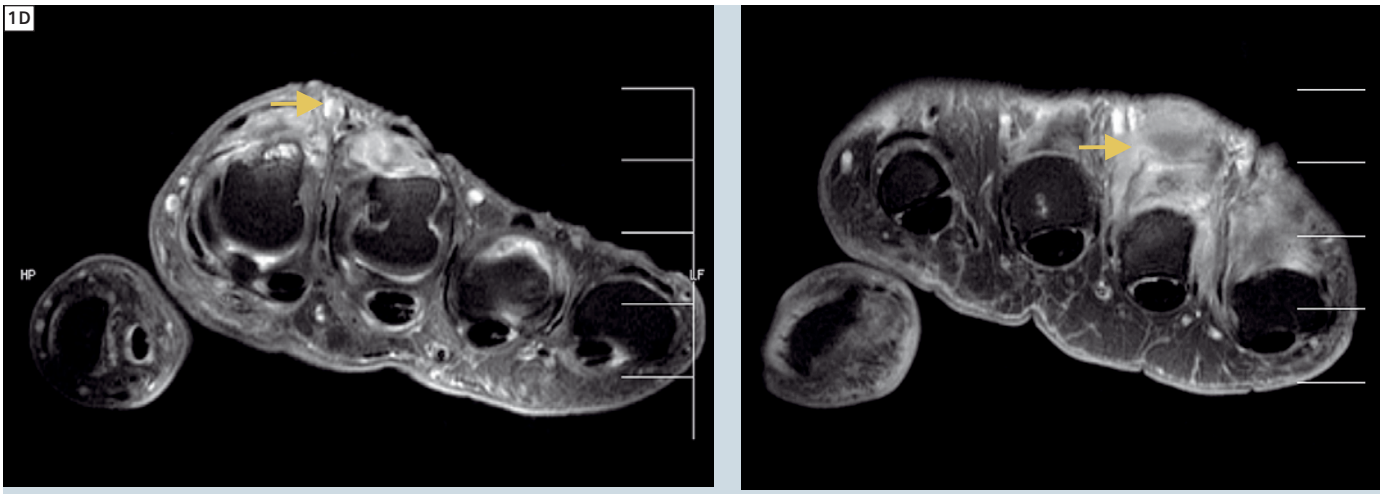

1D, E Axial fat-saturated T1-weighted post-gadolinium image, demonstrating extra-synovial inflammation.

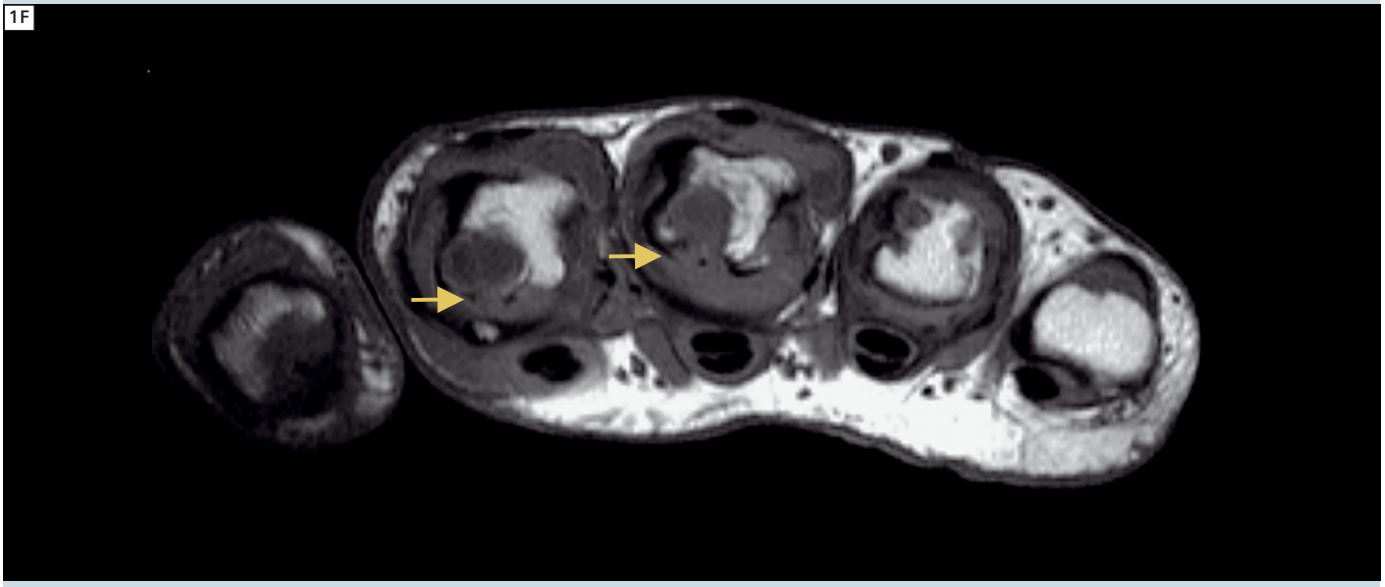

1F Axial non-enhanced T1-weighted image; synovial thickening can be delineated excellently due to the high resolution.

Image findings

On conventional radiographs of the hands (Fig. 2A), juxta-articular osteopenia, joint space narrowing with osteophyte formation (bony proliferation) was diagnosed in the wrist joint, intercarpal joint as well as to a lesser degree also in all other hand joints. Fusiforme swelling of the fingers was also noticed presumed to represent polydactylia.
High-resolution MRI of both hands using a dedicated hand coil and a 3T magnetic field (Siemens MAGNETOM Trio) revealed severe erosions in all joints, particularly in the wrist and the metacarpophalangeal joints (Fig. 2B). Note also tendon tear on the radial side of the wrist joint (arrow). Fig. 2C shows strong inflammation and thickening of the flexor tendon sheaths along the metacarpal bones. Note destruction of the Vth metacarpal head which differs in its morphology from the classical erosion by rheumatoid arthritis. The latter lacks new bone formation and is mainly localized at the so-called bare area. At the level of the wrist, the destructive character of this inflammatory arthritis becomes more evident. Note also the strong synovial hypertrophy of both extensor and flexor tendon sheaths (Fig. 2D).

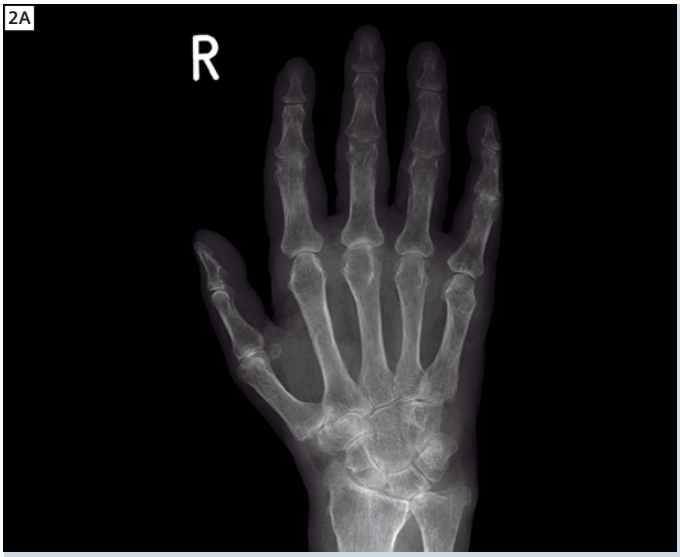

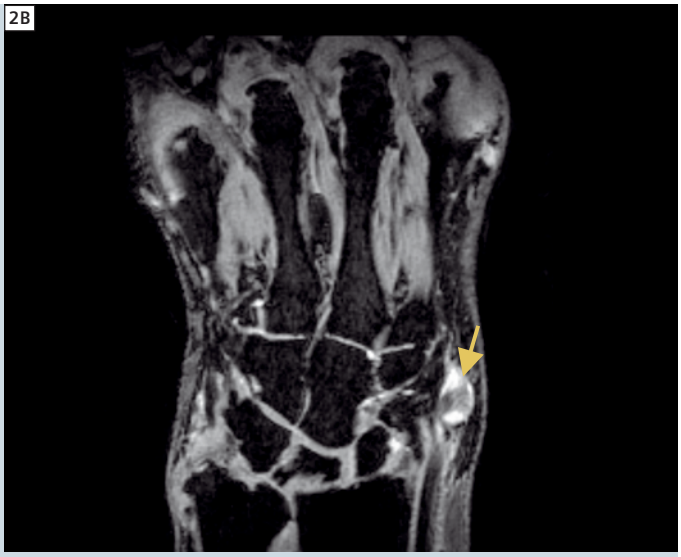

2A, B **A:** Conventional radiograph of the hand; juxta-articular osteopenia and joint space narrowing with osteophyte formation (bony proliferation) and fusiforme swelling of the fingers are present. **B:** Coronal DESS image visualizing severe erosion in all joints.

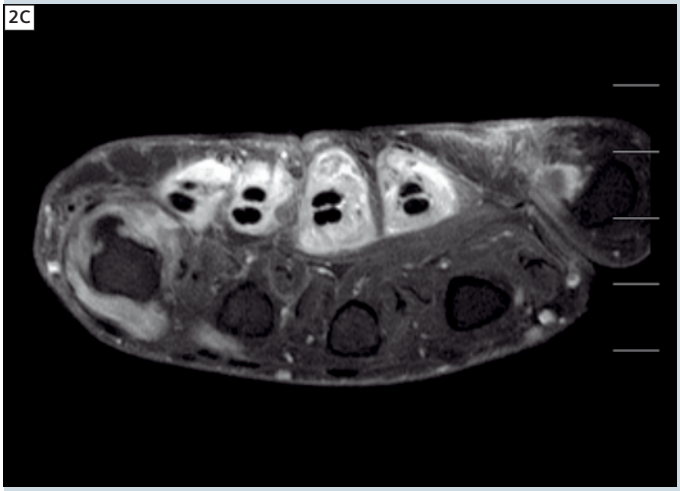

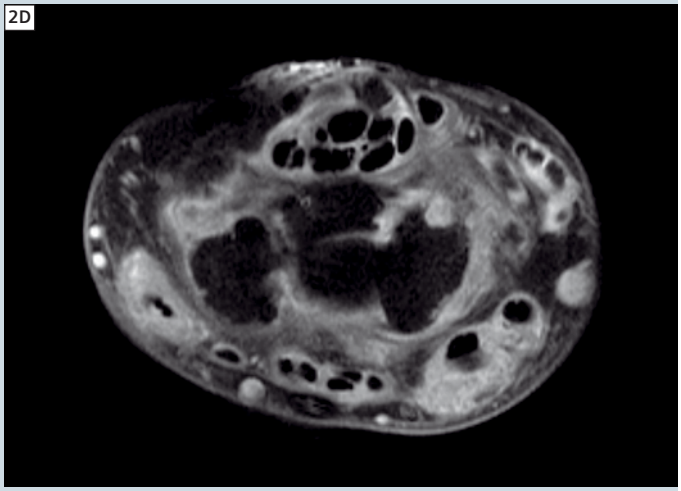

2C, D Axial fat-saturated T1-weighted post-gadolinium images.

Case 3
Systemic lupus erythematodes (SLE)-induced arthritis

This case compiles images of three different patients suffering from systemic lupus erythematodes (SLE) and complaining about joint pain. In the 1st patient, conventional X-ray of the hand did not disclose any pathologic findings (Fig. 3A). Axial fat-saturated T1-weighted post-gadolinium image however, shows strong synovial thickening and enhancement involving all joints, but in particular the metacarpophalangeal (MCP) joints (Fig. 3B). Note also extrasynovial extension of inflammation and accompanying tenosynovitis. The latter represents a frequent image finding in SLE-patients. There is no erosion at the level of MCP joints. At the 3rd metacarpal head, partial average volume simulated the presence of a prelesion which was not confirmed in the coronal plane.

In the second patient, a child* with SLE-associated arthritis, coronal DESS image demonstrates incomplete ossification of the carpal bones and open growth plates of the long bones (Fig. 3C). There is also small erosion in the capitate bone which represents an unusual finding for SLE-arthritis.
Nevertheless, axial fat-saturated post-gadolinium image at the level of the basis of the MCP demonstrates further erosions (arrow) and also strong enhancement in the thickened synovial membrane (Fig. 3D).
In the third patient with SLE, focal erosion of the 3rd metacarpal head (arrow) is nicely depicted on axial non-enhanced T1-weighted image (Fig. 3E). There is also thickening of the articular synovia. However, it is only the use of intravenous contrast material that allows appreciation of inflammatory activity of such findings. On the corresponding axial fat-saturated post-gadolinium image, mild enhancement is seen in the synovial membrane of the 3rd and 4th MCP, but none in the intraosseous pannus of the 2nd MCP (Fig. 3F). This finding is compatible with inactive pannus.

*The safety of imaging fetuses / infants has not been established.

Contact
Prof. Dr. Marius Horger
Department of Radiology
University Hospital of Tuebingen,
Hoppe-Seyler-Straße 6
72076 Tuebingen
Germany
marius.horger@med.uni-tuebingen.de

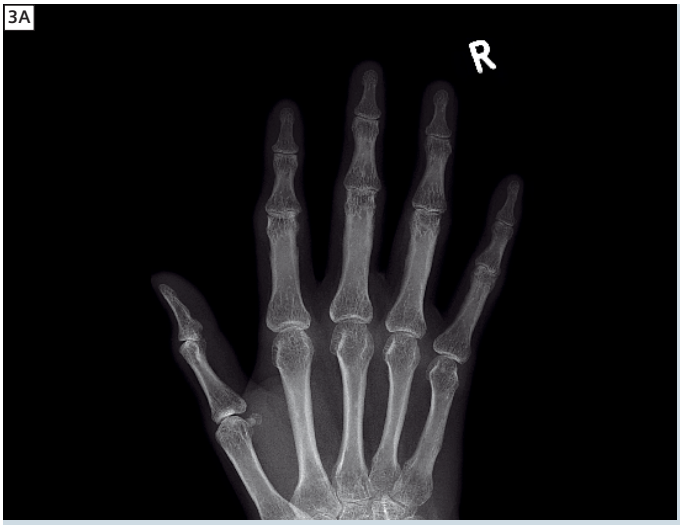

3A Conventional radiograph of the hand; no pathologic findings are disclosed.

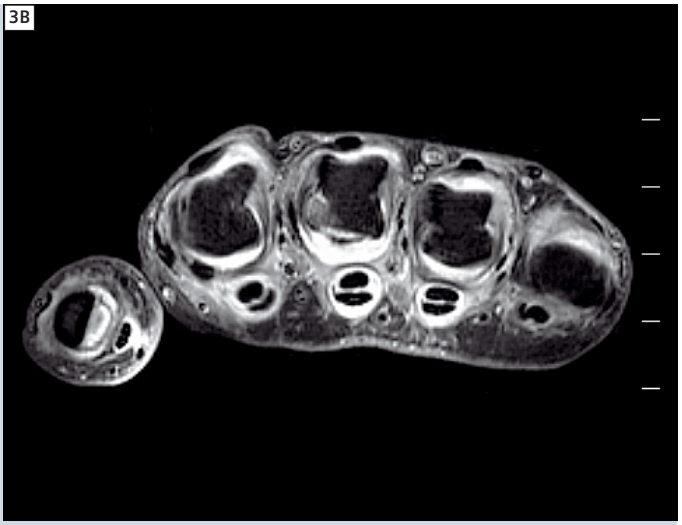

3B Axial fat-saturated T1-weighted post-gadolinium image; strong synovial thickening and enhancement involving of all joints are present.

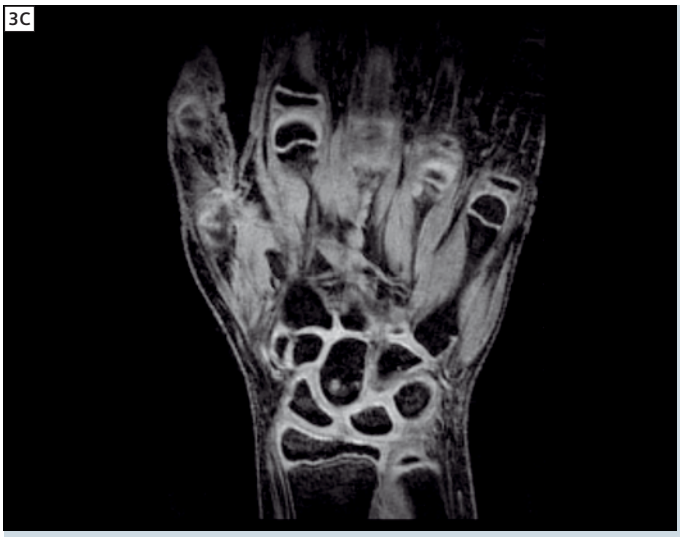

3C Coronal DESS image showing incomplete ossification of the carpal bones and open growth plates of the long bones.

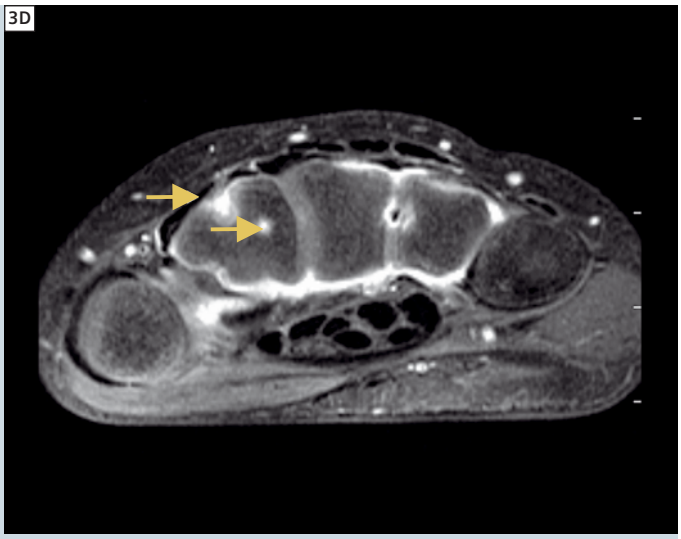

3D Axial fat-saturated T1-weighted post-gadolinium image showing erosions and also strong enhancement in the thickened synovial membrane.

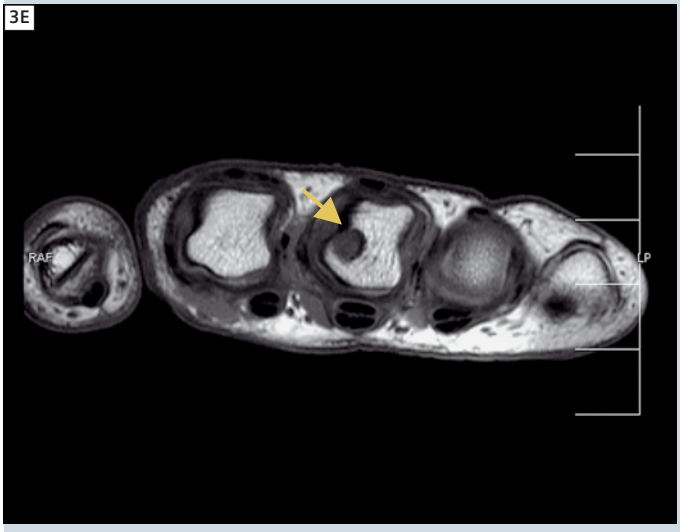

3E Axial non-enhanced T1-weighted image; a focal erosion of the 3rd metacarpal head is delineated in detail.

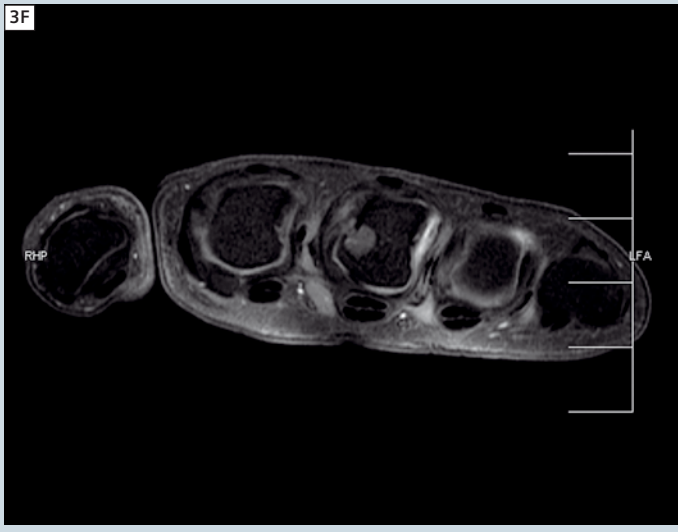

3F Axial fat-saturated T1-weighted post-gadolinium image.

The Composer

Sandra Winsor

Centre for Advanced MRI, University of Auckland, New Zealand

The composing software is an image stitching program similar to stitching scenic photographs into a panoramic picture. The difference with the composer is that it stitches the image in the vertical direction. The reason we do this is that our MR systems have a maximum field-of-view (FOV) of 35–50 cm. The human anatomy is often larger than this, and by composing the images we can achieve an effective FOV of up to 205 cm. The software is able to compose multiple slices for example; eleven sagittal slices from the upper and lower spine can be composed to create a composite image of eleven sagittal slices of the whole spine. Multiple data sets can be composed to create whole body images (Fig. 1A and B), or simply two regions for a smaller area of interest (Fig. 1C). Whilst most radiologists are used to and prefer the original smaller data sets to report from, clinicians and patients benefit from the composed images by having a better perspective of lesions and their location in relation to the rest of the body. The simplest and most useful function of the composing software is composing localiser scans especially with the use of the Inline Composing. Workflow is optimised by scout images being automatically composed and loaded into the exam card for subsequent planning of images.

Most parts of the anatomy can be composed using the spine algorithm, which is based on bone structure but not limited to just the spine. Similarly, vascular studies can be composed using the angio algorithm.

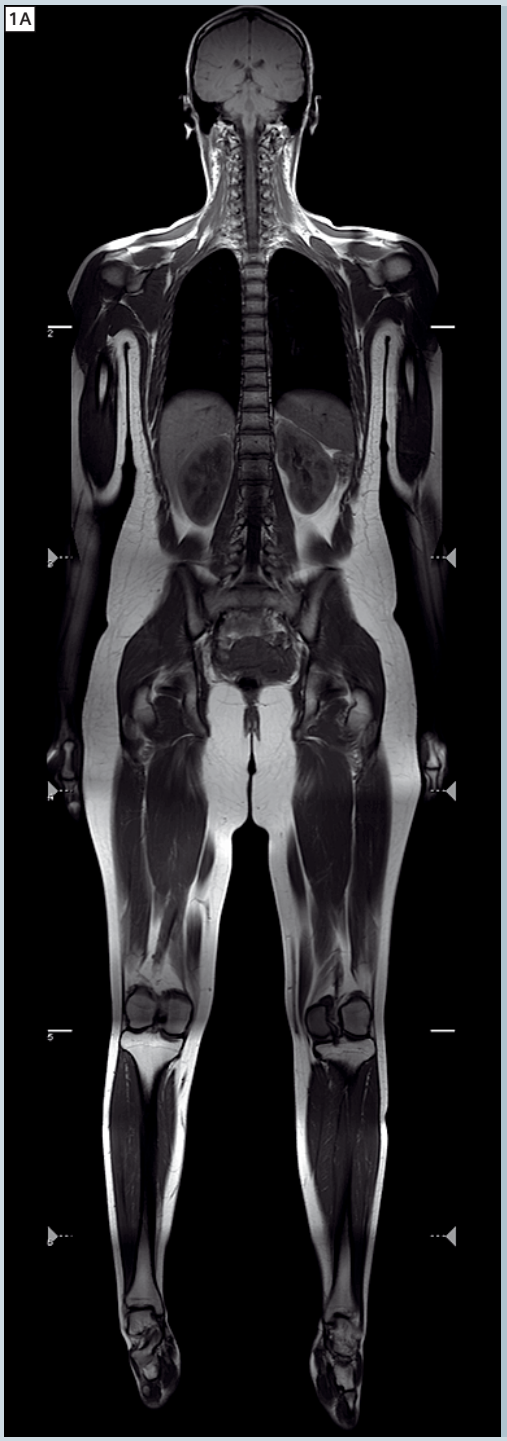

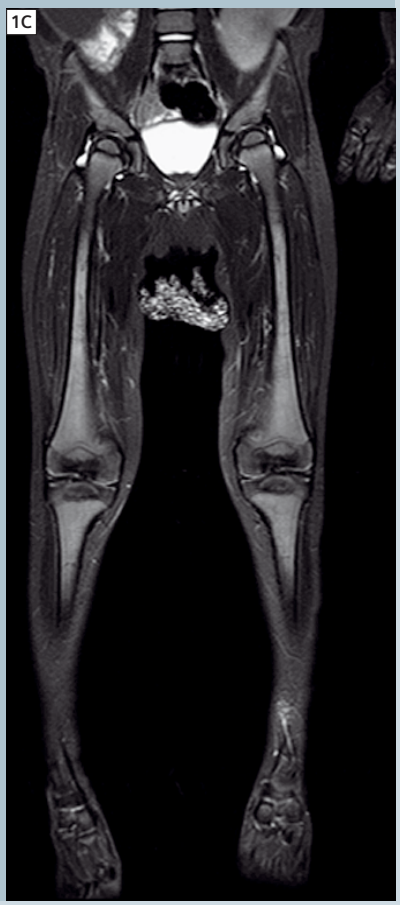

1 **(A)** is a composed whole-body MR image that consists of six different data sets, each covering a different anatomical area as shown in **(B)**. The *syngo* composing software can also be used for image integration from all types of multi-step MR examinations as demonstrated in **(C)**.

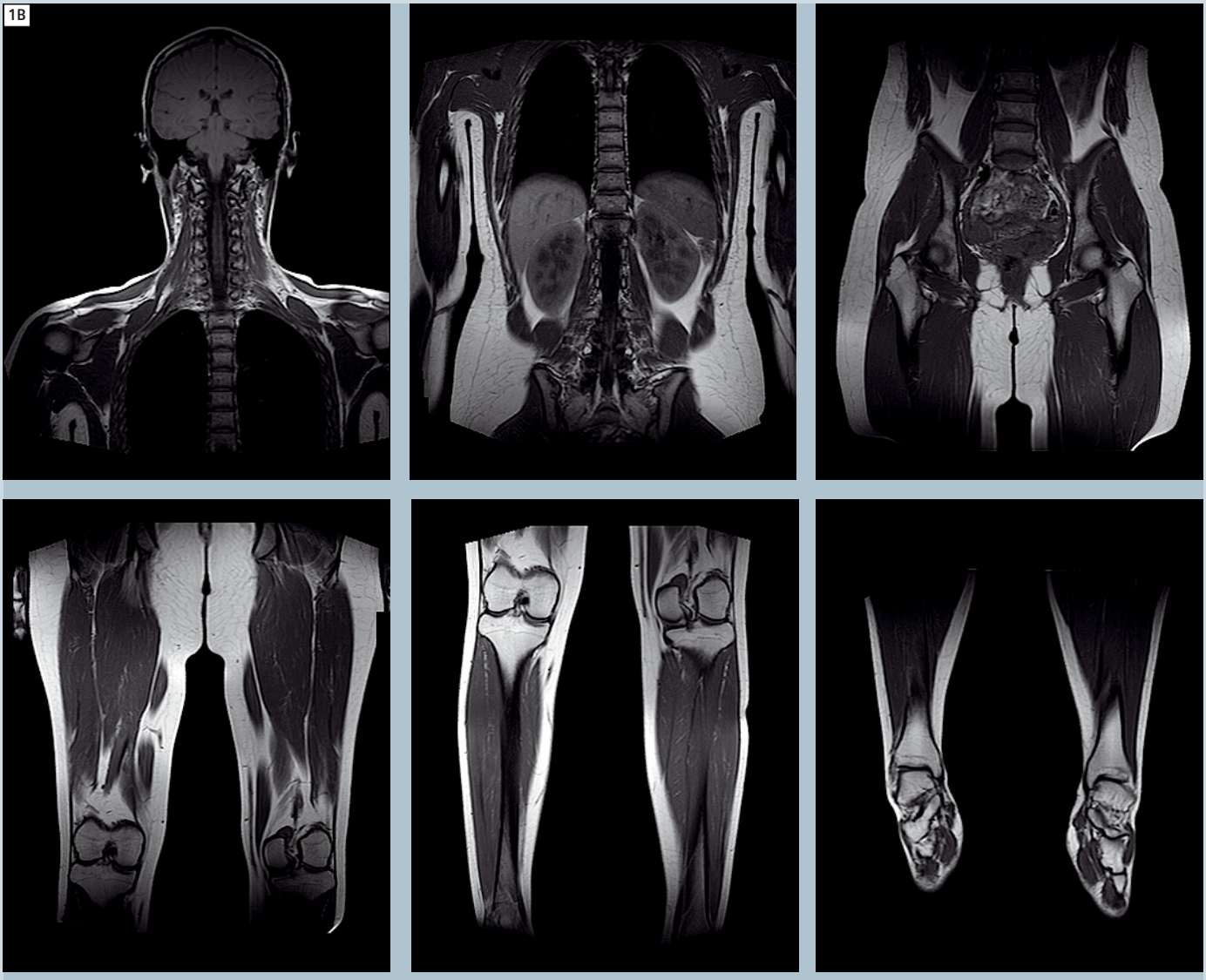

1 **(A)** is a composed whole-body MR image that consists of six different data sets, each covering a different anatomical area as shown in **(B)**. The *syngo* composing software can also be used for image integration from all types of multi-step MR examinations as demonstrated in **(C)**.

Once images are composed the software will advise if there has been any mismatch between data sets. Any inadequate matches are indicated by red triangles at the mismatch points. If necessary, the images can be adjusted up / down, right / left, or front / back. A normalise filter will even out any signal intensity variations between the different data sets. (Visit www.siemens.com/magnetom-world for the technical aspects of the normalise filter: "Image Quality Improvement of Composed MR Images by Applying a Modified Homomorphic Filter" by V. Jellus et al.)

Certain criteria are required for the software to be able to compose the images:

1. Must come from the same frame of reference.
2. Must be distortion corrected.
3. Must be the same image type.
4. Cannot be rotated about the feet-head (FH) axis.
5. Can angle by 45° in the other axes.
6. Can have different matrix size, FOV, slice thickness or number of slices between data sets.

Frame of reference

To ensure that the series come from the same frame of reference, they need to be distortion corrected.
Once distortion correction has been applied, the images belong to the whole body coordinate system and have the same frame of reference.

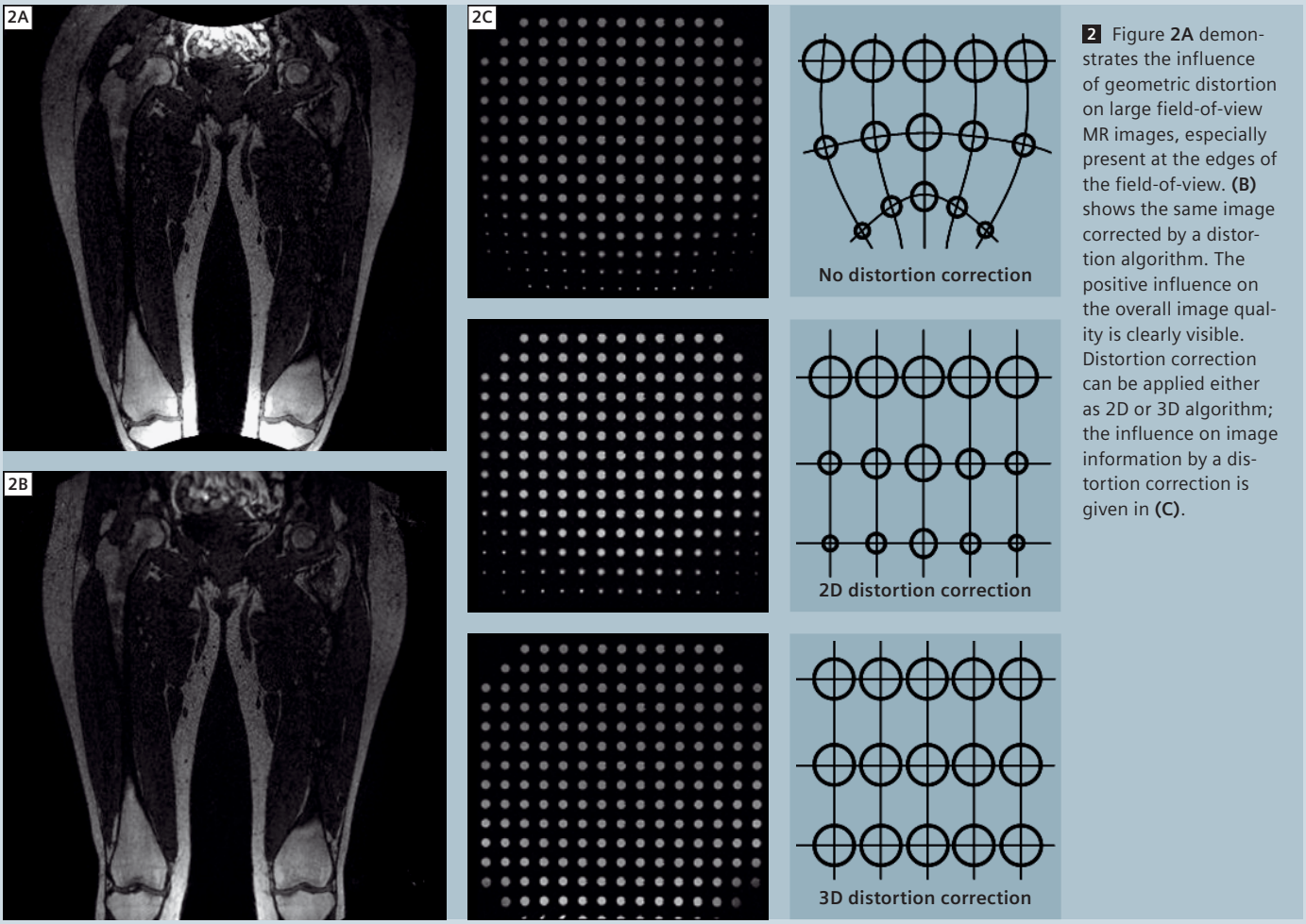

2 Figure **2A** demonstrates the influence of geometric distortion on large field-of-view MR images, especially present at the edges of the field-of-view. **(B)** shows the same image corrected by a distortion algorithm. The positive influence on the overall image quality is clearly visible. Distortion correction can be applied either as 2D or 3D algorithm; the influence on image information by a distortion correction is given in **(C)**.

Distortion correction

Images acquired on a large FOV will suffer from geometric distortion at the edges of the FOV (Fig. 2A). This is due to nonlinearity over the length of the gradients. Geometric distortion can be corrected by applying either a 2D or 3D distortion correction filter (Fig. 2B). The advantage of the 3D distortion correction filter is the additional corrections in the through-plane direction (Fig. 2C).

Same sequence type

This requires the data to have been acquired by the same technique.
It is not possible to compose gradient echo sequences with spin echo, or 2D sequences with 3D.

Planning the scan

When planning sagittal or coronal images, it is important not to rotate about the feet-head axis (Fig. 3B).

If scans are rotated in this direction, the subsequent regions must be of the same angle. A difference of more than one degree will render the data sets unable to be composed.
Angulations of up to 45 degrees in the other planes are acceptable for 2D sequences (Fig. 3 A and C), but with steeper angulations a limited number of composed images may result.

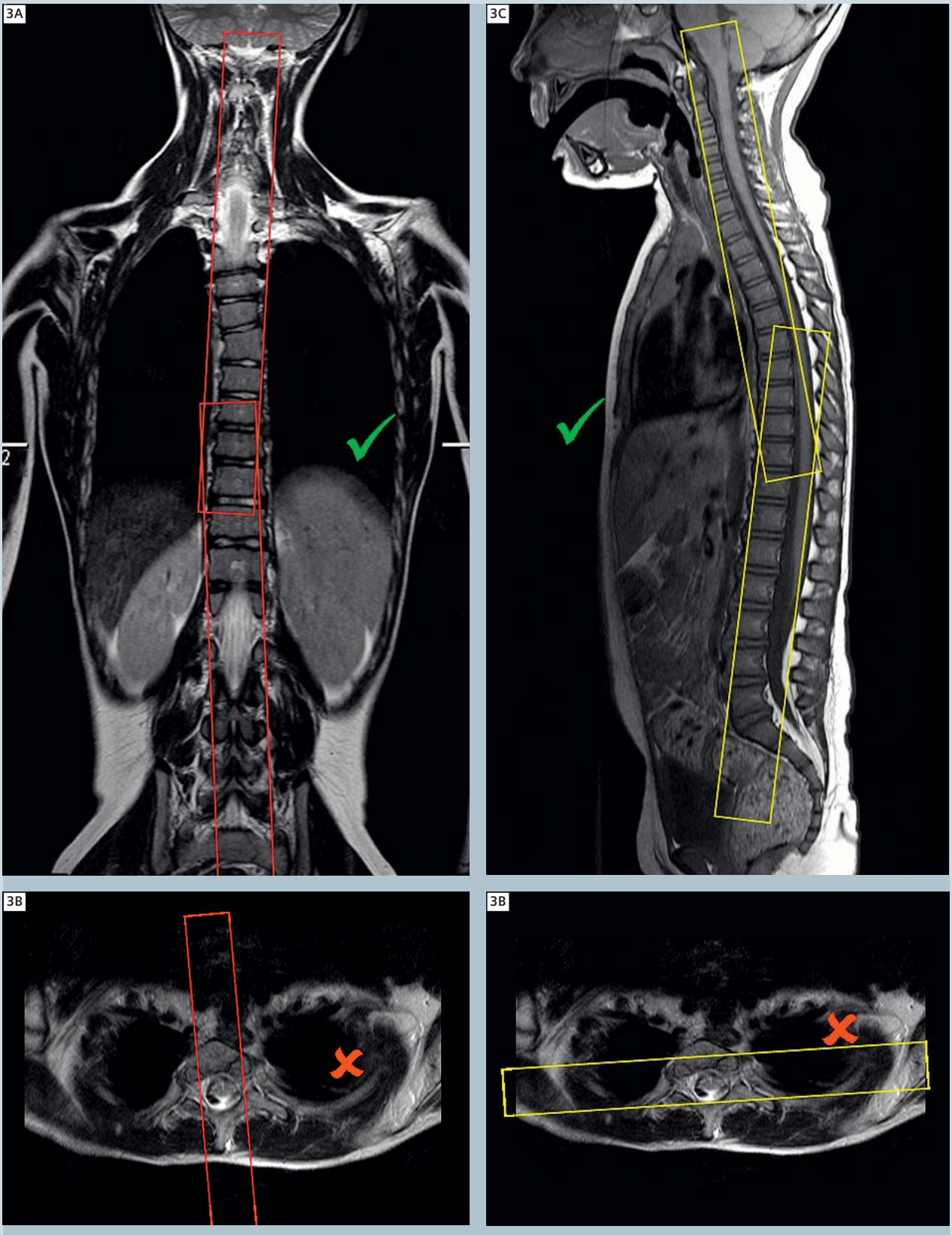

3 Planning the scan.

4 A composed 3D multi-step MR examination. **(A)** shows the regions of interest **(B)** their relative angulations. The resulting image provides a fast overview of the vessels **(C)**.

Be careful when planning 3D data sets as there is less leeway between angulations. While 3D data sets angled more than six degrees will compose, they may not be able to be used in any subsequent post processing such as MultiPlanar Reconstructions (MPR) or Maximum Intensity Projections (MIP). A warning will appear on screen that the images will be saved as secondary capture images. To avoid this, it is recommended to plan the sequences as straight as possible to ensure the regions will compose (Fig. 4A). This may require additional slices to include the required anatomy, but in vascular studies slice increases should not be to the detriment of accurate contrast timing (Fig. 4 B and C). Composing is a useful and rewarding post processing step applicable in almost any two or more region scans. With the use of Inline composing, original data sets can be automatically composed and saved to the database at the end of the last sequence acquisition.

Contact
Sandra Winsor
Charge Clinical MRT MRI
Centre for Advanced MRI
UniServices
University of Auckland
New Zealand
s.winsor@auckland.ac.nz

What's your favorite Dot Feature?

Dot (Day optimizing throughput) is the most comprehensive MRI workflow solution, and it helps take the complexity out of MRI. Dot has now established itself in the field and our customers have told us what they like best about Dot:

"In some pathologies, we need to obtain inter-examination reproducibility and to be able to carry out examinations swiftly. In the area of knee pathology in particular, Dot and its AutoAlign function have enabled us to position slices automatically without the need for user intervention."

Alexandre Fuchs, MD
Radiologist
Imagerie Médicale Sainte Marie, Osny, France

"One of the major benefits of Dot is that it provides us with a relatively easy way to perform slice positioning through a library of images, which guide the user to specific anatomical points by means of landmarks."

Romain Olliac, Technologist
Service de Radiologie Polyvalente Diagnostique et Interventionnelle Hôpital Pitié-Salpêtrière, Paris, France

"AutoAlign is helpful especially for colleagues who rarely perform knee examinations because the slices are positioned automatically, which saves a lot of time. Furthermore, our knee examinations have become reproducible."

Linda Willeke
Technologist
St. Franziskus Hospital, Münster, Germany

Experience a Dot workflow yourself and hear from more customers at

www.siemens.com/Dot

Dot is now available for 3T MAGNETOM Skyra and MAGNETOM Verio and for 1.5T MAGNETOM Aera and MAGNETOM Avanto.

Visit our site optimized for tablets and smartphones

3D High Resolution MRI of the Knee at 3T Using a Moderately T2-weighted 3D-TSE-fs (*syngo* SPACE) sequence – Useful or Not?

A. Horng[1], M. Notohamiprodjo[1], J. Raya[1], J. Park[1], W. Horger[2], A. Crispin[1], M. F. Reiser[1], C. Glaser[1]

[1]*Department of Clinical Radiology, University of Munich – Grosshadern Campus, Munich, Germany*
[2]*Siemens Healthcare, Erlangen, Germany*

Background

Magnetic resonance imaging (MRI) of the knee is justifiably one of the most commonly performed MRI examinations, as it offers excellent direct depiction of cartilage, ligaments, menisci and periarticular soft tissue. This can be achieved by standard application of fat-saturated moderately T2-weighted 2D Turbo Spin Echo (TSE)-sequences in three orientations [1, 2]. However, conventional TSE-sequences are not isotropic, hence structures and signal alterations / lesions with a size less than the usual slice thickness of 3 to 6 mm, i.e. meniscal roots, may not be completely detected. A slice thickness below 3 mm is rarely acquired because of its reduced signal-to-noise ratio (SNR) and contrast-to-noise ratio (CNR) and because of the prolonged acquisition time for complete joint coverage. Furthermore post-processing options for 2D-sequences for the assessment of structures, which are captured in an oblique course through several slices, like the anterior cruciate ligament or the femoral trochlear cartilage [3] are limited.
In this setting the introduction of a highly resolved 3D moderately T2-weighted (3D-T2w-TSE) sequence may be useful. In the literature time efficient 3D-T2w-TSE sequences have already been evaluated for the central nervous system [4] and recently for the body trunk [5, 6]. They enable data acquisition with high isotropic spatial resolution and allow for an interactive 3-dimensional visualization. Such post-processing after an initial isotropic data acquisition has been proven successful in many other MR and CT-based applications.

Technical considerations for *syngo* SPACE

Recently a 3D-TSE-sequence with moderate T2-weighting called "Sampling Perfection with Application optimized Contrasts using different flip angle Evolutions" (*syngo* SPACE), was developed for 3T systems. A restore pulse and variable flip angle distribution enable extremely large turbo factors. The variable flip angles provide a particular evolution of the signal during the echo train resulting in a "pseudo steady-state" with constant signal level neglecting relaxation [7]. Additionally, SAR is reduced by this acquisition scheme. The usage of this technique on a high field 3T system allows integration of parallel imaging with excellent SNR and CNR at reasonable acquisition times [8, 9].
The application of *syngo* SPACE at 3T might establish a new approach to MRI of the knee. Parallel imaging facilitates blockwise 3D-data acquisition with isotropic spatial resolution for evaluation of the whole knee in a reasonable time window. The acquisition time should be either less or at least comparable to acquisition times of conventional 2D TSE datasets in three planes. The advantage of an isotropic 3D-dataset is the possibility of 3-dimensional multiplanar reformatting (MPR), which may enhance the evaluation of small delicate or oblique structures like meniscal roots or the fascicles of the anterior cruciate ligament. Disadvantages might be slightly decreased in-plane resolution as compared to conventional 2D-TSE-fs-sequences and some additionally required time for the 3D reconstructions.
Recently our research group evaluated *syngo* SPACE for isotropic highly resolved MRI of the knee at 3T (MAGNETOM Trio, Siemens Healthcare, Erlangen, Germany) with consecutive 3-dimensional-MPR in comparison to conventional 2D-TSE-fs-sequences in three planes (coronal, sagittal, axial) [10].
Sequence parameters for *syngo* SPACE and for the moderately T2w-2D-TSE-fs-sequence are given in table 1. Fat saturation in *syngo* SPACE was performed with the SPectral selection Attenuated Inver-

sion Recovery (SPAIR) technique. Parallel imaging was performed with the k-space based technique *syngo* GRAPPA with an acceleration factor R = 2. For signal reception, a dedicated multichannel knee coil with 8 independent RF-channels was used. Reformation of the datasets was performed on a *syngo* MultiModality Workstation (Leonardo, software version VB15A, Siemens Healthcare, Erlangen, Germany).

Analysis of axial, sagittal and coronal reformations (MPR) of 0.5 mm, 1 mm and 2 mm slice thickness suggest a slice thickness for MPR of 1 mm ($SPACE_{1mm}$) to be optimal for the visualization of anatomical structures (Fig. 1). This slice thickness provides significantly higher SNR for ligaments, subchondral bone and menisci and at least equal SNR for cartilage, bone marrow, muscle and fat of *syngo* SPACE as compared to conventional 2D-TSE-fs. Though identification of anatomical structures was comparable for *syngo* SPACE and 2D-TSE-fs, the $SPACE_{1mm}$ showed significantly better visualization of menisci in axial sections and meniscal roots in coronal sections despite slightly inferior CNR (joint fluid/cartilage, joint fluid/menisci, fat/ligaments and bone marrow/subchondral bone) as compared to 2D-TSE-fs.

Clinical application

The reconstruction time for one *syngo* SPACE dataset was below 30 s, the data acquisition time was 10 min 35 sec with *syngo* SPACE versus 12 min 48 sec with 2D TSE in three planes (table 1). Thus the overall acquisition time for *syngo* SPACE was comparable to the acquisition of the 2D-TSE-fs datasets in three

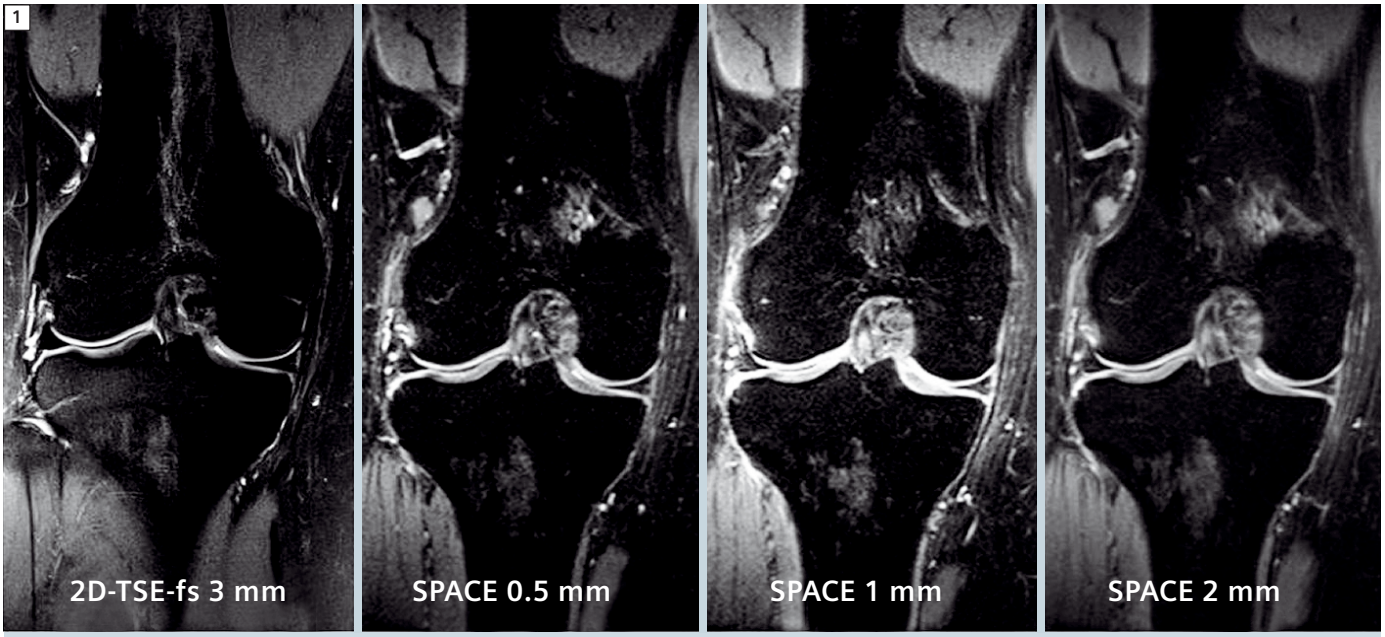

1 Coronal *syngo* SPACE reconstructions in 0.5 mm, 1 mm and 2 mm show a good homogeneity throughout the image as compared to the T2w-2D-TSE-fs.

Table 1: Sequence parameters for the *syngo* SPACE and the T2w-2D-TSE-fs-sequences.

	TR [ms]	TE [ms]	FA [°]	Resolution [mm^3]	FOV [cm]	Matrix	Parallel Imaging	T_{akqis}
***syngo* SPACE**	1200	30	120	0.5	16	320 x 320	GRAPPA r=2	10'35"
T2w-2D-TSE-fs	3200	30	180	0.36 x 0.36 x 3	16	448 x 448	GRAPPA r=2	12'34"

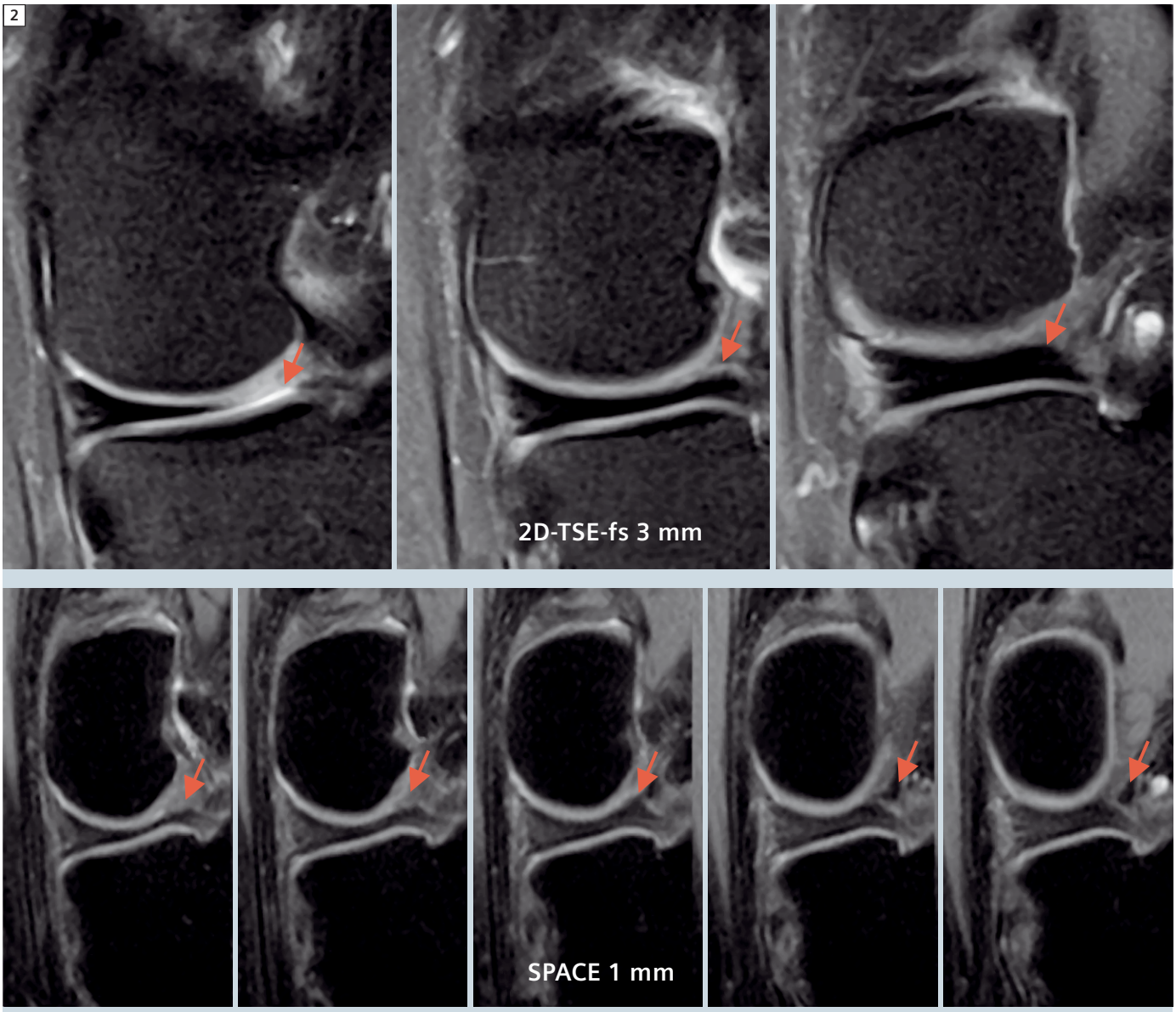

2 Coronal reconstructed *syngo* $SPACE_{1mm}$ and 2D-TSE-fs of a healthy volunteer. SPACE provides better visualization of the posterior medial meniscal root as compared to T2w-2D-TSE-fs, where the insertion of the root is blurred because of larger partial volume effects.

planes suggesting that the technique is feasible for daily clinical use.
The advantage of *syngo* SPACE over 2D-TSE-fs is the possibility of free multiplanar isotropic reconstructions at comparable SNR resulting in a slightly improved detection and differentiation of relevant small ligamenteous (Fig. 2) and meniscal structures (Figs. 3, 4). Clinical relevance thus might be better visualization of small avulsive ligamenteous lesions, e.g. of meniscal roots and of radial or complex meniscal tears whose configuration is challenging to interpret on conventional angulated thick sagittal or coronal sections (Fig. 5). The signal / image characteristics of *syngo* SPACE appear more similar to TSE image characteristics than to GRE and therefore are unlikely to require a big adjustment of the radiologist's reading and interpretation habits to the new sequence.
Usage of the free 3D-reformation according to the course of oblique anatomical structures as seen for femoral trochlear cartilage (Fig. 6) and the anterior cruciate ligament (Fig. 7) may aid in the evaluation of primarily difficult anatomical sites or a complicated situation after injury.

Conclusion

Blockwise acquired *syngo* SPACE is a new approach to MRI of the knee at 3T. It allows highly-resolved isotropic true 3-dimensional acquisition and subsequent reconstruction. Overall acquisition time is shorter than that of three separate 2-dimensional datasets and SNR for 1 mm reconstructions is similar to con-

Continued on page 46

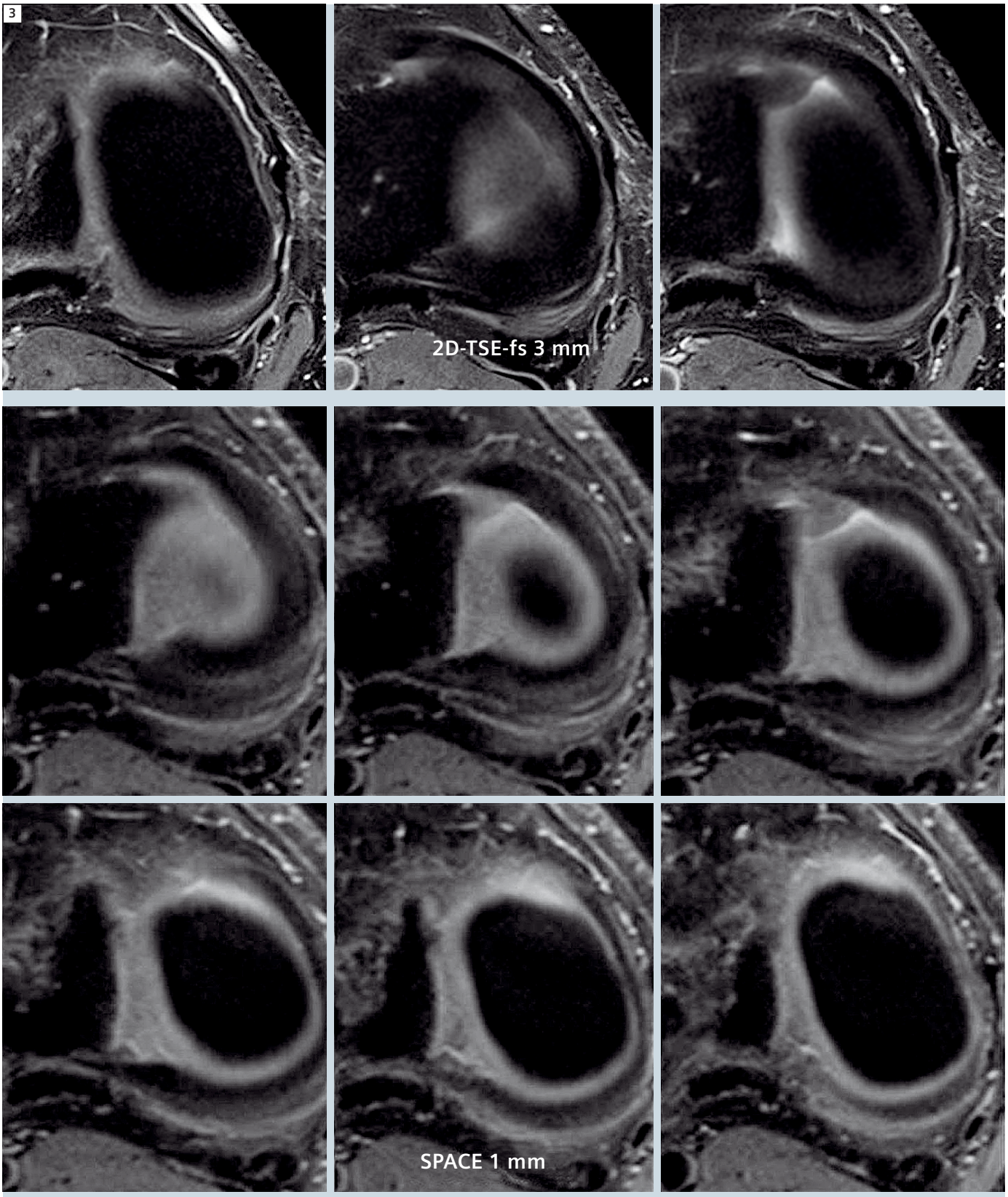

3 Axial sections of the medial meniscus of a healthy individual. *syngo* SPACE provides more detailed depiction of the meniscus throughout a higher number of slices as compared to 2D-TSE-fs. Both the meniscal body and its attachments (meniscal roots) are clearly visualized in SPACE while in 2D-TSE-fs parts of those are masked by partial volume effects.

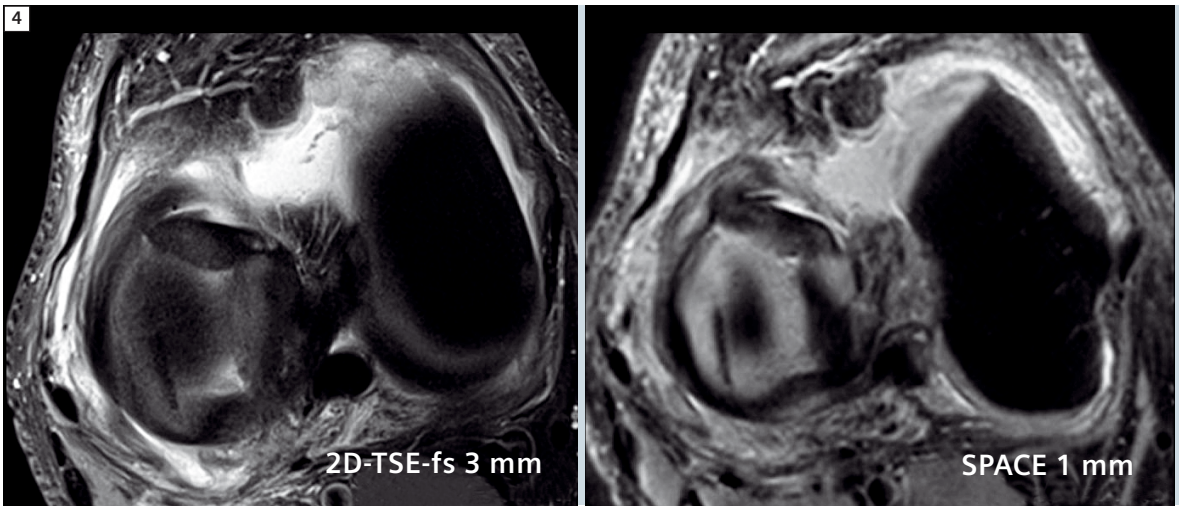

4 Axial reconstructed *syngo* SPACE$_{1mm}$ and 2D-TSE-fs of a patient with a bucket handle tear. SPACE provides better visualization of the configuration of the bucket handle tear as compared to T2w-2D-TSE-fs, in which delineation is impaired due to partial volume effects.

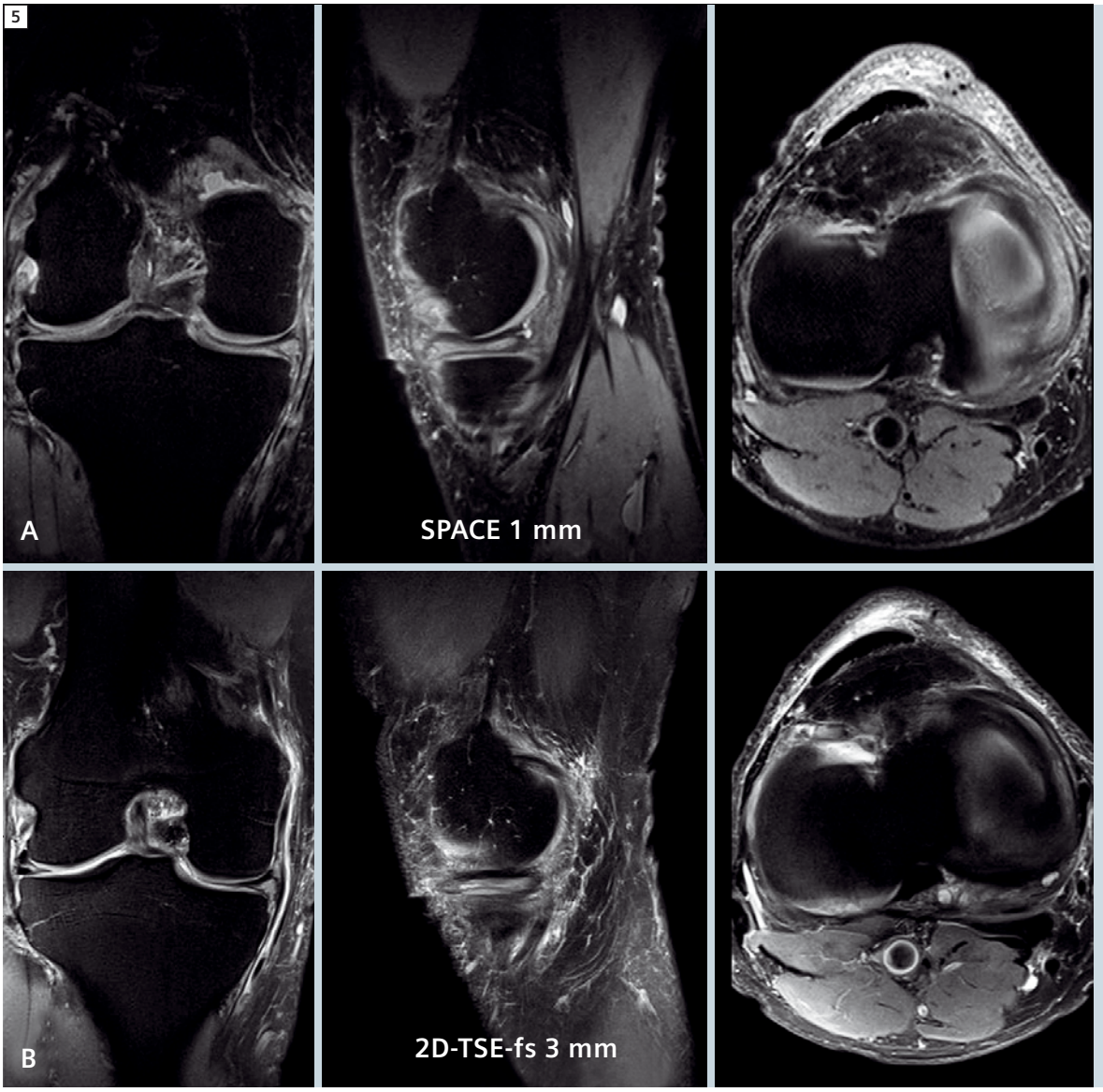

5 Coronal, sagittal and axial reconstructed *syngo* SPACE$_{1mm}$ images (row A) show a good delineation of a horizontal tear within the medial meniscus which approach the quality of the T2w-2D-TSE-fs sequence (row B) and provide an even clearer depiction of the lesion's borders and its extent.

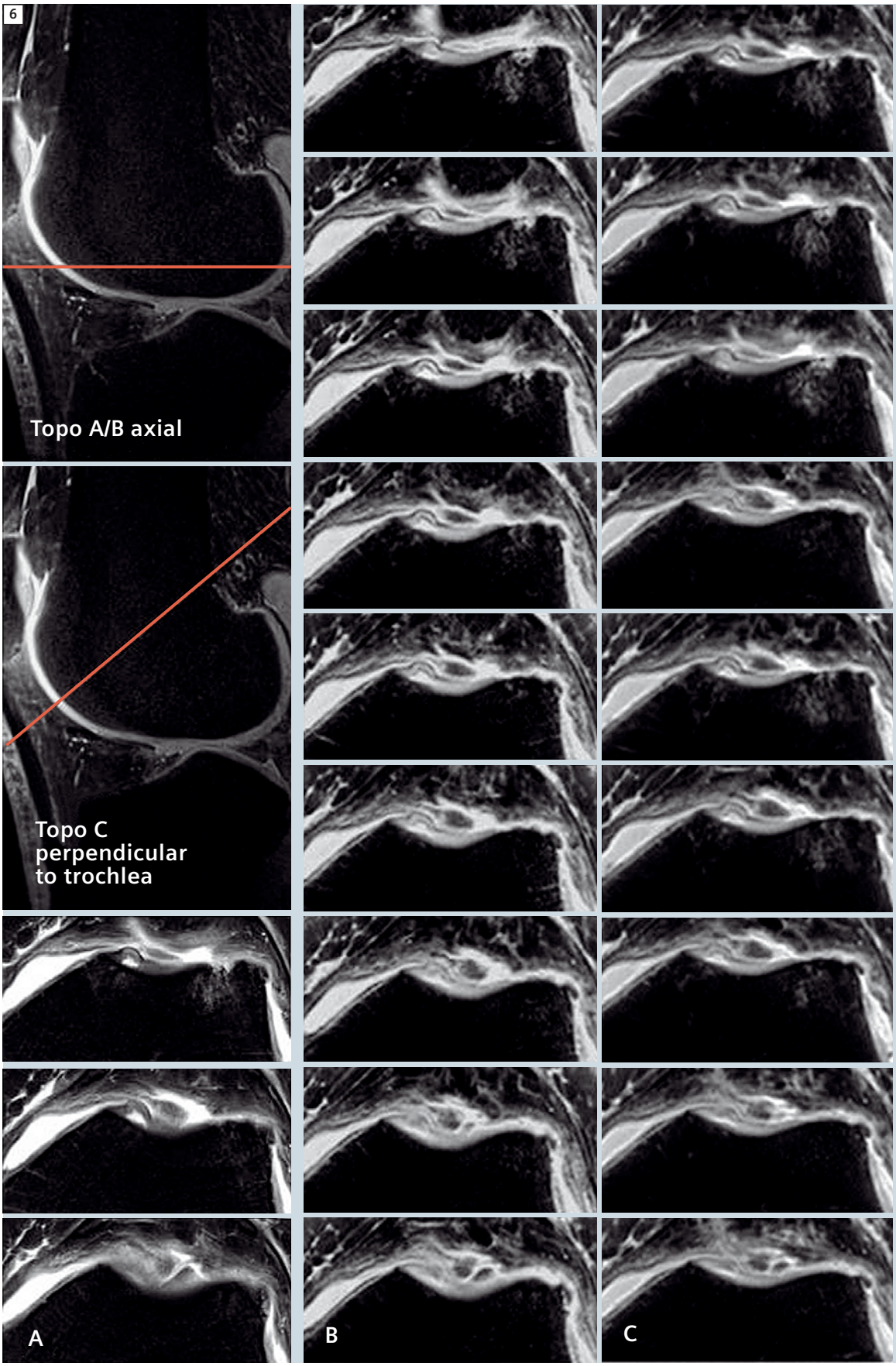

6 Axial reconstructed *syngo* $SPACE_{1mm}$ and 2D-TSE-fs of a patient with a trochlear cartilage delamination. In strictly axially acquired 2D-TSE-fs (Topo A/B and series A) the femoral trochlear cartilage is partially blurred because of partial volume effects, whereas depiction in $SPACE_{1mm}$ (B/C) is sharper. Axially reconstructed $SPACE_{1mm}$ (Topo A/B and series B) is able to cover the trochlear cartilage on more slices than 2D-TSE-fs enabling a more detailed depiction. MPR perpendicular to the trochlear cartilage (Topo C and series C) even allows a clearer depiction of cartilage height and the lesion.

Continued from page 86

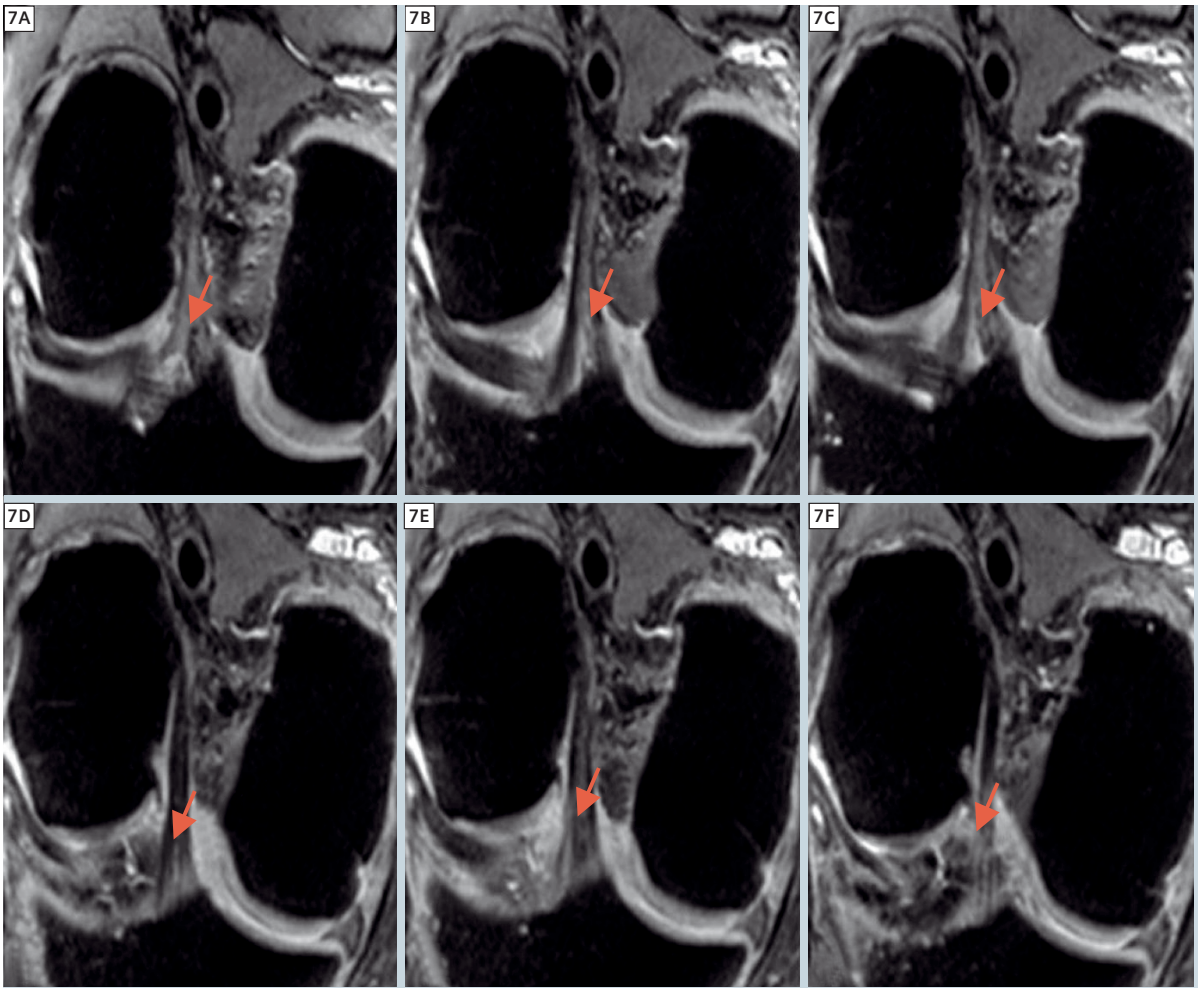

7 Anterior cruciate ligament of a healthy volunteer (sequence A–F). *syngo* $SPACE_{1mm}$ tilted to the course of the anterior cruciate ligament allows excellent traceability of the two bundles.

ventional 2D-TSE-fs. The identification of anatomical structures at least equals the conventional sequence and allows superior discrimination of relevant small ligamentous structures.

These data suggest that a protocol comprising 1 mm *syngo* SPACE reconstructions in three orientations would be useful for clinical evaluation. The additional possibility of free 3-dimensional reconstruction depending on the specific clinical need may become useful for the diagnosis of difficult anatomical situations and presurgical planning, i.e. for traumatic ligamenteous lesions or complex meniscal tears.

References

1 Glaser, C., et al., [Meniscus and ligament injuries]. Radiologe, 2006. 46(1): p. 26-35.
2 Protocols for MRI examinations of joints and the spine as recommended by the AG MSK of the Deutsche Röntgengesellschaft. Rofo, 2006. 178(12): p. 128-130.
3 Mosher, T.J., Musculoskeletal imaging at 3T: current techniques and future applications. Magn Reson Imaging Clin N Am, 2006. 14(1): p. 63-76.
4 Mugler, J.P., 3rd, et al., Optimized single-slab three-dimensional spin-echo MR imaging of the brain. Radiology, 2000. 216(3): p. 891-9.
5 Lichy, M.P., et al., Magnetic resonance imaging of the body trunk using a single-slab, 3-dimensional, T2-weighted turbo-spin-echo sequence with high sampling efficiency (SPACE) for high spatial resolution imaging: initial clinical experiences. Invest Radiol, 2005. 40(12): p. 754-60.
6 Isoda, H., et al., MRCP imaging at 3.0 T vs. 1.5 T: preliminary experience in healthy volunteers. J Magn Reson Imaging, 2007. 25(5): p. 1000-6.
7 Alsop, D.C., The sensitivity of low flip angle RARE imaging. Magn Reson Med, 1997. 37(2): p. 176–84.
8 Masi, J.N., et al., Cartilage MR imaging at 3.0 versus that at 1.5 T: preliminary results in a porcine model. Radiology, 2005. 236(1): p. 140-50.
9 Link, T.M., et al., 3.0 vs 1.5 T MRI in the detection of focal cartilage pathology--ROC analysis in an experimental model. Osteoarthritis Cartilage, 2006. 14(1): p. 63-70.
10 Notohamiprodjo, M., et al., A New Approach for High Resolution MRI of the Knee at 3T – Evaluation of a Moderately T2-Weighted 3D-TSE-Fs (SPACE) Sequence, Investigative Radiology, 2009 44(9): p.585-597.

Contact
Annie Horng, M.D.
Department of Clinical Radiology
University Hospitals Munich –
Campus Grosshadern
Marchioninistrasse 15
81377 Munich
Germany
Phone: +49 89 7095 3620
annie.horng@med.uni-muenchen.de

Relevant clinical information at your fingertips

From technology to clinical applications, you will find all the latest news on Siemens MR at

www.siemens.com/magnetom-world

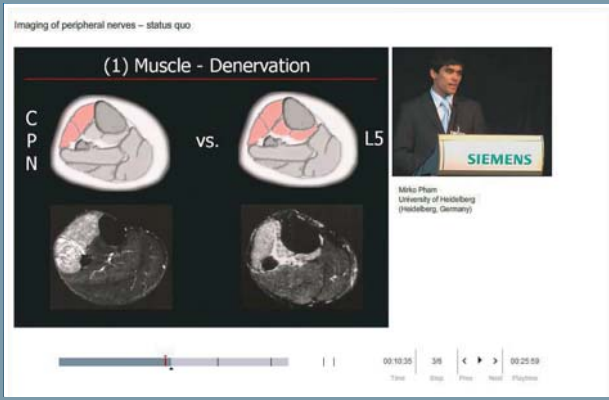

Don't miss the talks of international experts on Magnetic Resonance Imaging.

Go to
Education > e-trainings & Presentations

The centerpiece of the MAGNETOM World Internet platform consists of our users' clinical results. Here you will find case reports and clinical methods.

Go to
Clinical Corner > Case Studies

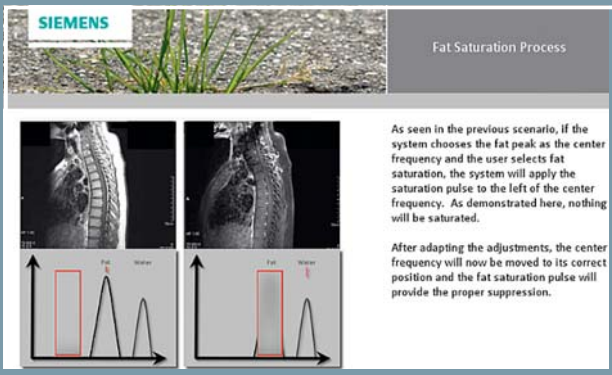

Just a mouse click away you will find application videos and useful tips allowing you to optimize your daily MR examinations.

Go to
Clinical Corner > Application Tips

For the whole range of clinical MR information visit us at

www.siemens.com/magnetom-world

FABS View of the Elbow for Visualization of Distal Biceps Tendon

Peter Cazares, RT (R) (CT) (MR)

MR Clinical Education Specialist, Siemens Healthcare, Iselin, NJ, USA

Introduction

Imaging of distal bicep tendon in MR can be somewhat difficult at times given the position of the elbow in relation to the general scanning environment. Common axial / coronal sequences demonstrate the tendon in an oblique projection that make it difficult to appreciate it in its entirety. By using the FABS (**f**lexed elbow, **ab**ducted shoulder, forearm **s**upinated) technique, imaging of the distal biceps tendon can be acquired "in plane" with excellent visualization and comfortable patient positioning.

Conclusion

Distal biceps tendon pathology will be greatly appreciated using this technique and can be incorporated with standard elbow imaging when this clinical referral is presented. Also greater success can be achieved with greater patient comfort using this technique and position.

Contact
Peter Cazares
Siemens Healthcare USA, Inc.
HQ Application Specialist – MR
170 Wood Avenue South
Iselin, NJ 08830
USA
peter.cazares@siemens.com

Procedure

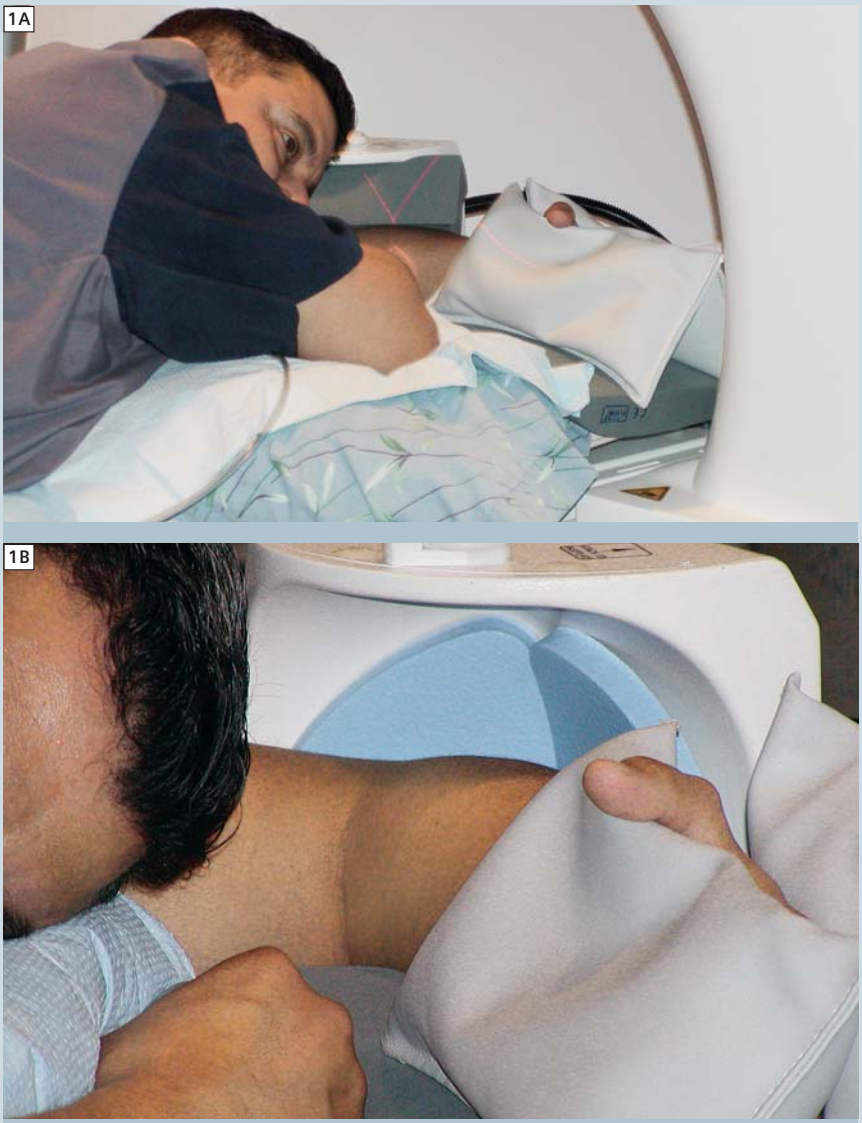

1 Step 1: We position the patient using our standard shoulder coil configuration. Have the patient lay on their stomach as comfortable as possible. Flex the elbow 90 degrees and place the elbow in the shoulder coil with the forearm and wrist supinated. Secure the forearm and wrist with either sandbags or a channeled positioning sponge to insure immobilization.

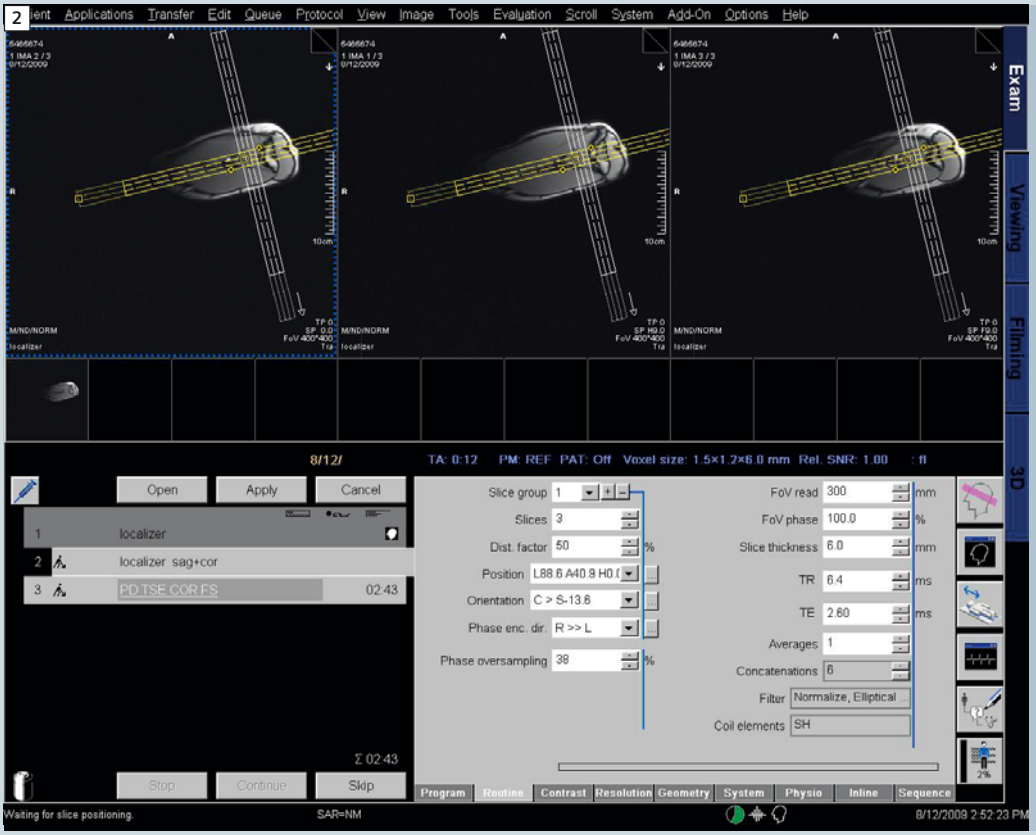

2 Step 2: Landmark at the center of the coil and localize. Perform two additional localizers in long and short axis in relation to the elbow.

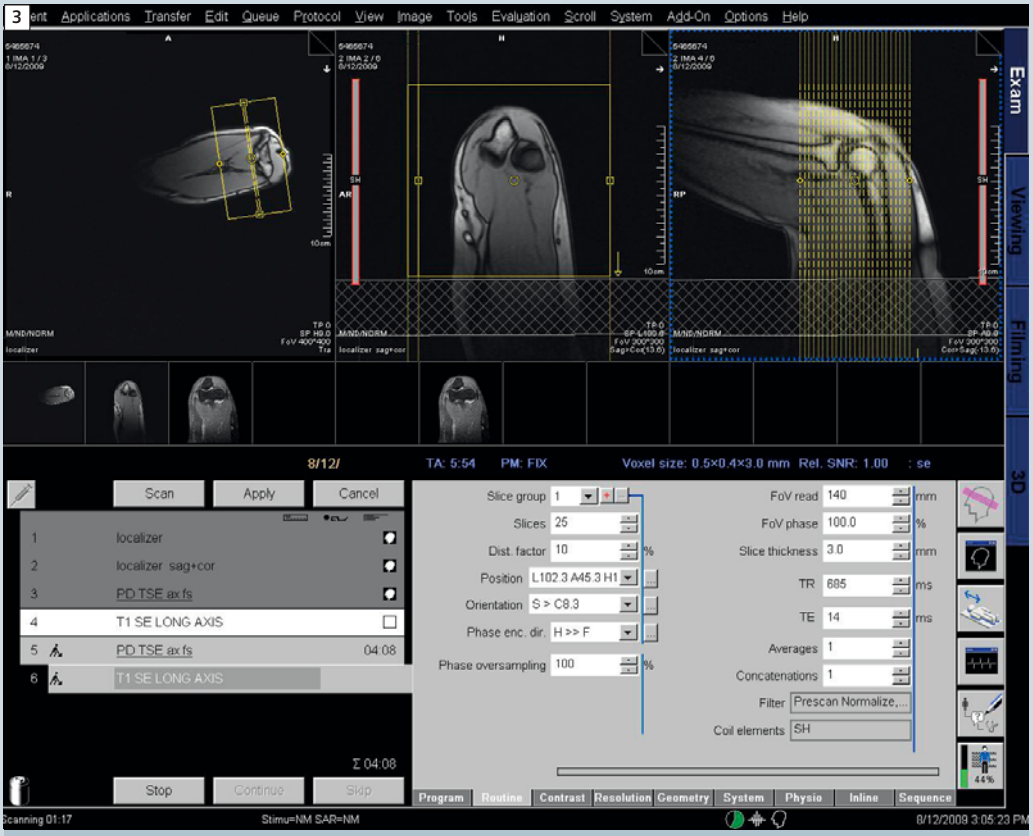

3 Step 3: Select sequences so as to image the biceps tendon "in plane". T1-weighted Spin Echo (SE) no fatsat, PD TSE fatsat are one recommendation.

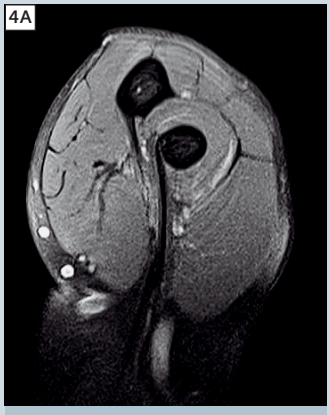

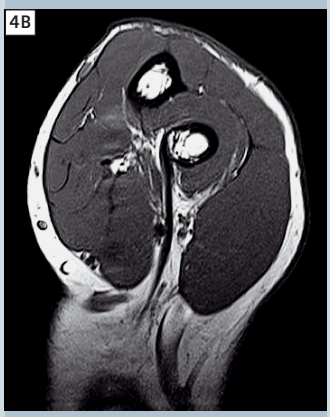

4 As seen, the distal biceps tendon is presented "in plane" along with the insertion at the radial tuberosity.

Case Reports: Musculoskeletal MRI in Sports Medicine

Heinz-Peter Schlemmer[1,3]; Tina Holder[1]; T. Nägele[1,2]; Claus D. Claussen[1,2]

[1]Radiologie SpOrt Stuttgart, Germany
[2]University Hospital of Tuebingen, Germany
[3]German Cancer Research Center, Heidelberg, Germany

Background

In contrast to its role in oncology, for example, MR imaging in sports medicine deals primarily with healthy and young individuals. This imaging technique is an invaluable tool in sports medicine, not only because of its excellent soft tissue contrast but also because of its non-invasive and non-ionizing nature. While imaging in recreational sports is mainly limited to an evaluation of the effects of severe traumatic events, such as a skiing accident, the role of musculoskeletal MRI in case of competitive sports is much more extensive. For example, following an injury, MRI is also used to assist in the detailed evaluation of the degree of performance impairment of the athlete – with direct impact on treatment / training actions taken for effective fast and full recovery. This implies that time-to-diagnosis and the easy access and availability of MRI scan time (also for follow-up exams) is important for these athletes. One should also take into account that the pattern and severity of injuries can differ between recreational and competitive sports. This has a direct impact on the indication to MRI and the required knowledge of technologists and radiologists. But also non-traumatic pain and limitation of mobility, and as a consequence insufficient training and competitive performances, of athletes can have various causes and are one of the main indications for MRI. Because of the importance of the results of such MR exams to the athlete, the interdisciplinary approach is one of the key elements for optimal and responsible treatment and support. Consequently, all cases shown in this article were examined at and treated by an association of different facilities including the Department of Sports Medicine at Tuebingen University and the Olympic Training Center Stuttgart.

In this article, we present a selection of cases. Whilst not being a representative selection, they do reflect very well the variety and range of musculoskeletal imaging in sports medicine: in cases 1 and 2, MRI was used to support the clinical diagnoses of ligamental tear / rupture. Cases 3 through 5 show typical patterns of muscular tears and haematoma after trauma. In these patients, MRI was used to evaluate the involvement and extension of the different muscles to evaluate and quantify the degree of performance impairment and to provide information for further rehabilitation training. And finally, in cases 6 and 7, the images of two young athletes with pain at training but without corresponding trauma are shown.

All MRI exams shown in this article were performed at 1.5 Tesla (MAGNETOM Avanto).

Case 1

22-year-old male soccer player with severe knee pain after traumatic knee injury.

An extensive effusion is obvious. Already suspected by clinical signs, oedema and tear of the anterior cruciate ligament supports the diagnosis of a complete rupture of the ligament (arrowhead in Fig. 1A). In addition, a horizontally shaped oedema within the dorsal medial meniscus supports the suspicion of a horizontal (smaller) meniscal tear (arrow in Fig. 1B).

Images were acquired with the dedicated CP extremity coil. Sequence parameters for the shown images were:

- Sagittal PDw TSE with spectral fat suppression: TR / TE = 3754 / 37 ms, SL 1.5 mm, FOV 140 x 140 mm, Matrix 269 x 384 px
- Coronal PDw TSE with spectral fat suppression: TR / TE = 3754 / 37 ms, SL 1.5 mm, FOV 140 x 140 mm, Matrix 269 x 384 px

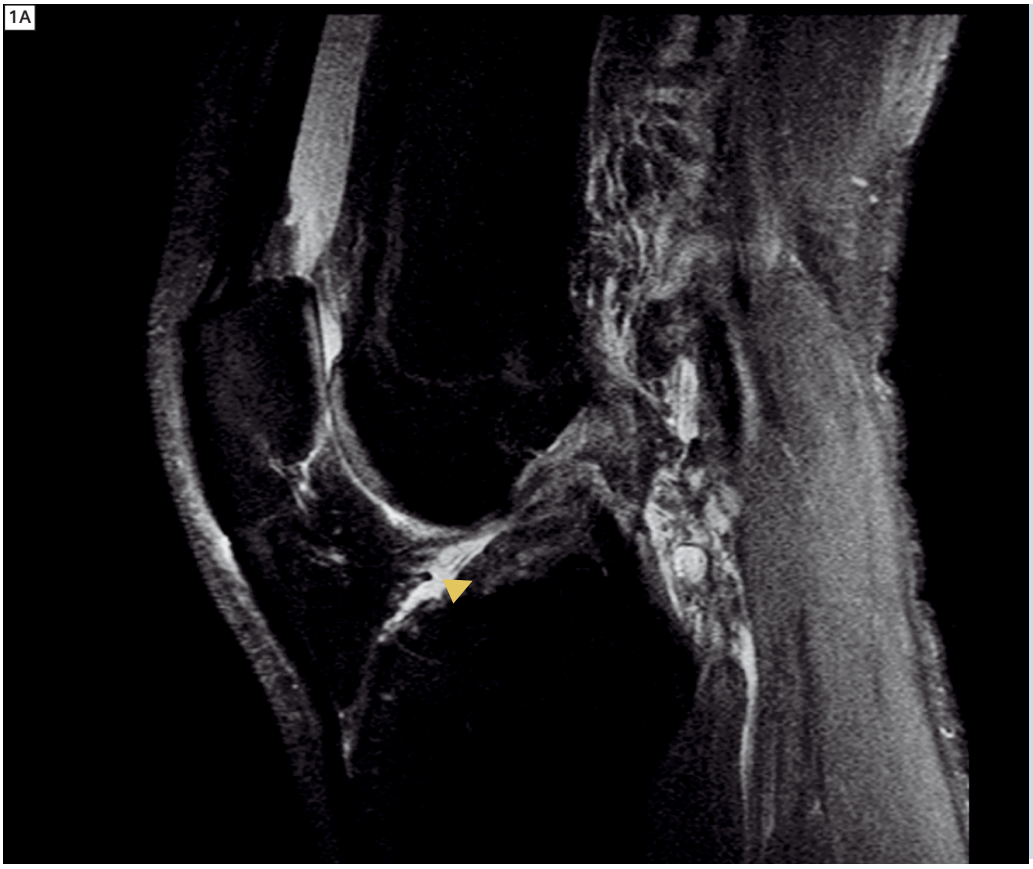

1A Sagittal PDw STIR.

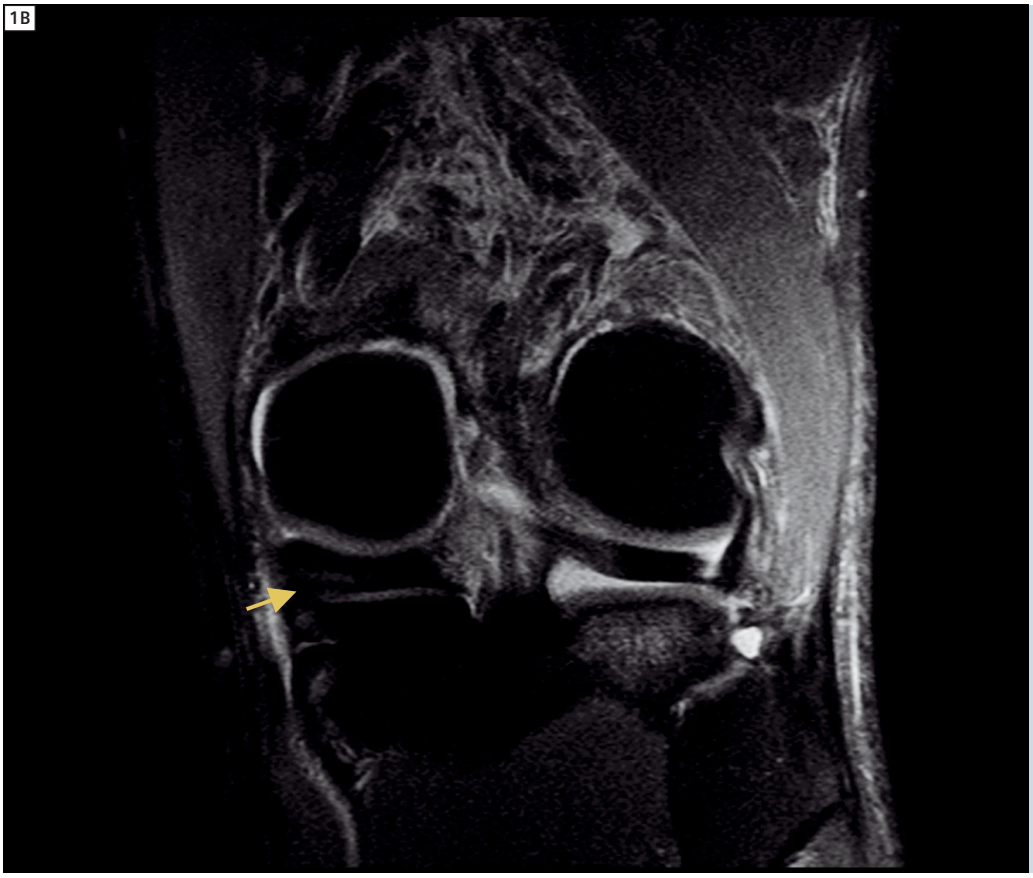

1B Coronal PDw STIR

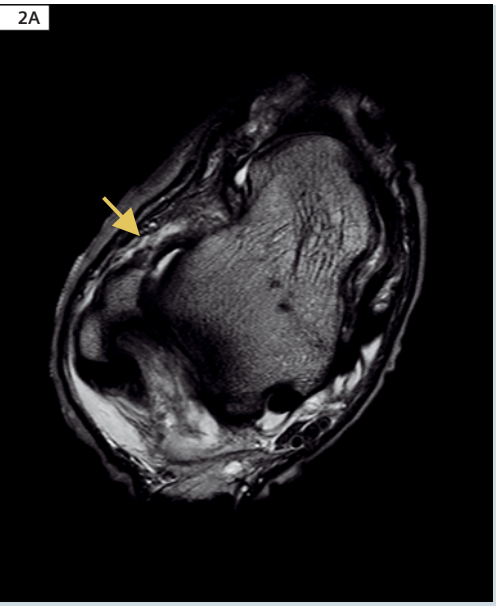

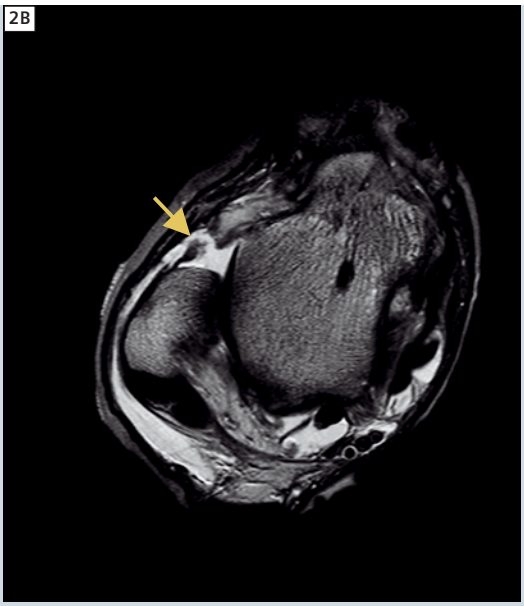

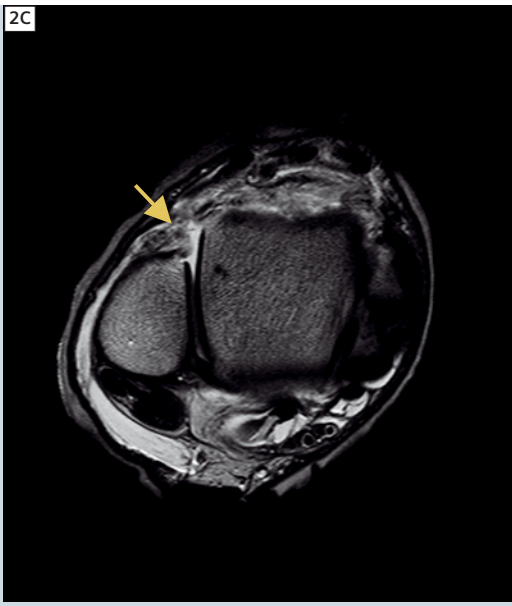

2A–C 1st trauma: transversal T2w TSE.

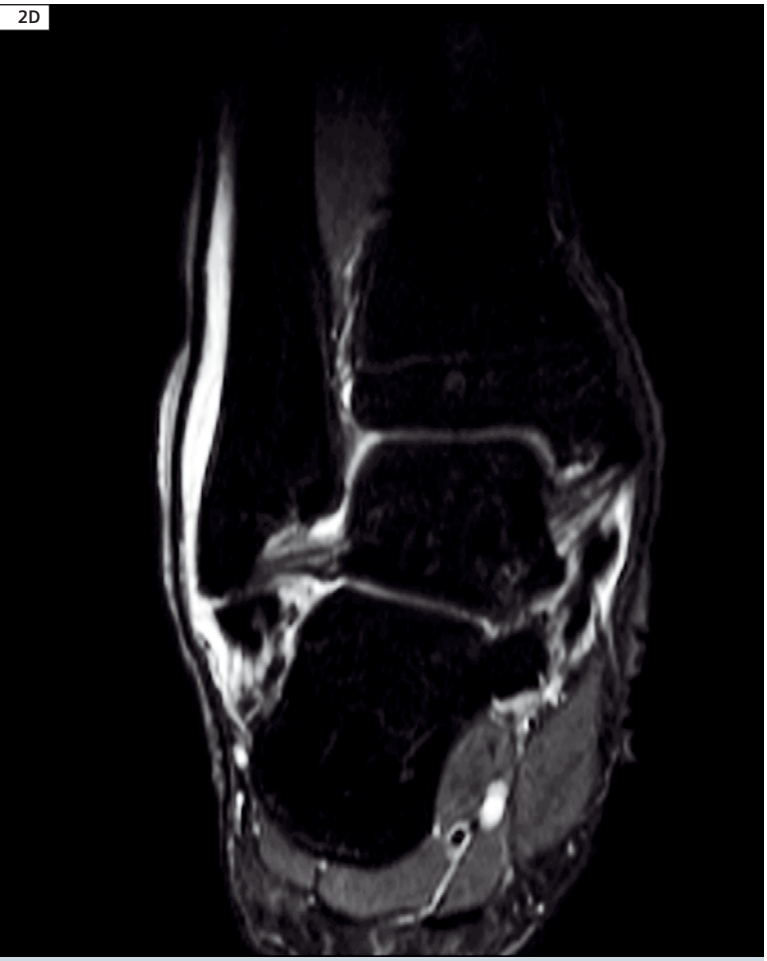

2D 1st trauma: coronal PDw STIR.

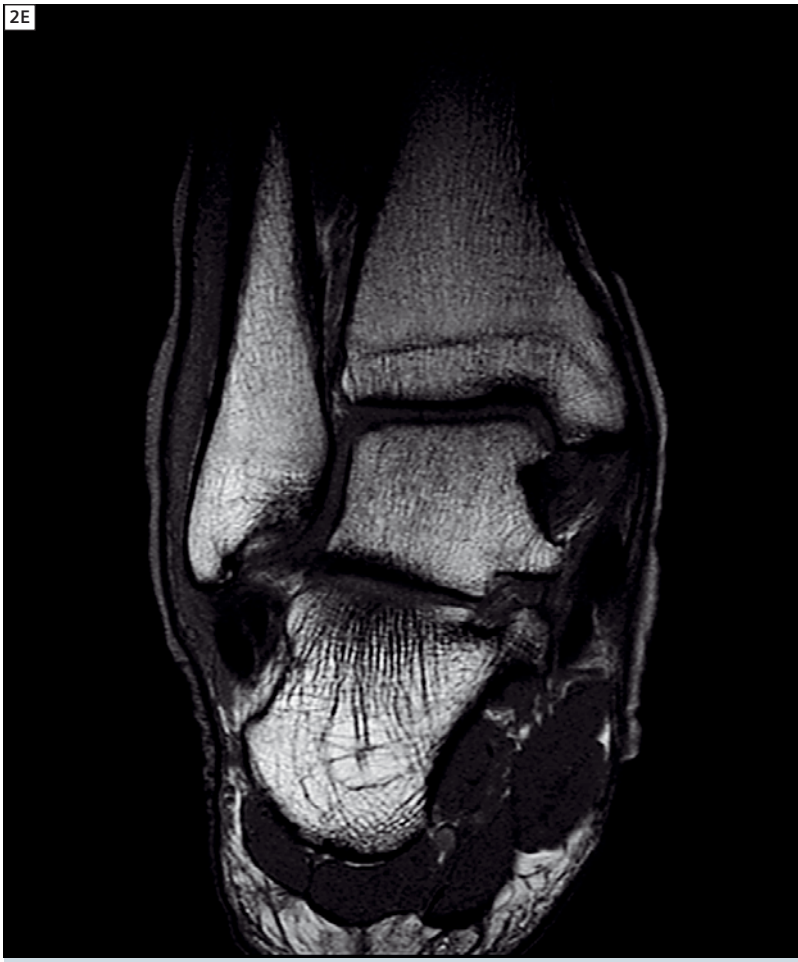

2E 1st trauma: coronal T1w TSE.

Case 2

23-year-old male soccer player after traumatic ankle injury.
MRI demonstrates a complete rupture of the anterior fibulotalar ligament (arrow in Figs. 2A–C). In addition, a partial rupture of the anterior syndesmosis ligament is present and an extensive oedema and haemorrhage of the surrounding soft tissue can also be observed (Figs. 2D and E). 7 months after the initial traumatic event, another trauma of similar type occurred. Follow-up MRI showed a thickened but now continuous fibulotalar ligament and ventral syndesmosis (arrowheads in Figs. 2D–F); no re-rupture was found.
Images were acquired with the 4-channel flex coil. Sequence parameters for the shown images were:

- Transversal T2w TSE: TR / TE = 5259 / 85 ms, SL 3 mm, FOV 140 x 140 mm, Matrix 269 x 448 px
- Coronal PDw STIR: TR / TE / TI = 6500 / 29 / 160 ms, SL 3 mm, FOV 160 x 160 mm, Matrix 169 x 256 px
- Coronal T1w TSE: TR / TE = 537 / 9.5 ms, SL 3 mm, FOV 111 x 160 mm, Matrix 250 x 448 px, TA
- Follow-up MRI transversal T2w TSE: TR / TE = 4110 / 105 ms, SL 3 mm, FOV 110 x 110 mm, Matrix 512 x 512 px

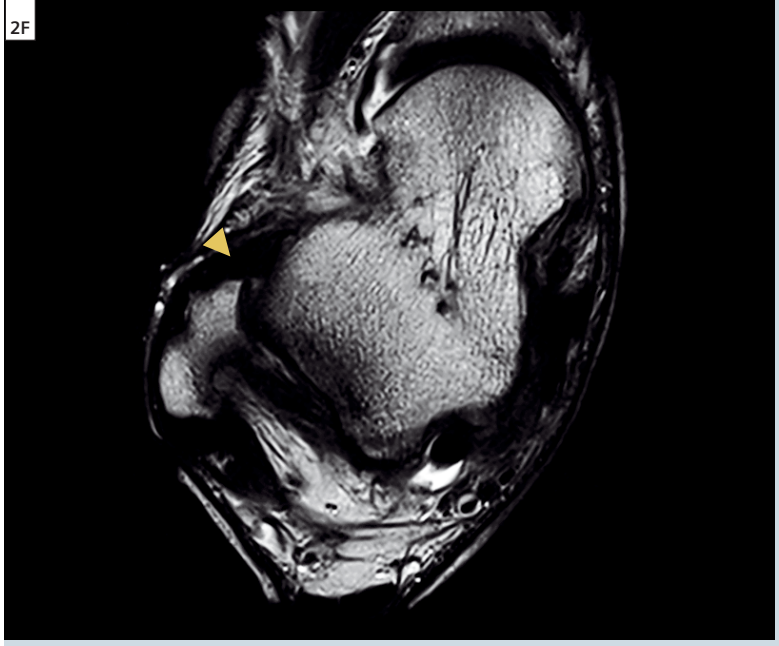

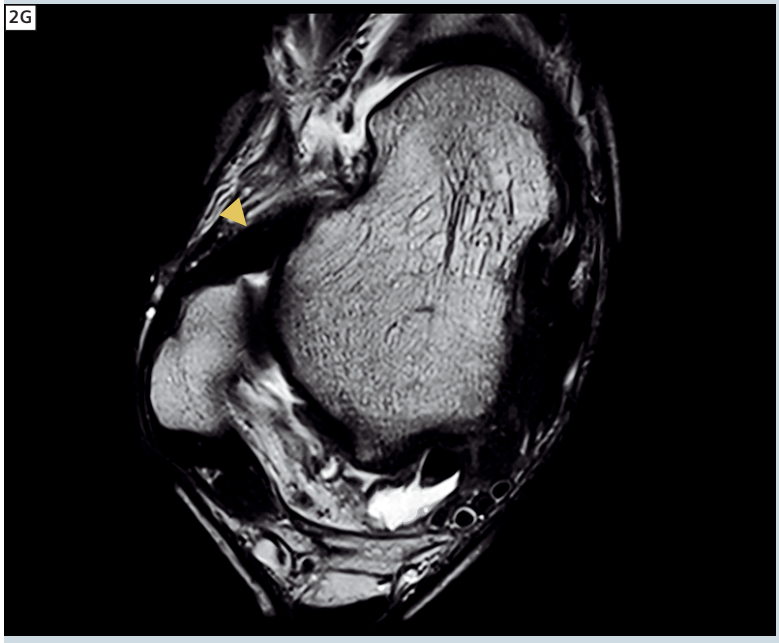

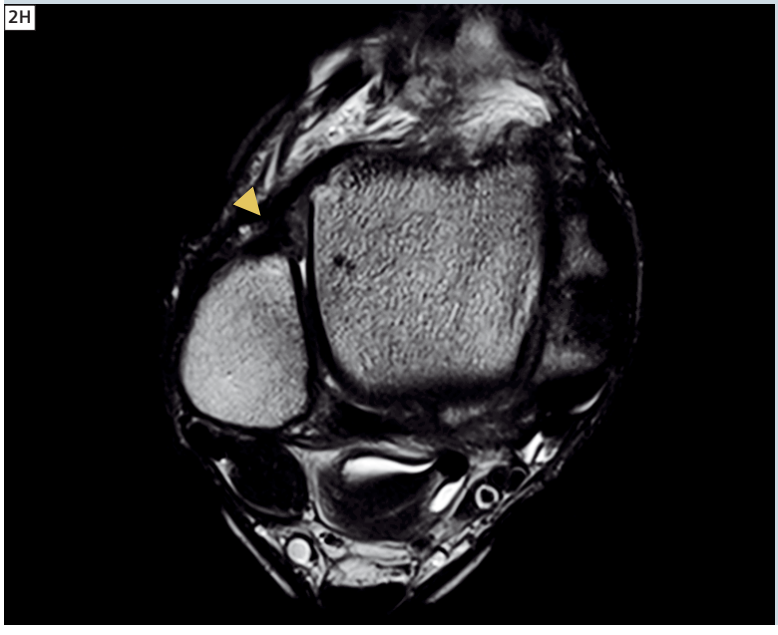

2F–H 2nd trauma: transversal T2w TSE.

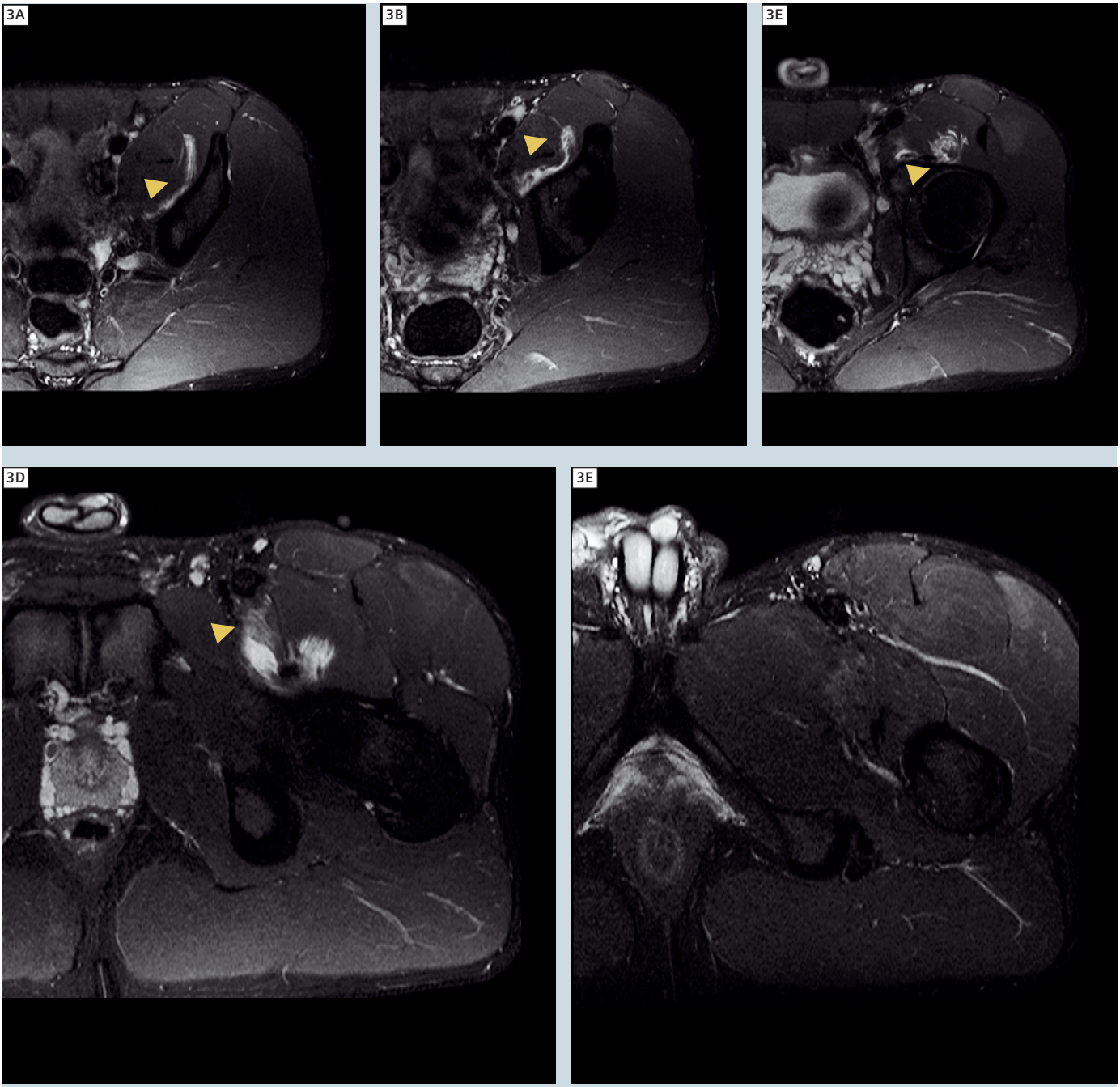

3A–E Transversal PDw STIR.

Case 3

22-year-old male soccer player after trauma of the left upper leg.
Tear of the fascia of the left iliac muscle at the ventral border of the acetabulum and less prominent tear of the iliac muscle itself (arrowheads in Fig. 3).
Images were acquired with the Spine and Body Matrix coil. Sequence parameters for the shown images were:

- Transversal PDw STIR: TR / TE / TI = 5390 / 29 / 160 ms, SL 4 mm, FOV 220 x 200 mm, Matrix 224 x 320 px
- Oblique coronal PDw TSE with spectral fat saturation: TR / TE = 4340 / 13 ms, SL 3 mm, FOV 250 x 250 mm, Matrix 240 x 320 px, TA
- Obliques sagittal PDw STIR: TR / TE / TI = 7540 / 29 / 160 ms, SL 4 mm, FOV 189 x 270 mm, Matrix 157 x 320 px

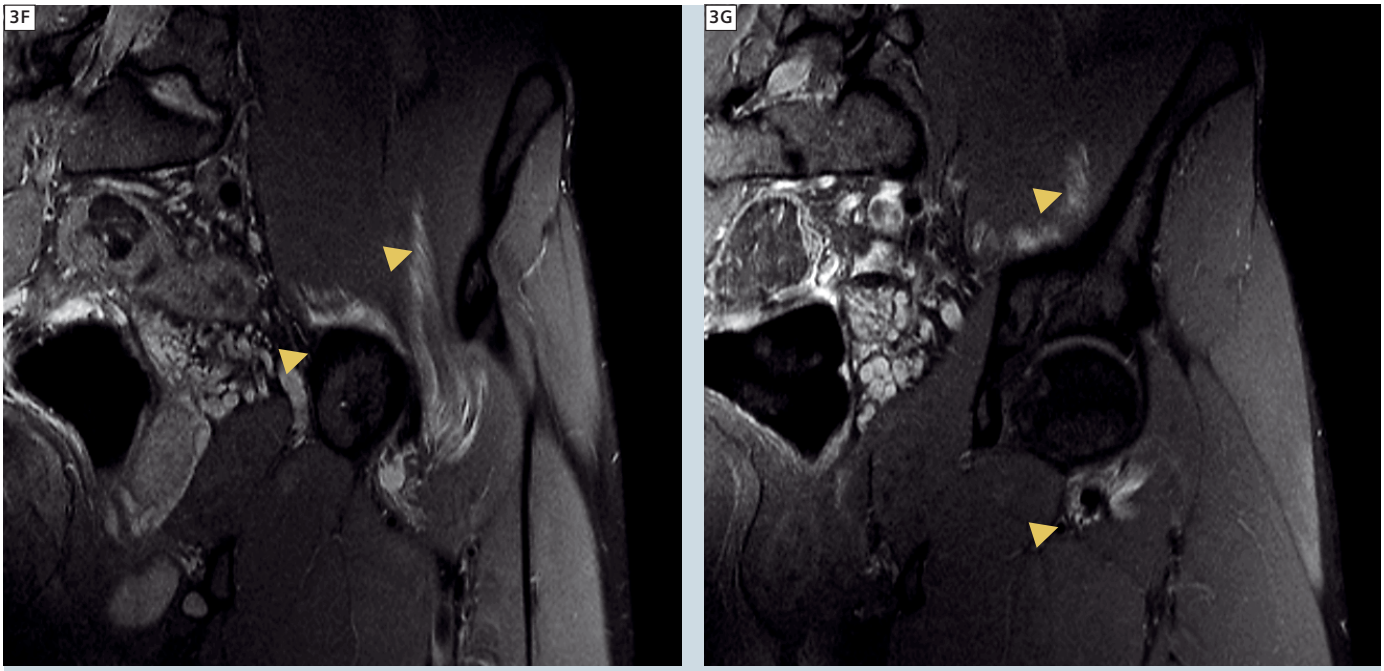

3F–G Oblique coronal PDw STIR.

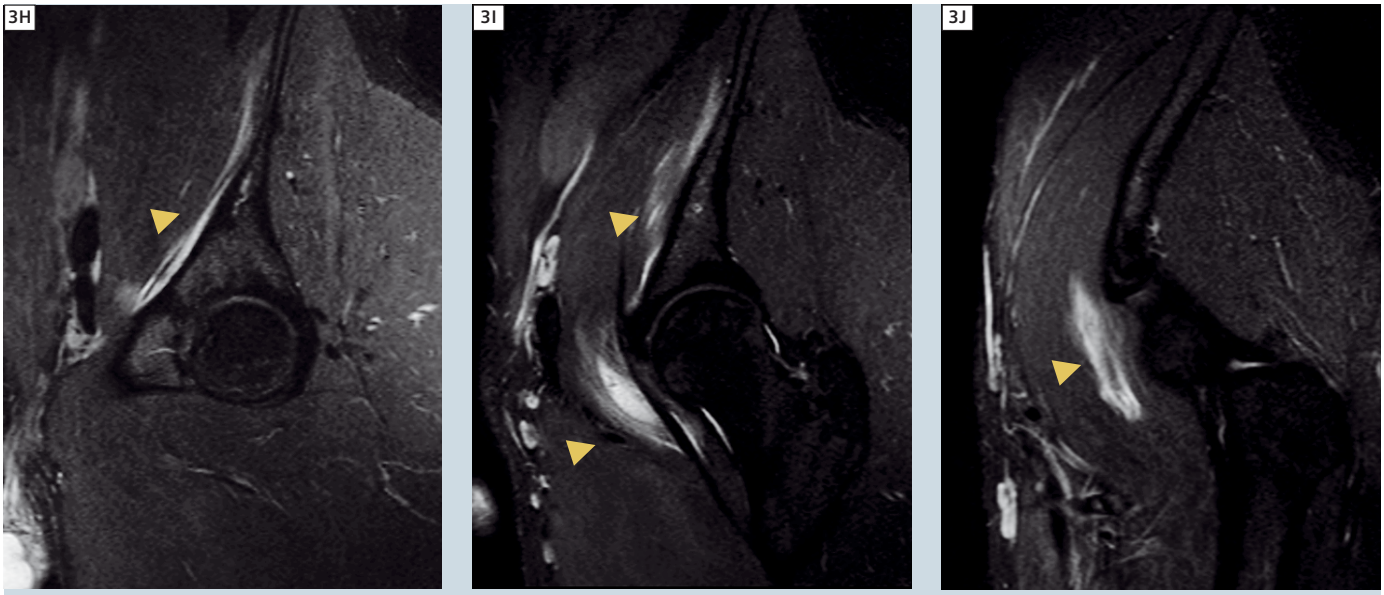

3H–J Oblique sagittal PDw STIR.

→ **Visit**
www.siemens.com/magnetom-world
to check out the protocols of the MSK Advisory Board.

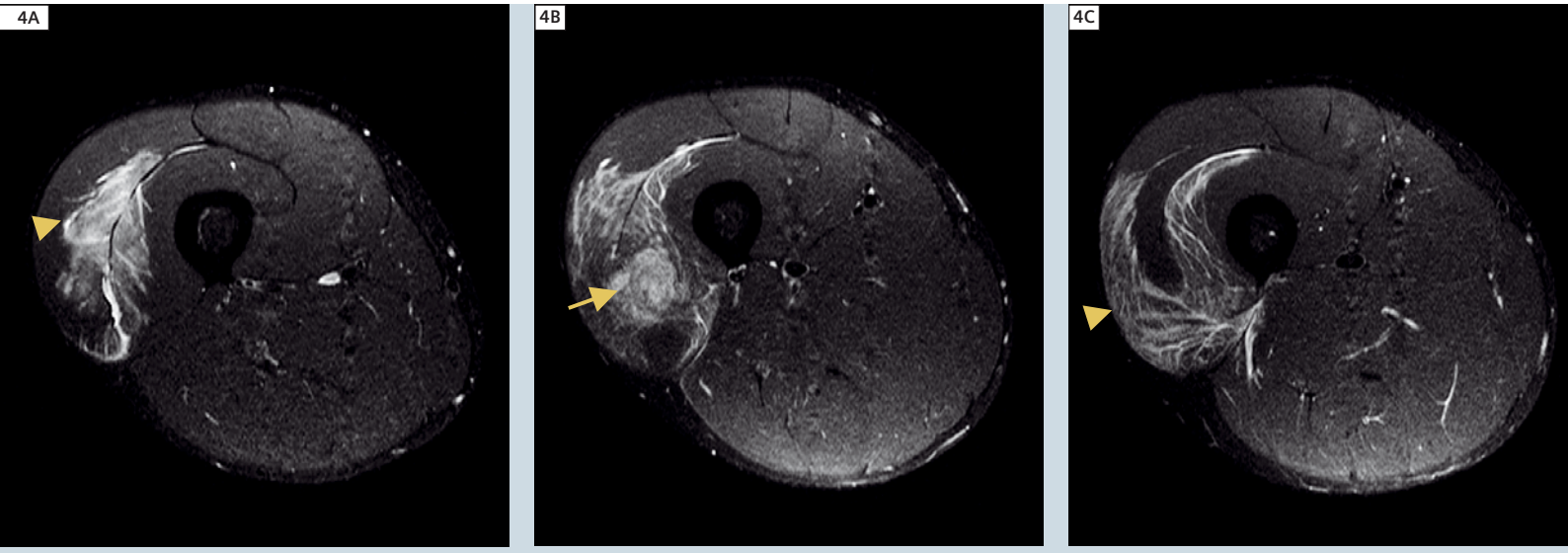

4A–C Transversal PDw STIR.

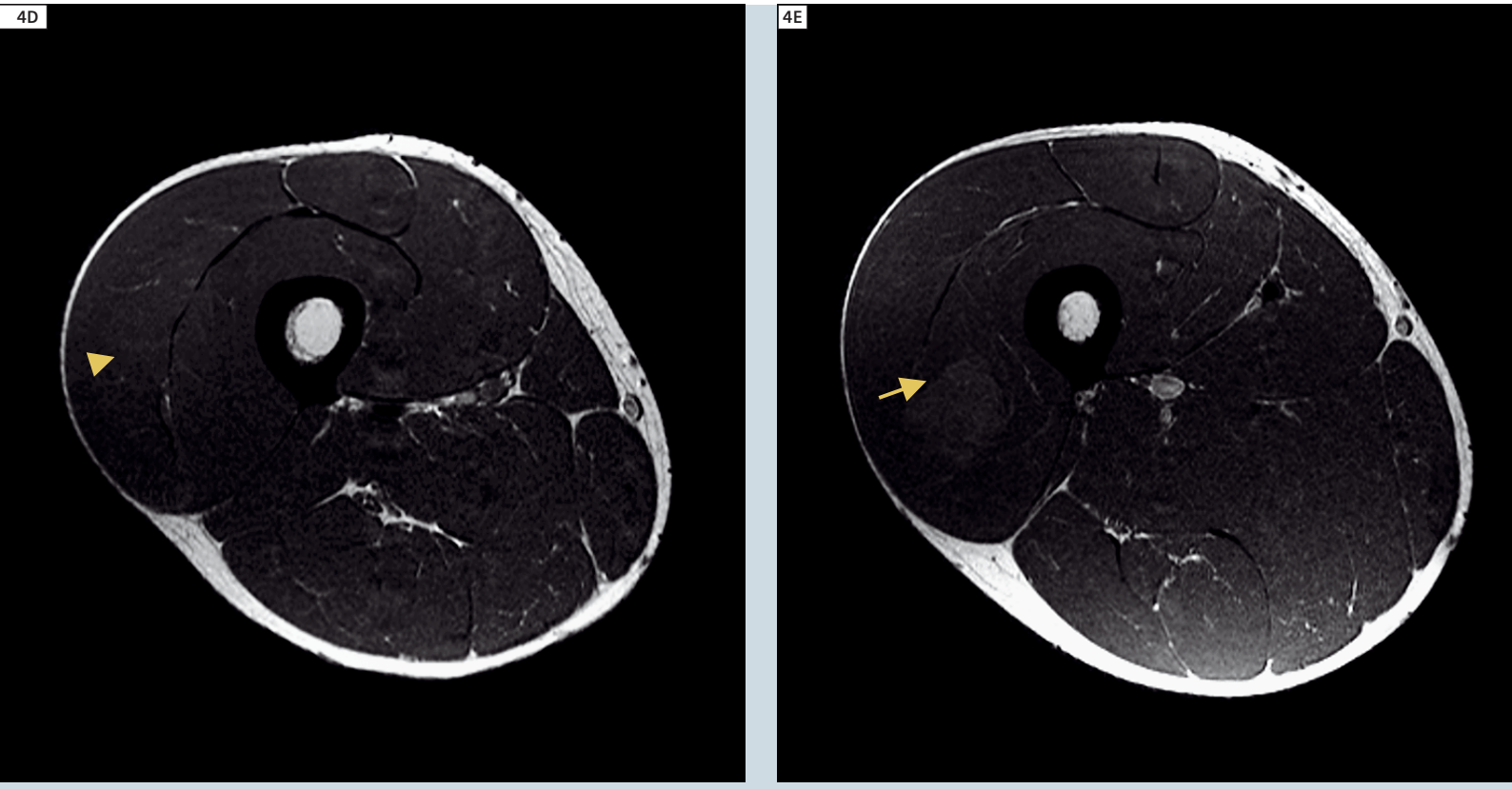

4D–E Transversal T1w TSE.

Case 4

24-year-old male soccer player after direct trauma (pound on right upper leg). On T2w images, a space occupying lesion within the lateral vastus muscle (arrow) and slight increased signal intensities on T1w images was seen, representing an extensive haematoma. Also a surrounding haemorrhage (arrowheads) was obvious. There were no clear signs of a tear in the muscles. The femur showed neither a fracture nor abnormalities of the signal intensities of the bone marrow.
Images were acquired using the Spine and Body Matrix coil. Sequence parameters for the shown images were:

- Transversal PDw STIR: TR / TE / TI = 8073 / 29 / 160 ms, SL 4 mm, FOV 220 x 220 mm, Matrix 224 x 320 px
- Transversal T1w TSE: TR / TE = 580 / 13 ms, SL 4 mm, FOV 200 x 200 mm, Matrix 256 x 320 px
- Sagittal PDw STIR: TR / TE / TI = 4580 / 29 / 160 ms, SL 4 mm, FOV 280 x 400 mm, Matrix 157 x 320 px
- Coronal T2w TSE: TR / TE = 7130 / 86 ms, SL 4 mm, FOV 281 x 399 mm, Matrix 216 x 384 px

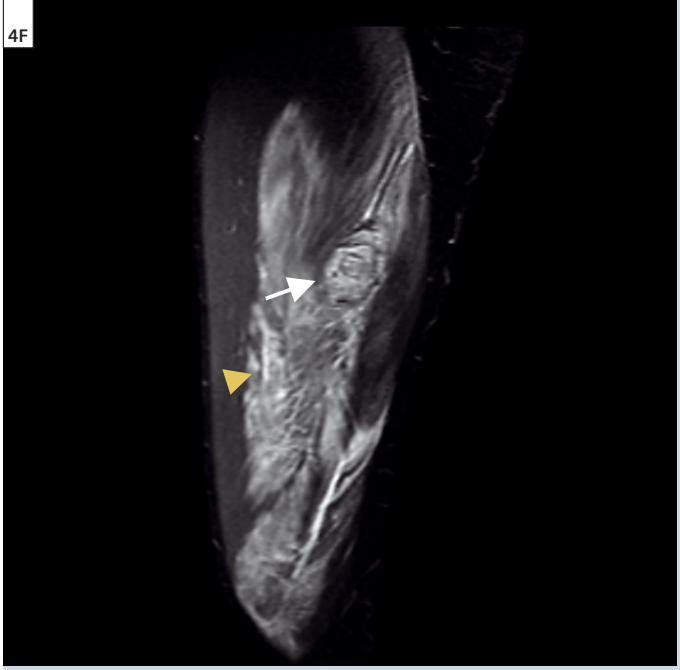

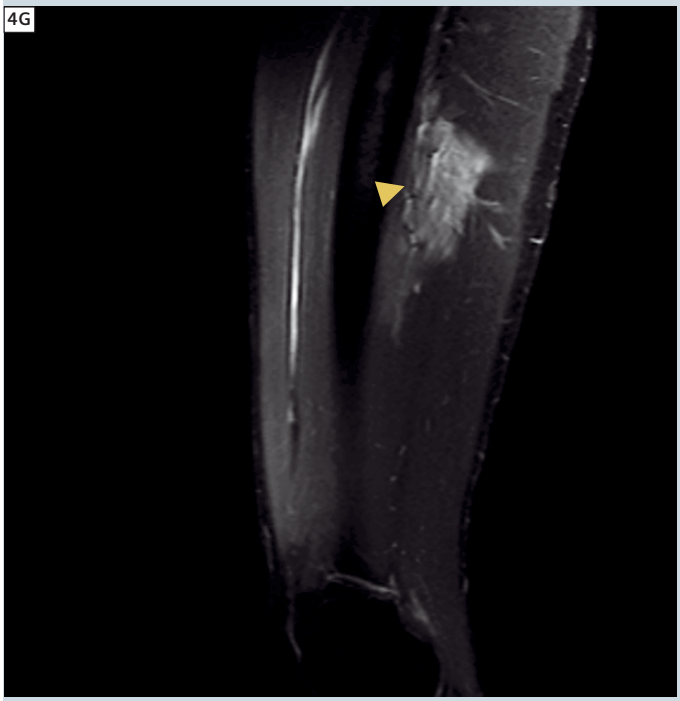

4F–G Sagittal PDw STIR.

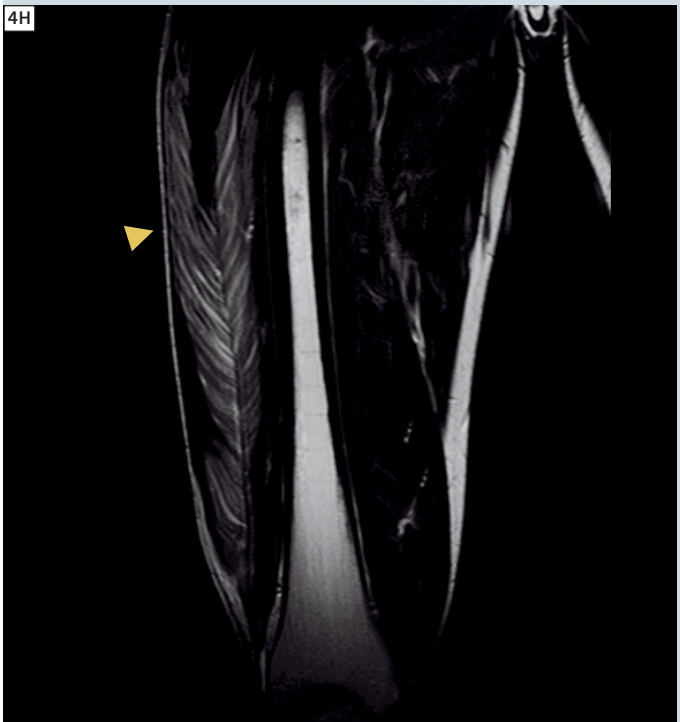

4H Coronal T2w TSE.

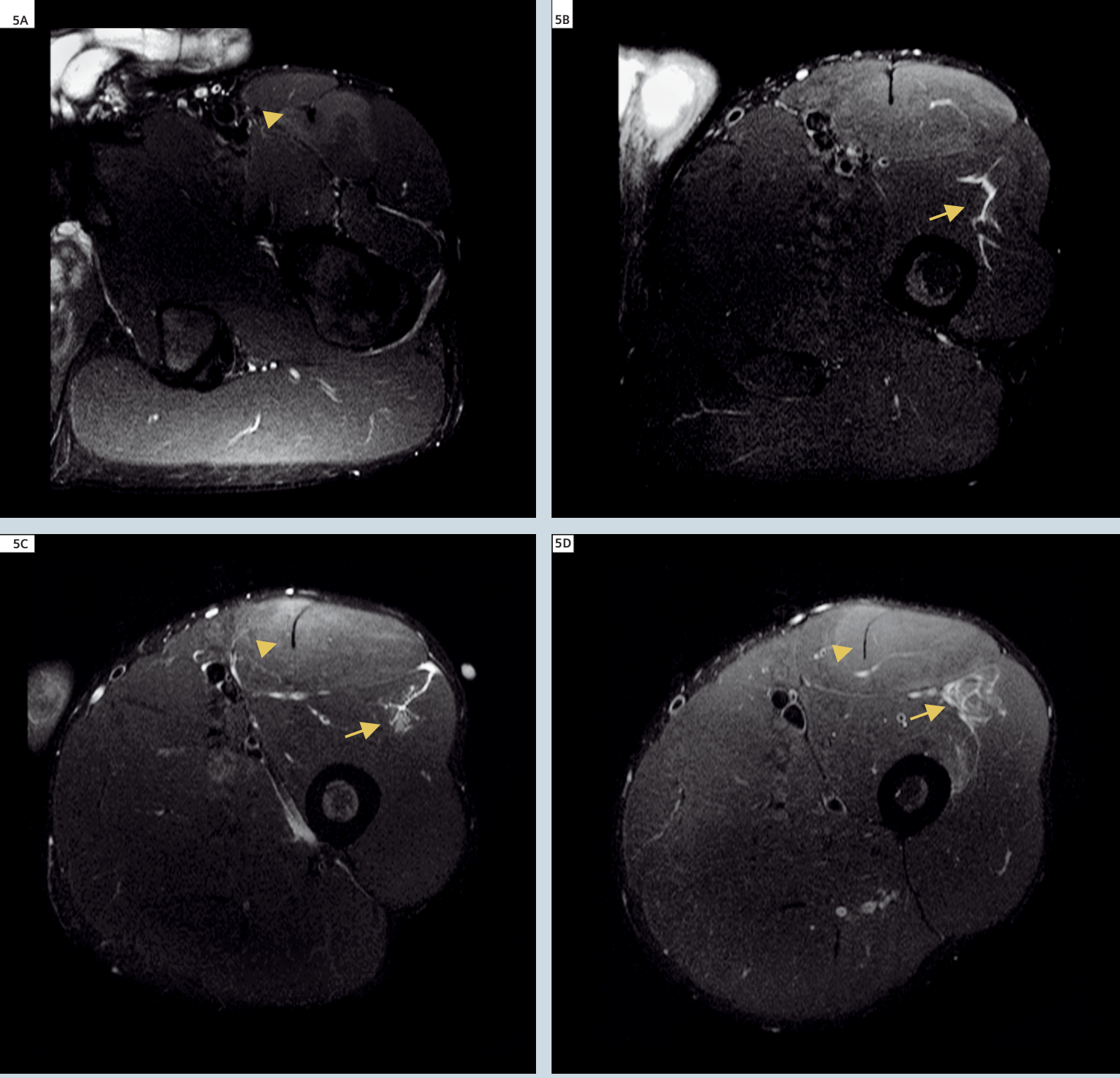

5A–D Transversal PDw STIR.

Case 5

24-year-old male soccer player after trauma.
In contrast to case 4, an approximate 15 mm long acute tear of the lateral vastus muscle (arrow) was seen in this patient but there were no signs of a dehiscence of the muscles. Slight increase of the signal intensities on PDw images within the vastus intermedius and rectus femoris muscles were rated as a strain.
The patient was positioned feet first and the images were acquired with the Spine and Body Matrix coil. Sequence parameters for the shown images were:

- Transversal PDw STIR: TR / TE / TI = 5390 / 29 / 160 ms, SL 4 mm, FOV 220 x 220 mm, Matrix 224 x 320 px

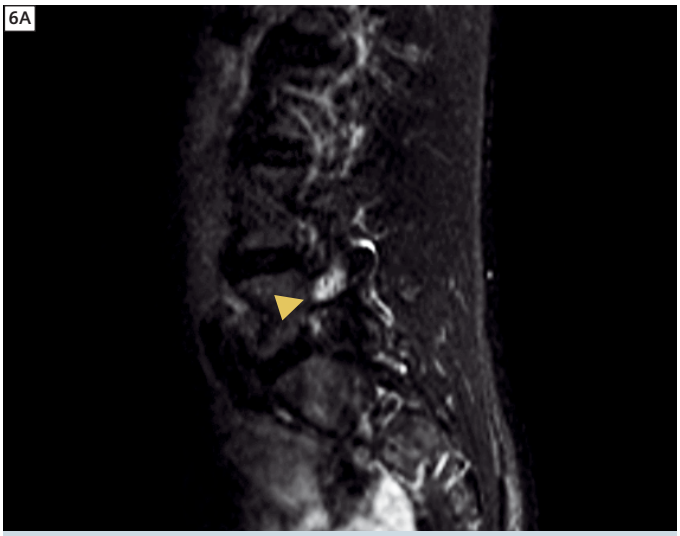

6A Sagittal T2w STIR.

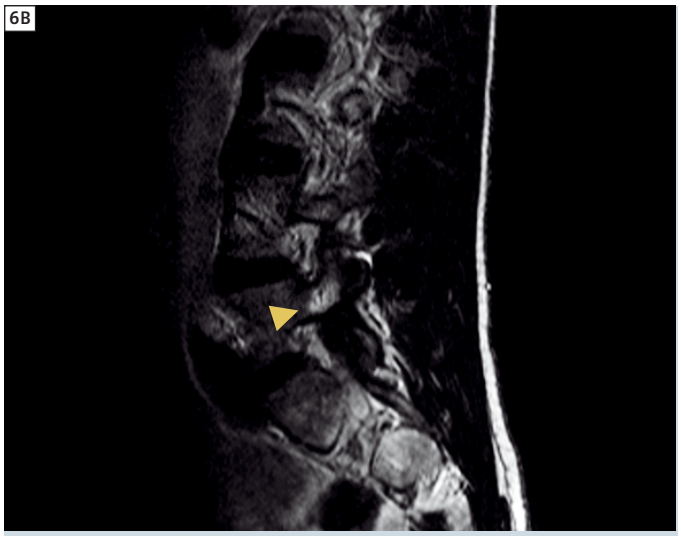

6B Sagittal T2w TSE.

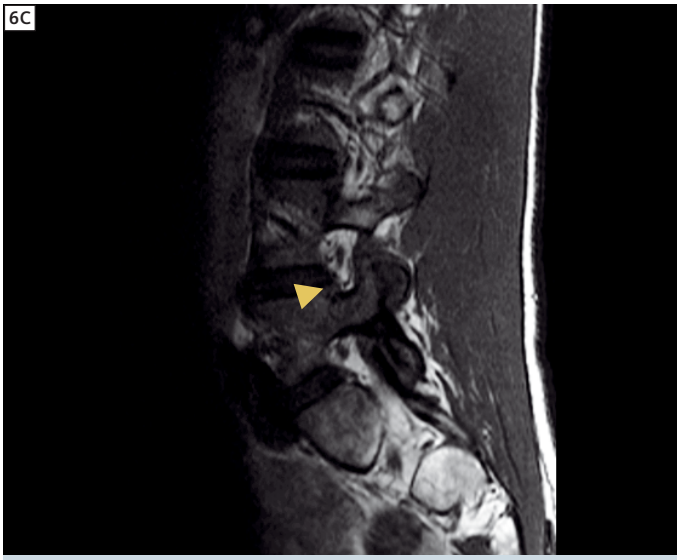

6C Sagittal T1w TSE.

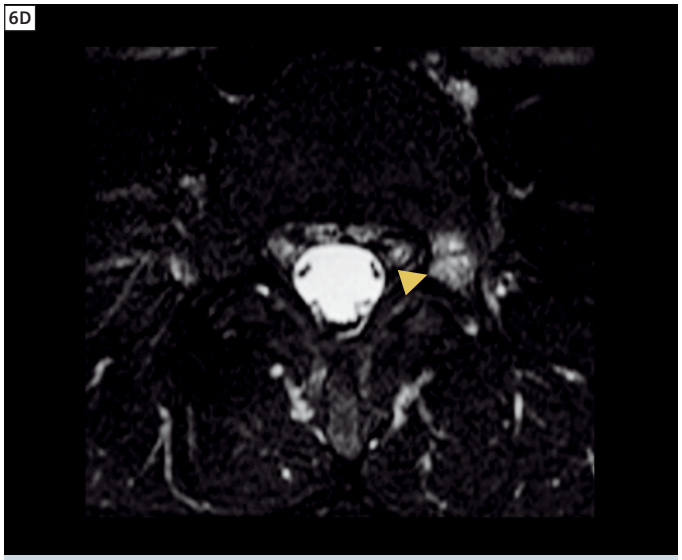

6D Oblique transversal T2w STIR.

Case 6

16-year-old female high-jumper with consistent pain during training sessions and while making sudden jerky movements.
High signal intensity within the bone marrow of the left pedicel of the 5th vertebra could be seen. Within this oedema, a continuous hypointense line was crossing the pedicel. This finding was rated as a 1st degree spondylolysis without signs of listhesis or cleft.
Images were acquired using the spine coil. Sequence parameters for the shown images were:

- Oblique transversal T2w TSE with spectral fat saturation: TR / TE = 3800 / 105 ms, SL 3 mm, FOV 180 x 180 mm, Matrix 192 x 256 px
- Sagittal T2w STIR: TR / TE / TI = 7300 / 63 / 150 ms, SL 3 mm, FOV 300 x 300 mm, Matrix 195 x 256 px
- Sagittal T1w TSE: TR / TE = 621 / 12 ms, SL 3 mm, FOV 280 x 280 mm, Matrix 269 x 384 px
- Sagittal T2w TSE: TR / TE = 8660 / 120 ms, SL 3 mm, FOV 280 x 280 mm, Matrix 269 x 384 px

Case 7

13-year-old female soccer player with pain within the right forefoot but without adequate corresponding trauma. Caudal of the epiphyseal line of the second metatarsal bone, an oedema of the bone marrow and very apical loss of shape of the bone and compression of bone trabeculae. The epihyseal line is of regular shape. The caudal head of the metacarbal bone is also surrounded by oedema and an effusion of the joint was present, too. These findings were concordant with an osteonecrosis in the stadium of vitrification (Morbus Köhler-Freiberg / Morbus Köhler II).

Images were acquired with the 4-channel flex coil. Sequence parameters for the shown images were:

- Coronal T2w STIR: TR / TE / TI = 4180 / 70 / 140 ms, SL 2 mm, FOV 140 x 140 mm, Matrix 460 x 512 px
- Coronal T1w TSE: TR / TE = 684 / 13 ms, SL 2 mm, FOV 140 x 140 mm, Matrix 256 x 512 px
- Sagittal T2w STIR: TR / TE / TI = 3700 / 70 / 140 ms, SL 2 mm, FOV 140 x 140 mm, Matrix 460 x 512 px
- Transversal T2w TSE: TR / TE = 3880 / 103 ms, SL 3 mm, FOV 89 x 130 mm, Matrix 352 x 512 px

Contact
Prof. Heinz-Peter Schlemmer, M.D; Ph.D.
Radiologie SpOrt Stuttgart
Fritz-Walter-Weg 19
D-70372 Stuttgart
Germany
h.schlemmer@Dkfz-Heidelberg.de
www.radiologie-neckarpark.de
www.sport-medizin.eu

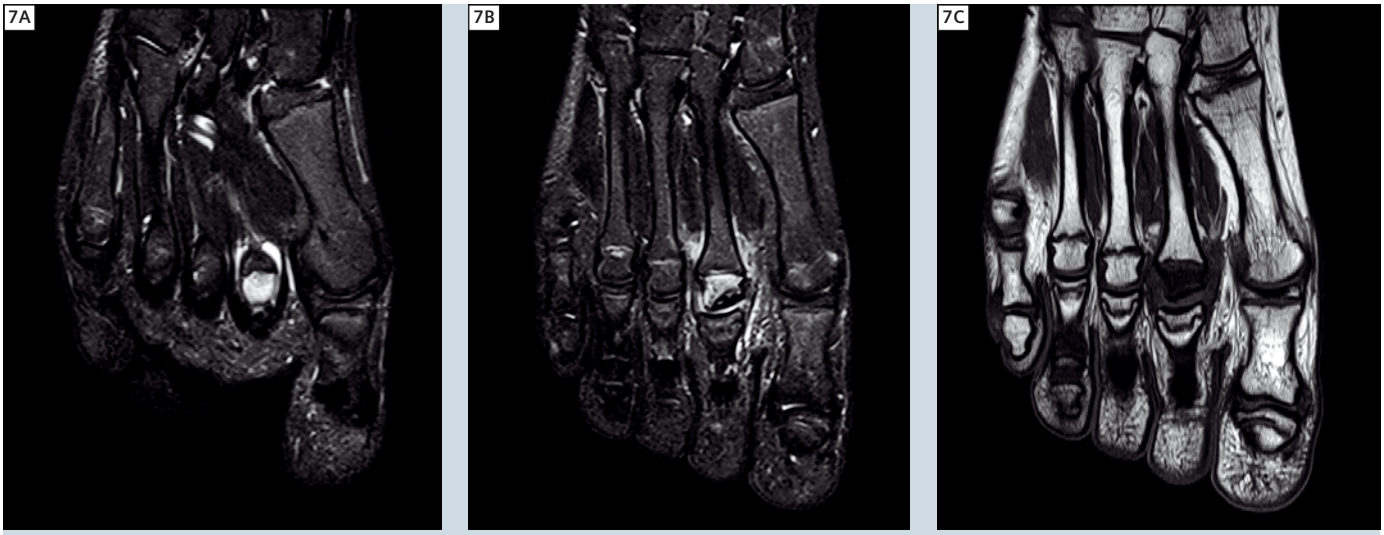

7A–C **A** and **B:** Coronal T2w STIR. **C:** Coronal T1w TSE.

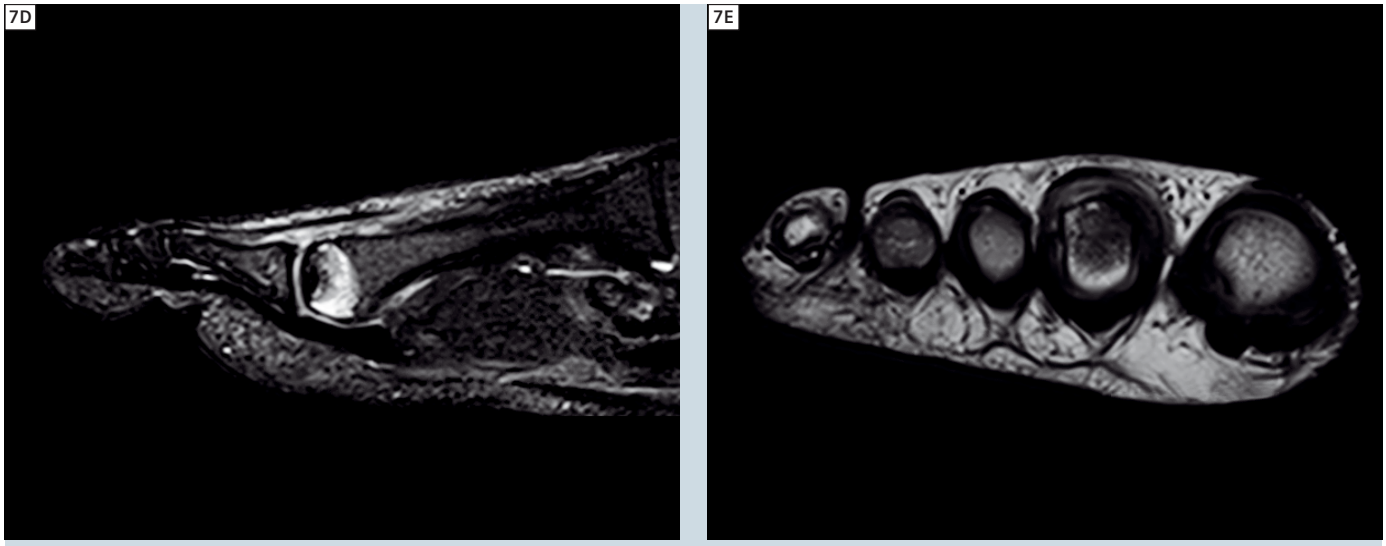

7D–E **D:** Sagittal T2w STIR. **E:** Transversal T2w TSE.

Missing information?

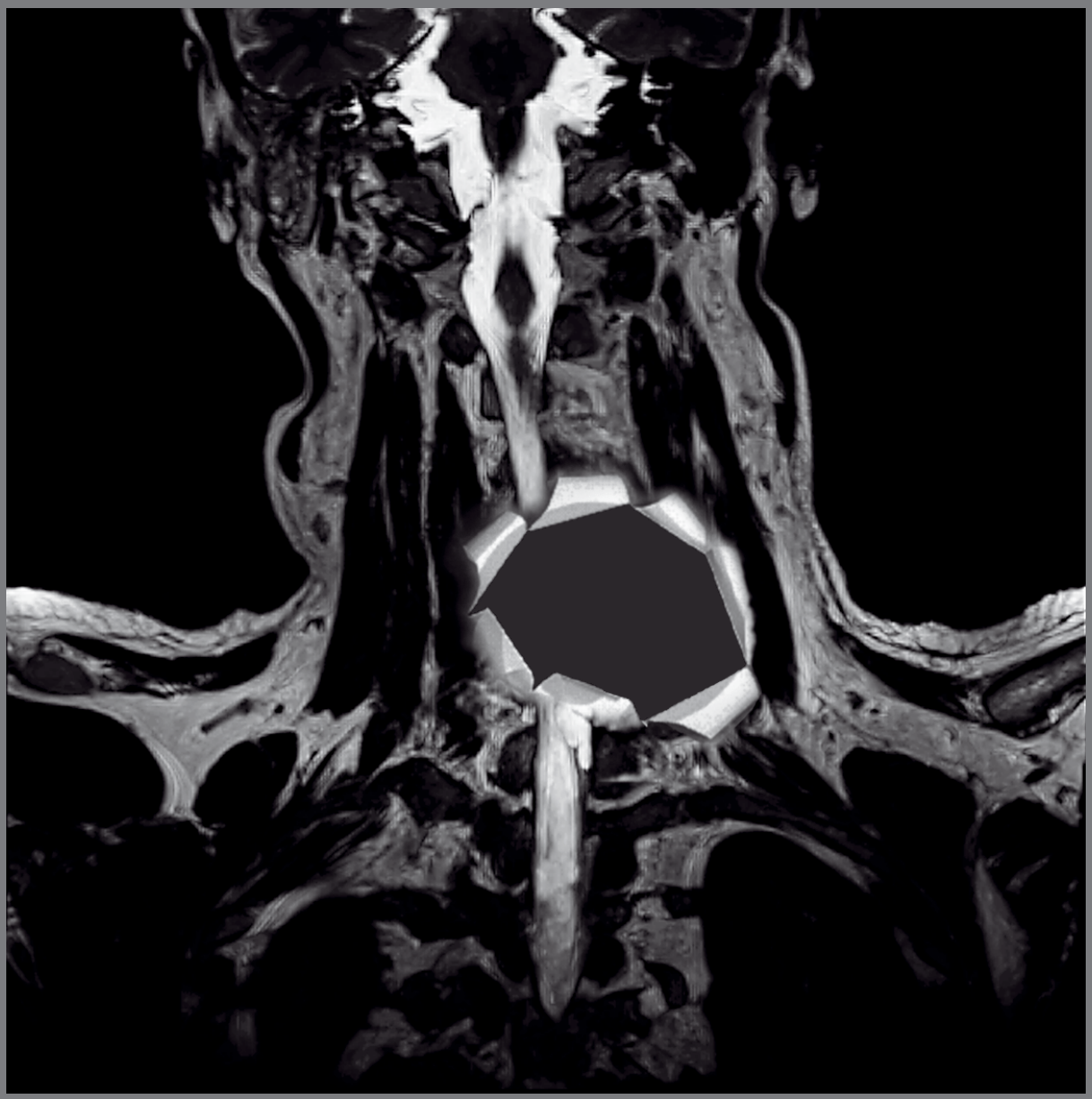

To make sure you have all the information you need, register for our free monthly newsletter on clinical MRI information.
Check out case reports from MAGNETOM users around the world and stay up-to-date with Siemens software applications.

Register at
www.siemens.com/magnetom-world
Go to
Publications > Subscriptions

Knee Imaging with 4-Channel Flex Coils. The Influence of Patient Positioning and Coil Selection on Image Quality

Birgit Hasselberg; Marion Hellinger

Siemens Healthcare, Erlangen, Germany

2

2 Patient positioned for an examination of the right knee. Both knees are positioned in one plane.

3

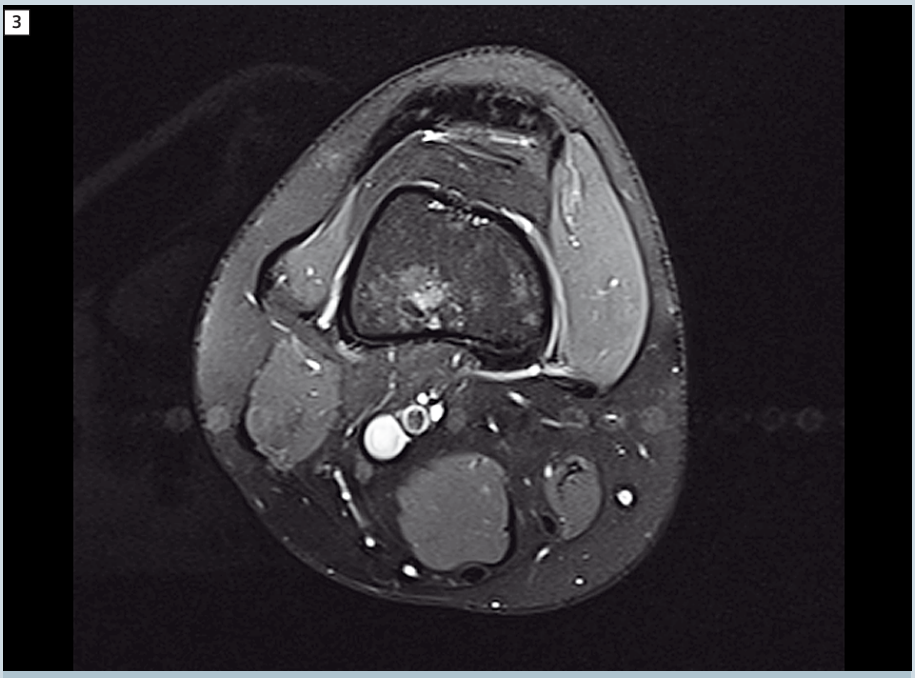

3 Using the Siemens protocol from clinical library arthrography Pd_tse_fs_tra_320, due to incorrect patient positioning, infolding effects of the not examined left knee are visible.

– Wrong

Correct patient positioning and the selection of the right coil have a huge influence on image quality as the following examples clearly show.

The patient is positioned supine on the table in feet-first orientation.
In the first case, the patient lies straight on the table; both knees are positioned in one plane.
The resulting transversal clinical image shows aliasing effects from the left knee (which is not being examined) in the left-right phase-encoding direction.

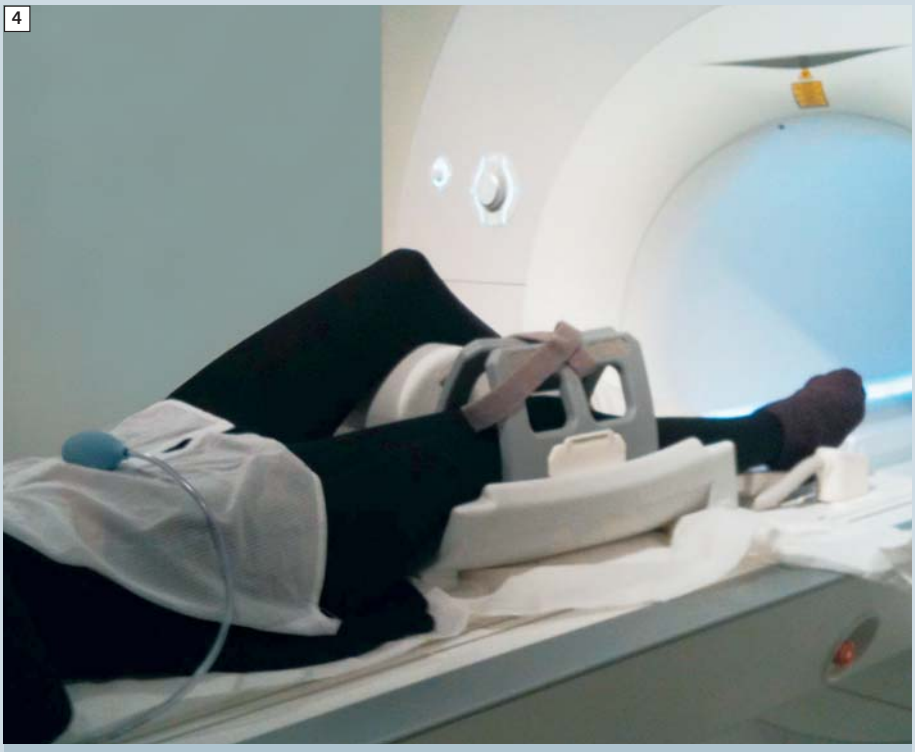

4 Patient correctly positioned for knee exam. The knee not being examined is positioned on a cushion.

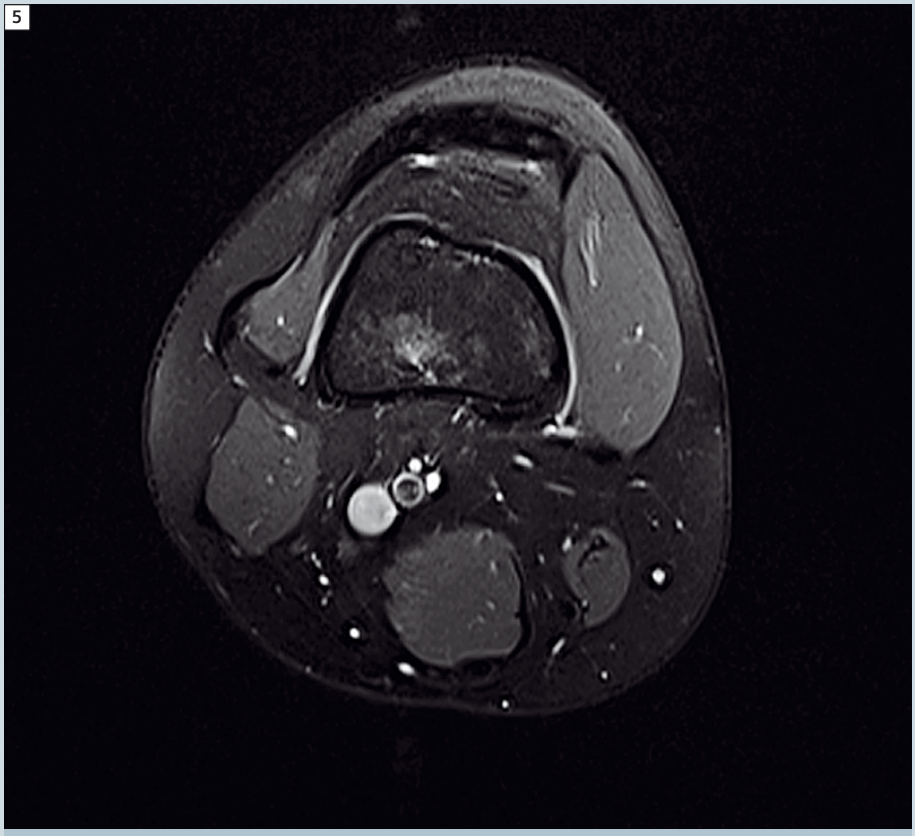

5 Again using the Siemens protocol from the clinical library arthrography Pd_tse_fs_tra_320. No infoldings due to correct patient positioning.

Right

Done right, the patient is again positioned supine on the table in feet first orientation. However, in this case the left knee is raised by a cushion in order to avoid the aliasing effect. The knee which is not examined is positioned higher than the examined knee.
The resulting transversal image shows no aliasing effects.

6

6 A small knee positioned in a large 4-channel flex coil.

7

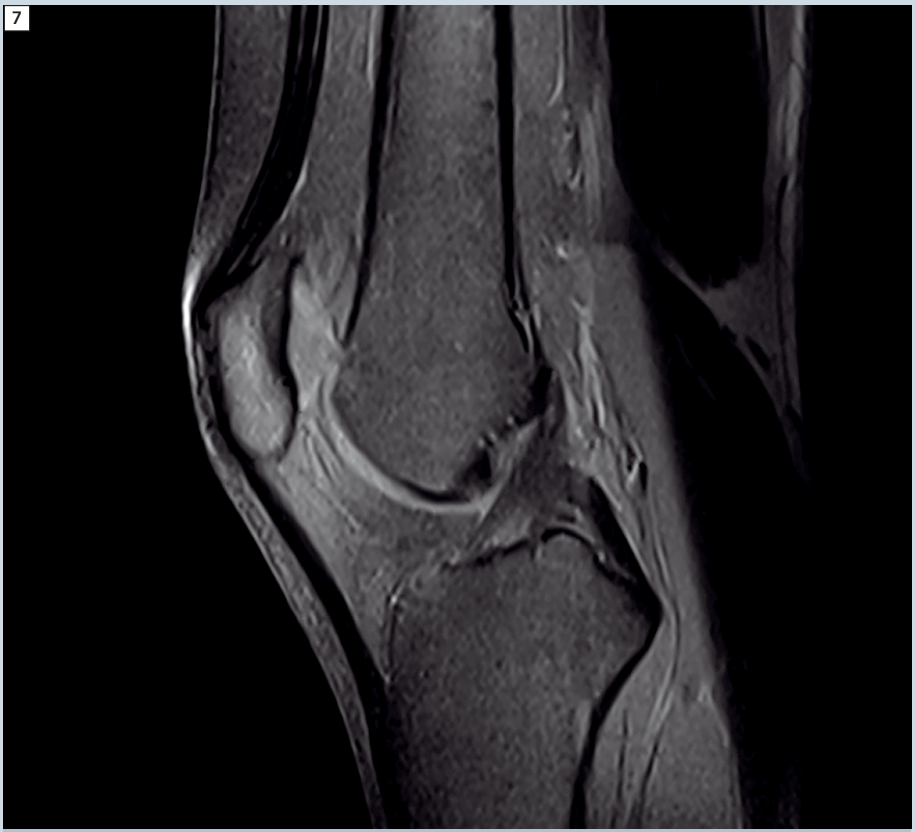

7 T1_tse_fs_sag_256 of a small knee in a large 4-channel flex coil, resulting in minor image quality.

Wrong

Besides correct patient positioning, the size of the knee in combination with the chosen coil has an effect on the image quality. The so-called "coil filling-factor" is demonstrated below. When you choose a coil which is too large for the examined body part, you get less overall signal which results in a minor image quality.

In the first case, the large 4-channel flex coil is used for the examination of a small knee.
The resulting sagittal series shows minor image quality: apart from minor signal-to-noise ratio, this also results in inhomogeneous signal distribution as well as fat suppression.

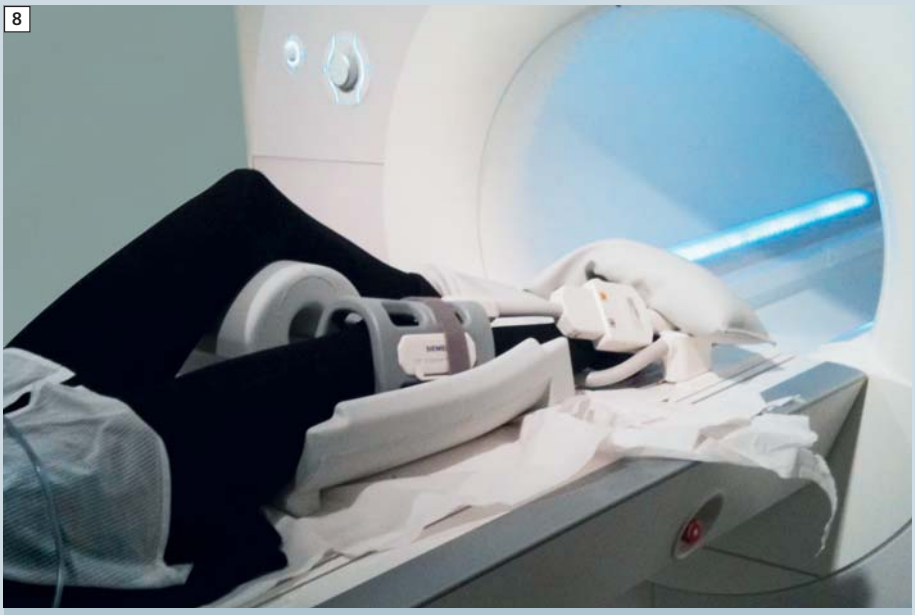

8 A small knee positioned correctly in a small 4-channel flex coil.

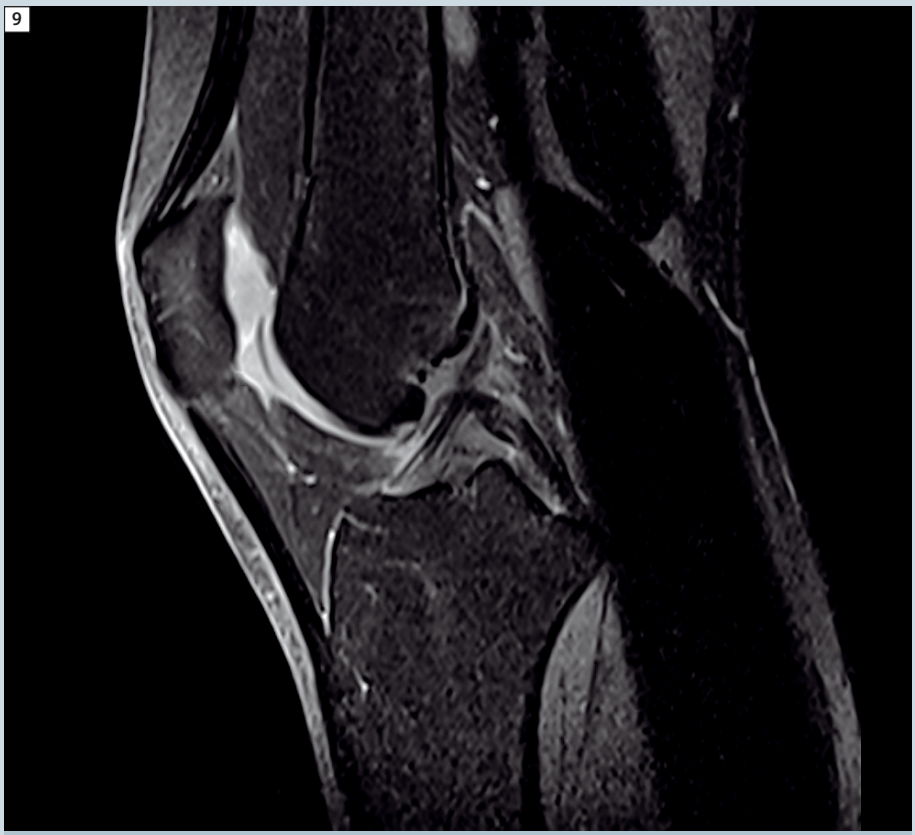

9 T1_tse_fs_sag_256 of a small knee examined with a small 4-channel flex coil, resulting in good SNR, good image quality. Compared to figure 7 there is good contrast and homogenous fat saturation in the bone.

Right

In the second case, the small 4-channel flex coil is used for the examination of a small knee. At the popliteal fossa we left the coil open
The resulting sagittal image shows a good SNR with an adequate image quality.

1

1 4-Channel Flex coil large and small

Finally, remember to position the patient in the isocenter of the magnet. The flexibility of the large and small 4-channel flex coils gives perfect support in optimal left-right positioning. As shown above, the 4-channel flex coils come in 2 sizes and are part of the standard system configuration. They provide superior signal-to-noise-ratio (SNR) and can be used for the examination of various body parts. The wrap around coil is made of soft and flexible material. Due to its 4-channel design it is iPAT-compatible. The coil can easily be combined with other coils such as Spine 32 and Body 18.

In summary, we can state that in knee examinations correct patient positioning and the selection of the right coil have a huge influence on the resulting clinical images.

Contact
Marion Hellinger
Siemens Healthcare
H IM MR PLM AW T Workflow
Allee am Roethelheimpark 2
D-91052 Erlangen
Germany
marion.hellinger@siemens.com

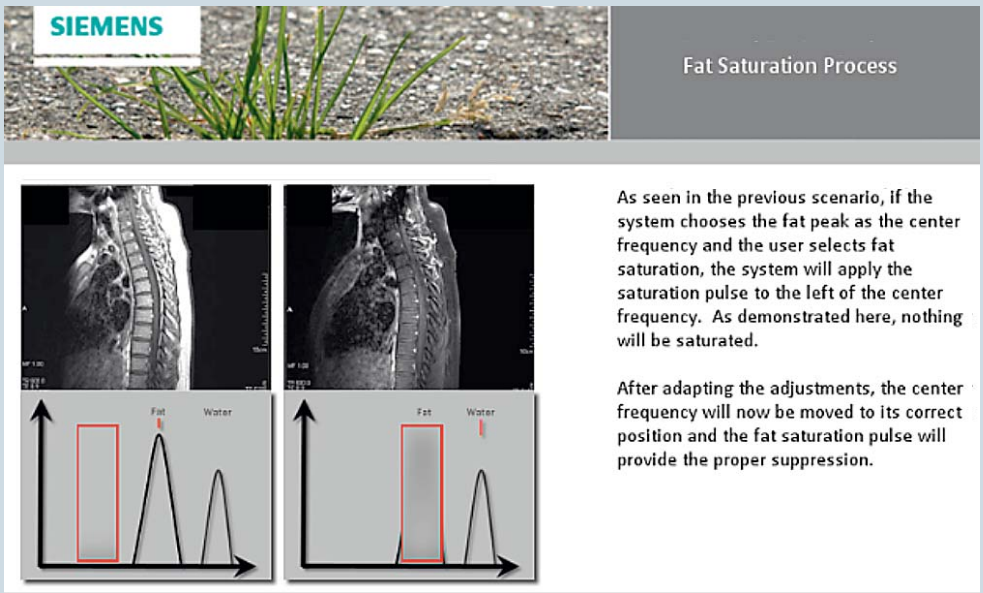

→ **Get free-of-charge application training at www.siemens.com/magnetom-world**

In this 8 min online training on fat saturation you will learn

- how to identify the fat and water peaks
- to calculate fat and water separation
- to perform the optimal fat saturation process

→ **Visit us at www.usa.siemens.com/fatsat-video**

Musculoskeletal Advisory Board Provides Protocols for 1.5 and 3T MAGNETOM systems

We have launched the MSK Advisory Board website, providing proven MSK protocols (.edx files) for download. To support Technologists there are also coil positioning videos and tips & tricks.

Board members are:

- Christian Glaser, LMU Grosshadern, Germany
- Jürg Hodler, University Hospital Zürich, Switzerland
- Young-Jo Kim, Harvard Medical School, Children's Hospital Boston, USA
- Tallal Charles Mamisch, Bern University, Switzerland
- Michael Recht, New York University, USA
- Siegfried Trattnig, AKH Wien, Austria
- Lawrence M. White, University of Toronto, Canada
- Marc-André Weber, University Hospital Heidelberg, Germany

Visit us at

www.siemens.com/magnetom-world

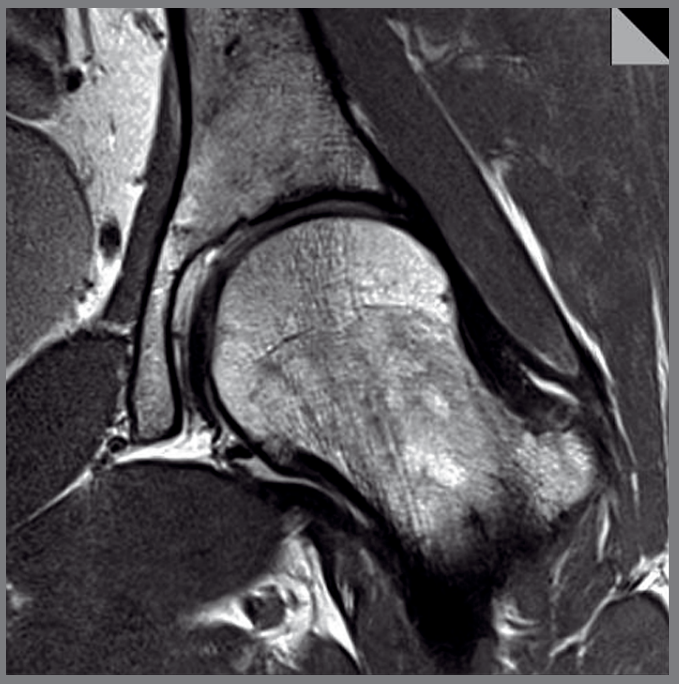

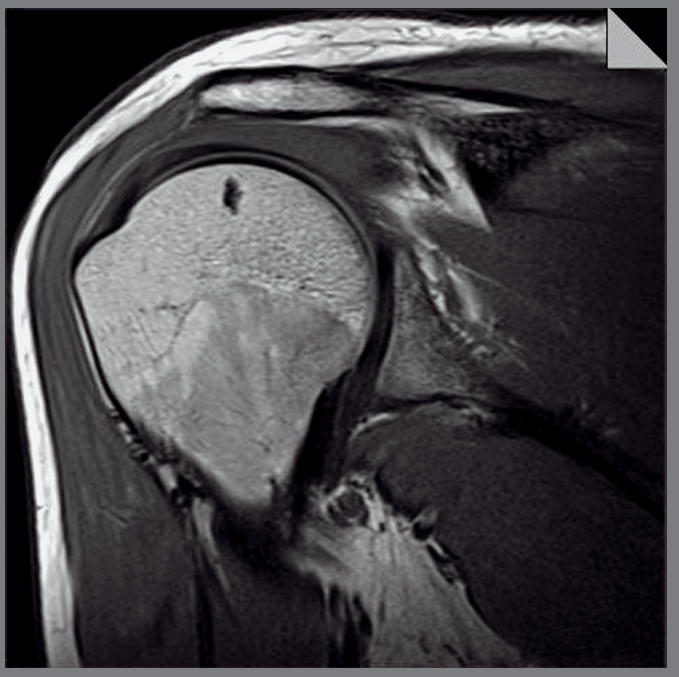

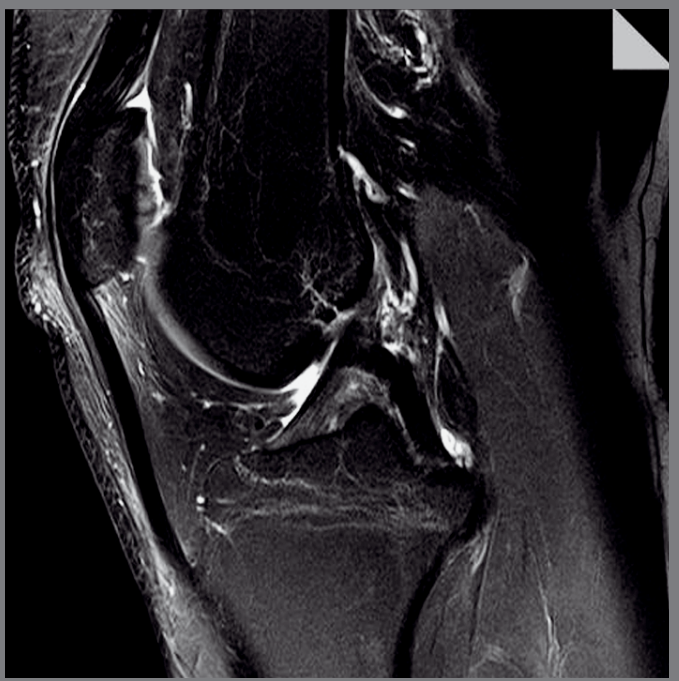

Case Report:
Snowboarding Injuries to the Middle Subtalar Joint. The Sustentacular Talocalcaneal Articulation

Anna K. Chacko, MD; Charles P. Ho, PhD, MD

Steadman Philippon Research Institute, Vail, Colorado, USA

In this case report we present two cases of injuries to the subtalar joint, specifically chondral defects of the middle facet of the talus and concomitant involvement of middle talocalcaneal or sustentacular articulation. These injuries were both sustained during snowboarding.

Patient history and imaging findings

A 26-year-old male snowboarder presents with a history of snowboarding injury 3 weeks prior to being scanned. Scarring and sprain of the anterior talofibular and calcaneofibular ligaments is observed. There is sprain and contusion of the deltoid ligament complex. A small talocrural effusion is seen with capsular sprain and scarring. Synovitis and debris are also seen in the anterior and posterior recesses. Bone edema and impaction fracture of the plantar medial aspect of the talar neck and head are seen with extension to the middle facet. At the sustentacular (middle facet) articulation an impaction fracture of the plantar medial aspect of the talar neck and head is observed (Fig. 1A). Chondral contusion, fracture and focal defects are also noted (Fig. 1B). There is ligamentous injury and partial tearing with sprain involving the talocalcaneal and interosseous cervical ligaments of the sinus tarsi. Bone edema, and impaction injury of the adjacent sustentaculum tali to medial portion of the body of the calcaneus are observed. Multiple chondral fragments are observed adjacent to the sustentaculum tali (Fig. 1C).

A 27-year-old male snowboarder presents with history of recent snowboarding injury. Clinically, a lateral process fracture was suspected. Mild impaction injury of the plantar aspect of the talar head with extension to the middle facet is seen (Fig. 2A). A focal sharply margin-

Table 1: Sequence details

Weighting and planes	FOV	TR	TE	Sequence	Slice thickness	Gap	Matrix size
T2- weighted axial	100	3860	108	Turbo Spin Echo	3 mm	0.3 mm	640 x 640
PD- weighted FS axial	100	3730	43	Turbo Spin Echo Fat suppressed	3 mm	0.3 mm	640 x 640
PD-weighted coronal	100	4340	33	Turbo Spin Echo	3 mm	0.3 mm	768 x 768
PD-weighted FS coronal	100	4660	43	Turbo Spin Echo Fat suppressed	3 mm	0.3 mm	640 x 640
PD-weighted sagittal	100	2840	34	Turbo Spin Echo	3 mm	0.3 mm	640 x 640
PD-weighted FS sagittal	100	2910	43	Turbo Spin Echo Fat suppressed	3 mm	0.3 mm	640 x 640

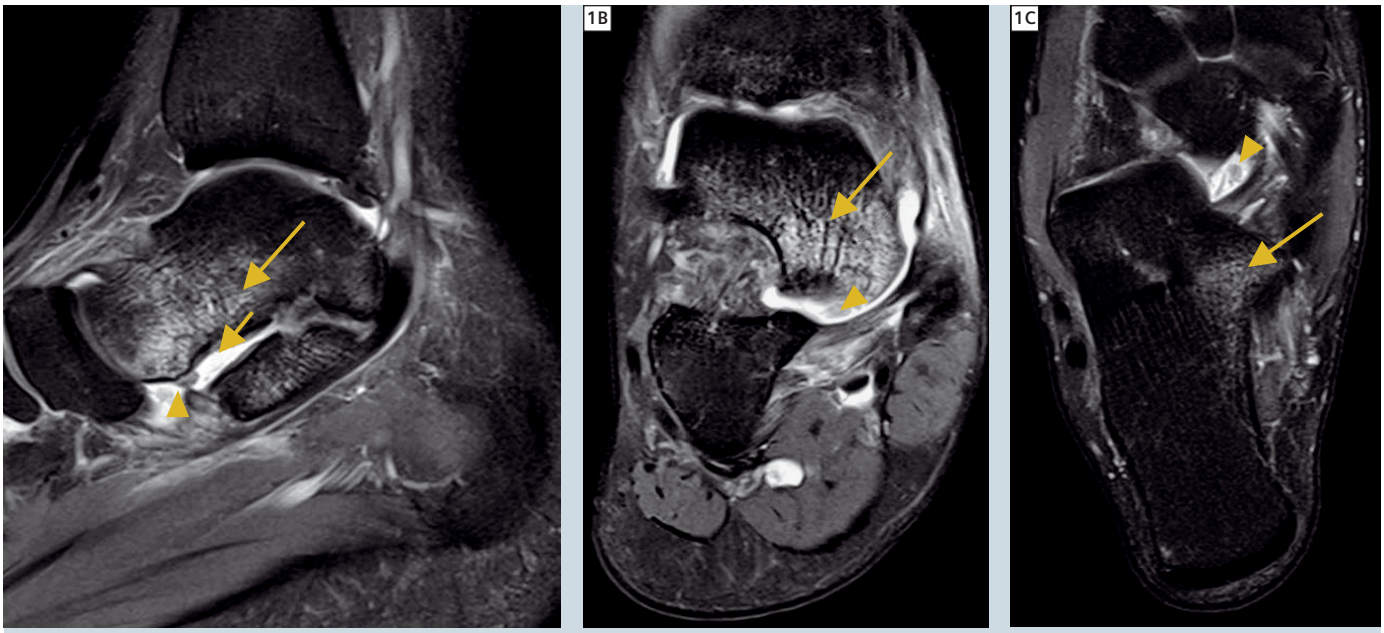

1 26-year-old snowboarder presents with subtalar injury. **1A:** PD-weighted Turbo Spin Echo fat suppressed sagittal images through the ankle demonstrate the multiple components of this injury. Bone marrow edema shows the site of the impaction fracture of the middle facet of the talus (long arrow). Chondral defect is noted in the articular cartilage of the middle facet on the inferior aspect of the talus (short arrow). Chondral fragment (arrow head). **1B:** PD-weighted Turbo Spin Echo fat suppressed coronal images through the ankle demonstrate bone marrow edema at the site of the impaction fracture of the middle facet of the talus (long arrow). Chondral fragment (arrow head). **1C:** PD-weighted Turbo Spin Echo fat suppressed axial images through the ankle. Bone marrow edema shows the site of the impaction fracture at the sustentaculum tali (long arrow).Chondral fragment (arrow head).

ated chondral defect is observed (Fig. 2B) with adjacent chondral fragment (Fig. 2C). For the MR evaluation of the ankle joint on the 3T MAGNETOM Verio MR scanner (Siemens Healthcare, Erlangen, Germany), the first of our axial image set is routinely a T2-weighted Turbo Spin Echo (TSE) sequence, paired with an axial Proton Density (PD) TSE fat suppressed (FS) sequence. These are then followed by PD-weighted TSE sequences with and without fat suppression in the sagittal and coronal planes. Details of our imaging parameters are presented in Table 1.

Discussion

There is a large body of radiologic literature describing both osseous and ligamentous injuries, to the ankle and hindfoot particularly involving athletic endeavours such as skiing, basketball, football etc. However, injuries to the subtalar joints do not find their way into these discussions. Furthermore, discussions of involvement of the middle facet of the talus and the middle talocalcaneal sustentacular articulation are even more sparse. This may very well have been due to the "inaccessibility" of the area to imaging examination. The advent of MR imaging and the ability to achieve finer resolution and better signal-to-noise ratios may have changed the landscape. Snowboarding is significantly so different from skiing that the prevalence and distribution of injuries are commensurately different. Snowboarders stand on their boards very similar to skateboarders or surfers. They stand sideways on their board with the rear foot at 90 degrees to the long axis of the board and the front foot positioned between 45 and 90 degrees to the long axis of the board. The snowboarder executes turns by shifting body weight to the front foot and by swinging the tail of the board to swing out. Since poles are not used, the arms and hands are used to break a fall. The bindings, the type of boot, the patterns of the lead foot etc. are believed to be responsible for the patterns of injury. Upper limb and ankle injuries are more common among snowboarders than skiers. Ankle injuries are the third most common injuries in snowboarders (16%) versus skiers (6%). These ankle injuries which are torsional could be accompanied by talocalcaneal/subtalar injuries which may go undetected. Undetected subtalar injuries and attendant instability can set the stage for significant chronic problems. These injuries are better dealt with acutely rather than chronically.

The talus and the subtalar joints are part of a complex biomechanical entity with multiple degrees of freedom where the talocrural (ankle) joint acts in concert with the subtalar and talocalcaneonavic-

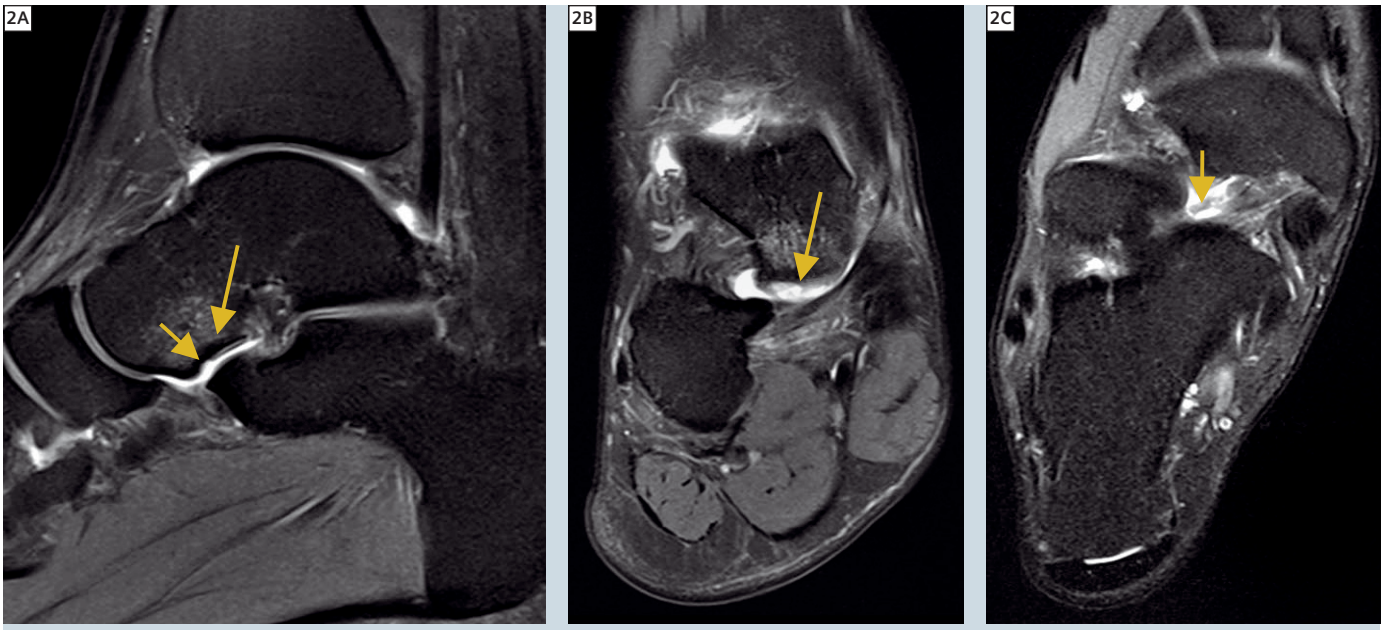

2 27-year-old snowboarder presents with subtalar injury. **2A:** PD-weighted Turbo Spin Echo fat suppressed sagittal images through the ankle demonstrate bone marrow edema at the site of the impaction fracture of the middle facet of the talus (long arrow). Chondral defect is noted in the articular cartilage of the middle facet on the inferior aspect of the talus (short arrow). **2B:** PD-weighted Turbo Spin Echo fat suppressed sagittal images through the ankle demonstrate the chondral defect in the articular cartilage of the middle facet on the inferior aspect of the talus (arrow). **2C:** PD-weighted Turbo Spin Echo fat suppressed axial images through the ankle demonstrate single chondral fragment adjacent to the sustentaculum tali (arrow).

ular joints providing significant complexity and multiaxiality of function. This allows the foot to accommodate to irregular terrain. Patients presenting with ankle/talocrural joint injuries must be examined carefully for subtalar injuries. The three talocalcaneal articulations can be visualized on standard planes on MR. However, subtle injuries with osteochondral fractures require greater attention to detail with high resolution.

The talus is shaped like a truncated cone and ligament stability of the talocrural and subtalar joints is dependent on the lateral collateral, the cervical and the talocalcaneal interosseous ligaments.

Contact
Charles P. Ho, PhD, MD
Steadman Philippon Research Institute
181 W. Meadow Dr. Suite 1000
Vail, CO 81657
USA
Karen.briggs@sprivail.org

References

1 PinoColville: Snowboard Injuries. American Journal of Sports Medicine: Vol 17, No 6, 1989.
2 Bladin C et al: Australian snowboard injury database study: A four year prospective study. American Journal of Sports Medicine: Vol 21, 701, 1993.
3 Ligamentous injuries about the ankle and subtalar joints. Zwipp H Clin Podiatr Med Surg 2002 Apr; 19 (2): 195-229.
4 Challenging fractures of the foot and ankle Prozuski LJ, Saltzman CL Radiol Clin North Am: 1997 May; 35 (3): 655-70.
5 Ankle and foot trauma. Mulligan ME. Semin Musculoskelet Radiol. 2000; 4 (2): 241-53.
6 Chronic ankle instability: biomechanics and Pathomechanics of ligamentous injury and associated lesions. Bonnel F, et al: Orthop Traumatol Surg Res 2010 Jun: 96 (4): 424-32.
7 Lateral ankle sprains: a comprehensive review, Part 1: etiology, pathoanatomy, histopathogenesis and diagnosis. Med.Sci. Sports Exerc., Vol 31, no. 7 (Suppl.) pp S429-S437,1999.
8 Fractures of the talus Skeletal Radiology Volume 26, Number 3, 137-142, DOI: 10.1007/s002560050209.
9 Wechsler RJ et alHelical Ct of fractures of the talus Skeletal Radiol (1997) 26:137-142 International skeletal Society 1997.
10 Osteochondral lesions of the talus – Canale and Belding RH JBJS Am 1980:62:97-102.
11 Osteochondral Lesions of the Talus Schachter et al. J Am Acad Orthop Surg.2005; 13: 152-158.
12 Characterizing osteochondral lesions by magnetic resonance imaging DiPaola JD et al Arthroscopy: The journal of Arthroscopic and related Surgery VOL 7 Issue 1 March 1991 101-104.
13 Osteochondritis dissecans: a review and new MRI classification Bohndorf K VOL 8 Number 1 103-112.
14 Osteochondral lesions of the talus in a sports medicine clinic. A new radiographic technique and surgical approach Thompson JP et al Am Journal of Sports Medicine December 1984 vol 12 no 6 460-463.
15 Challenging fractures of the foot and ankle Prozuski LJ, Saltzman CL Radiol Clin North Am: 1997 May; 35 (3): 655-70.
16 JBJS: Mulfinger GL and Trueta J Blood supply of the talus VOL 52B No. 1 February 1970.
17 Ankle and foot trauma. Mulligan ME. Semin Musculoskelet Radiol. 2000; 4 (2): 241-53.
18 Chronic ankle instability: biomechanics and Pathomechanics of ligamentous injury and associated lesions. Bonnel F, et al: Orthop Traumatol Surg Res 2010 Jun: 96 (4): 424-32.
19 Lateral ankle sprains: a comprehensive review, Part 1: etiology, pathoanatomy, histopathogenesis and diagnosis. Med.Sci. Sports Exerc., Vol 31, no. 7 (Suppl.) pp S429-S437, 1999.
20 Solomon MA et al CT scanning of the Foot and Ankle: I Normal anatomy AJR 146: 1192-1203 June 1986.

Case Report:
Chondral Fracture of the Talar Dome and Diastasis of the Os Trigonum

Anna K. Chacko, MD; Charles P. Ho, PhD, MD

Steadman Philippon Research Institute, Vail, Colorado, USA

Patient history

We present the magnetic resonance (MR) images of the right ankle of a 34-year-old male police officer complaining specifically of pain deep in the right ankle for 4 years. He has had a history of several small uneventful injuries over the past several years, since high school. Physical activity such as running is hampered by the pain in the right ankle as well as the right knee. On physical examination of his ankles, there is mild tenderness along the anterior aspect of the ankle joints. He is more tender on the anterolateral ankle joint and lateral gutter. He has negative tenderness posterior to his peroneal tendons. Anterior drawer and tilt tests were negative.

Imaging findings

We present Magnetic Resonance images of the right ankle with significant findings related to his complaints in his right ankle.

The right ankle was imaged using a 3T MAGNETOM Verio MRI scanner (Siemens Healthcare, Erlangen, Germany) with a dedicated 8-channel ankle coil. The ankle was imaged in the sagittal, coronal and axial planes. These included proton density (PD), T2-weighted non fat suppressed as well as fat suppressed images for the coronal and sagittal planes. Axial images were obtained with T2-weighting for the non-fat-suppressed images and PD-weighting for the fat suppressed images. We utilized slice thicknesses of 3 mm in all planes. Details of the techniques used are outlined in Table 1.

Several abnormalities involving the ligaments in and around the ankle joint were noted on multiple images. However, there are two findings which are well demonstrated in this case.

The first is the presence of the chondral fragment in situ noted on the images

Table 1: Sequence details

Weighting and planes	FOV	TR	TE	Sequence	Slice thickness	Gap	Matrix size
T2-weighted axial	100	3860	108	Turbo Spin Echo	3 mm	0.3 mm	320 x 256
PD-weighted axial fat suppressed	100	3730	43	Turbo Spin Echo fat suppressed	3 mm	0.3 mm	320 x 256
PD-weighted sagittal fat suppressed	100	2910	43	Turbo Spin Echo fat suppressed	3 mm	0.3 mm	320 x 256
PD-weighted sagittal	100	2660	35	Turbo Spin Echo	3 mm	0.3 mm	384 x 326
PD-weighted coronal fat suppressed	100	4660	43	Turbo Spin Echo fat suppressed	3 mm	0.3 mm	320 x 256
PD-weighted coronal	100	4340	35	Turbo Spin Echo	3 mm	0.3 mm	384 x 326

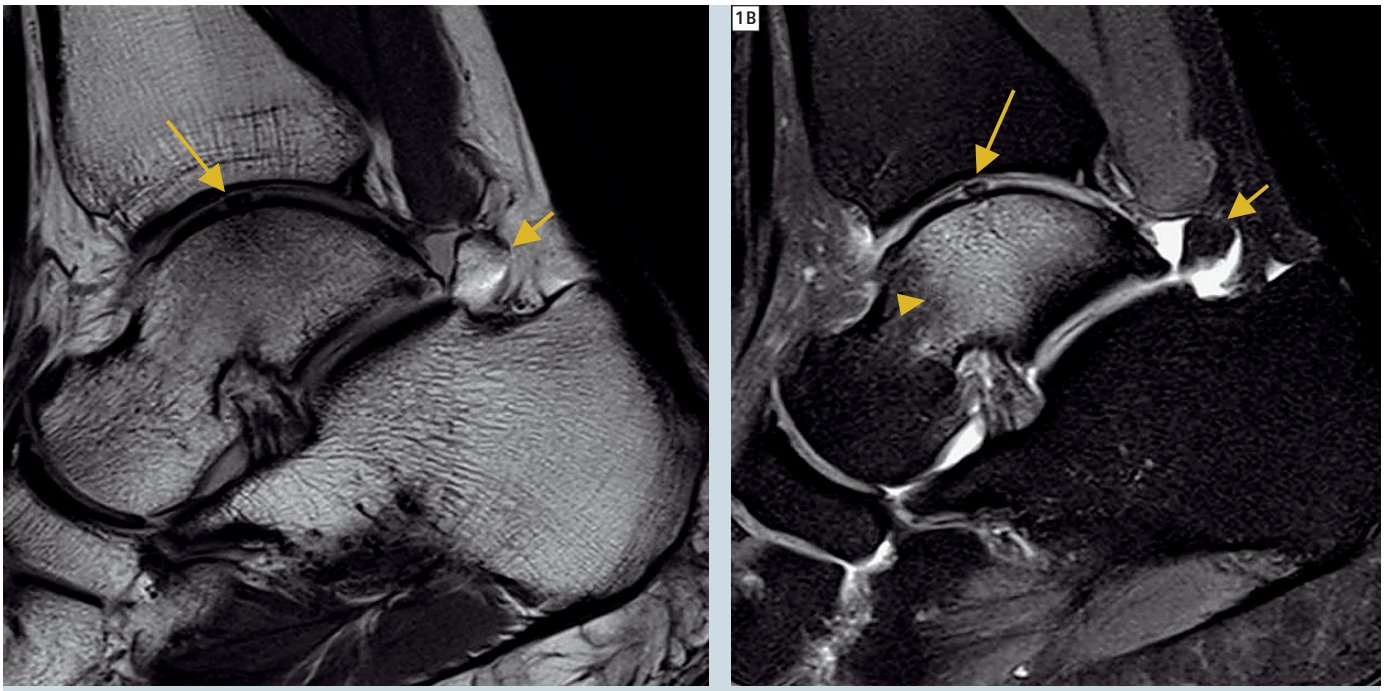

1 Sagittal images of the ankle. **1A:** PD-weighted sagittal image which shows the chondral fragment on the talar dome (long arrow) and the diastased os trigonum (short arrow). **1B:** Fat suppressed PD-weighted TSE image which again demonstrates the chondral fragment (long arrow) and the diastased os trigonum (short arrow). The increased signal in the body of the talus (arrowhead) is consistent with edema in the bone marrow as a result of the repetitive irritation caused by instability and ongoing motion of the chondral fragment.

displayed in Figures 1 and 2. The chondral fragment is particularly well delineated by the contrast provided by the effusion surrounding the fragment and the extensive prominent underlying bone edema in the ankle joint and talar dome areas. The chondral fragment measures approximately 3–4 mm and is seen along the mid talar dome. There is underlying osseous irregularity, surrounding chondral focal fissuring. Extensive prominent increased signal is noted in the talar dome and the body which may be reactive stress-related edema and/or contusion and possible ongoing motion/instability of the fragment. The adjacent tibial plafond demonstrates chondral thinning and fissuring to bone (Grade IV – Outerbridge). Cortical irregularity, sclerosis and remodeling are also noted. The presence of increased signal in the body of the talus on the fat suppressed Turbo Spin Echo images (Figs. 1B and 2B) signifies the presence of bone edema which is most likely due to the irritation of the chondral fragment which is located at a strategic point trapped at the mid weight bearing portion of the talar dome.

The second is the separation and posterior tilting of the os trigonum. The os trigonum appears diastased by approximately 3 mm from the lateral tubercle of the posterior process with high signal widening of the synchondrosis. This is most likely related to injury and chronic separation at the synchondrosis. The findings of the diastased os trigonum are visualized on the sagittal images seen in Figures 1A and B.

Discussion

1. Chondral or osteochondral fracture of the talar dome: Ligamentous injuries of the ankle are among some of the most common sports related injuries involving the ankle. When the pain becomes chronic or persistent, associated osteochondral contusion or fracture should be considered. Opposing lesions which involve the plafond and the adjacent talar dome as in this patient should be sought. While the clinical significance of bone contusion has not been established [1] osteochondral fractures do need to be treated.

Of the 146 ankles imaged in the series analyzed by Sijbrandij et al., it was found that bone contusion occurred in the tibial plafond while osteochondral fractures occurred more commonly in the talar dome. They conclude that the opposing lesions occur due to impaction of the talus on the tibia. In this case, however the lack of bone contusion in the plafond suggests that the plafond injury is chronic with resolution of the edema. The presence of the talar edema with the osteochondral fracture of the talar dome suggests that ongoing local movement and instability of the osteochondral fragment could be producing a localized bone injury and consequent stress related edema.

Sijbrandij also opined that the explanations for the higher occurrence of the subchondral fractures in the talus rather in the plafond is most likely due to the fact that the osteochondral lesions are more commonly observed on convex

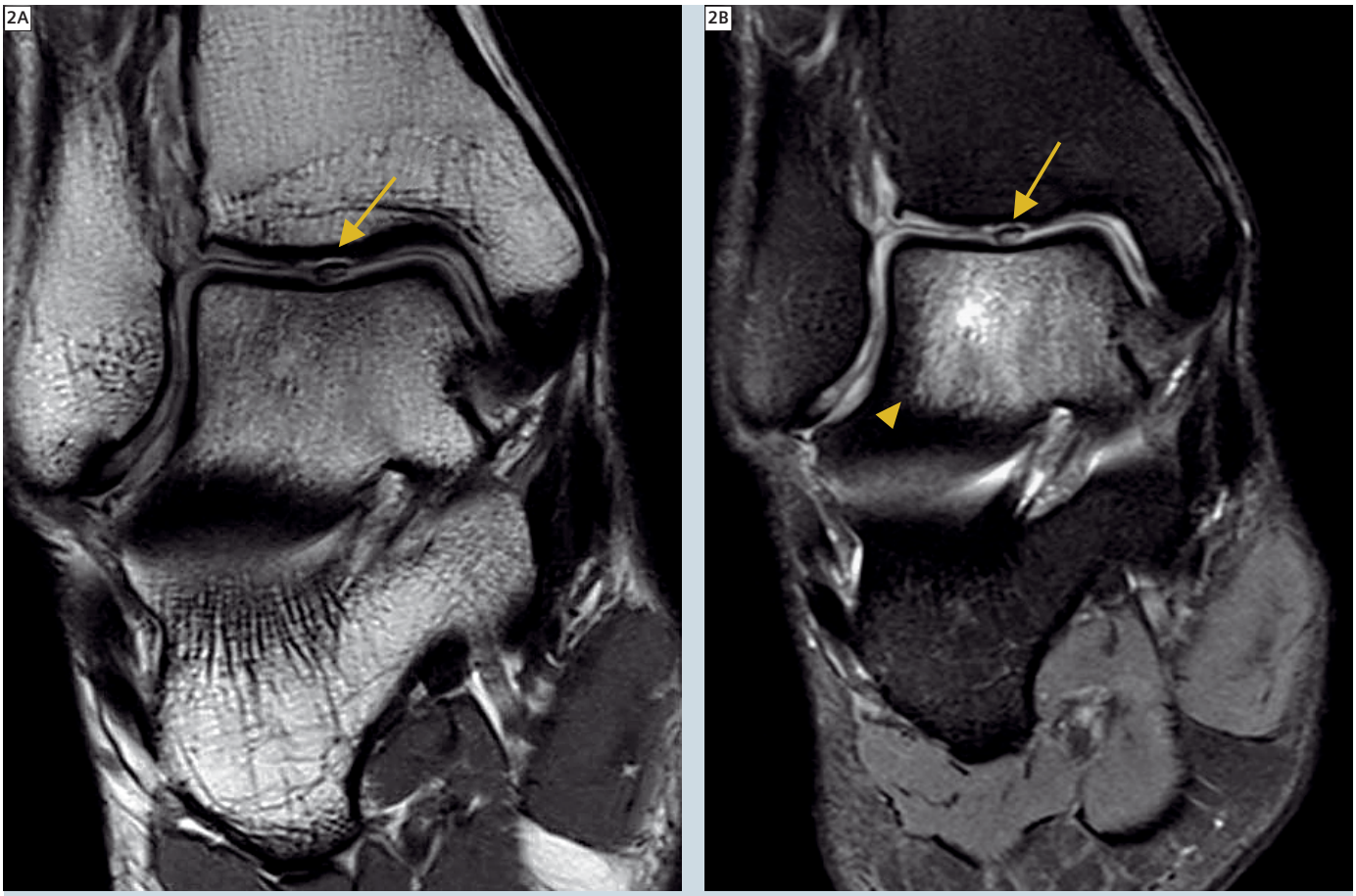

2 Coronal images of the ankle. **2A:** PD-weighted image which shows the chondral fragment on the talar dome (long arrow). **2B:** Fat suppressed PD-weighted TSE image which again demonstrates the chondral fragment (long arrow). The increased signal in the body of the talus (arrowhead) is consistent with edema in the bone marrow as a result of the repetitive irritation caused by the chondral fragment.

surfaces with preferentially sparing of the concave surfaces.

2. Os trigonum injury: The os trigonum is believed to be analogous to a secondary ossification center being formed from a cartilaginous extension of the posterior portion of the talus [2, 3]. It appears between 7–13 years of age, fusing with the posterior process of the talus within 1 year of appearance. In 7–14% patients it remains as a separate ossicle – often present bilaterally. A cartilaginous synchondrosis develops in this region in those adults where it remains separate. A painful os trigonum may be due either from an acute injury or, as likely in this case from a chronic repetitive microtrauma and resulting chronic diastasis of the synchondrosis [4]. The proximity of the flexor hallucis long tendon is a feature of which one has to be mindful since pressure from the diastased os trigonum can lead to tenosynovitis. When the involvement of the flexor hallucis tendon becomes chronic and there is degeneration/tendinosis and fibrosis of the tendon between the medial and lateral tubercles of the talus, there can be reduced flexion of the great toe.

References

1 Sijbrandij ES, van Gils APG et al Posttraumatic Subchondral Bone Contusions and Fractures of the Talotibial Joint: Occurrence of "Kissing" Lesions. AJR 2000; 175: 1707-1710.
2 Magee TH, Ginson GW Usefulness of MR Imaging in the detection of talar dome injuries. AJR 1998; 170: 1227-1230.
3 Karasick D, Schweitzer ME Pictorial Essay The Os trigonum Syndrome: Imaging Features AJR 1996: 166: 125-129.
4 Grogan DP, Walling AK et al Anatomy of the os trigonum J Pediatr Orthop 1990: 10:618-622
5 Hedrick MR, McBryde AM Posterior ankle impingement Foot Ankle 1994; 15: 2-8.

Contact
Charles P. Ho, PhD, MD
Steadman Philippon Research Institute
181 W. Meadow Dr. Suite 1000
Vail, CO 81657
USA
Karen.briggs@sprivail.org

Long Bone Imaging Distal Lower Limbs utilizing Tim Technology and the Tim User Interface

James Hancock

Benson Radiology, Adelaide, South Australia

Distal lower limbs with Tim

Positioning technique

- Head coil and C-spine coil removed from table.
- Spine coil on the table and plugged in.
- Create a bolster for the patient's feet using two triangular pads and sandbags to support them as shown in figure 1. This support needs to be placed in the region of the first spine element as indicated on the table.
- Position the patient on the examination table feet first with their feet dorsiflexed and placed on the support pads.
- Ensure the patient is in the middle of the table and that their legs are as close together as possible without actually touching.
- Place the two Body Matrix coils over the patient's lower limbs strap down and plug in.
- Use the laser to centre to the patients knee joint.
- Press the isocenter button to move the patient in to the magnet bore.

Set up the triangular sponges as shown in these images. Pay attention to the 1st spine element as you want to position them in that region. This allows you to position the patient with their feet dorsiflexed and in the correct anatomical position.

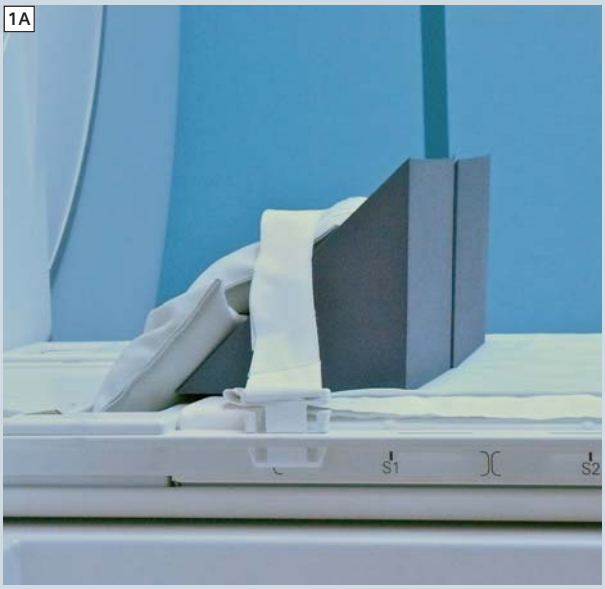

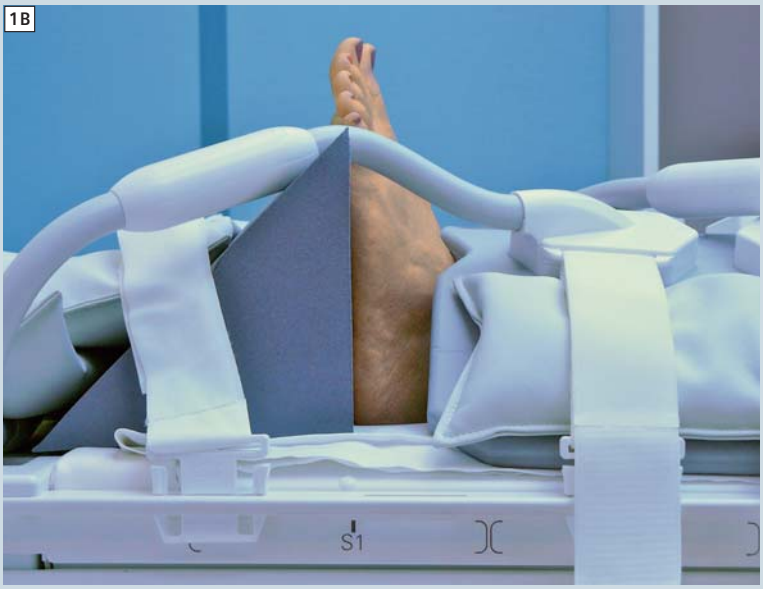

1C

1D

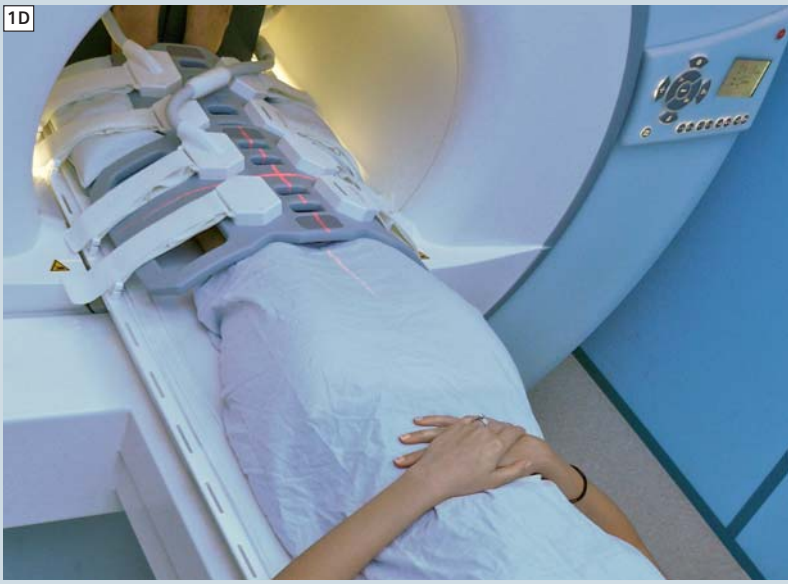

1E

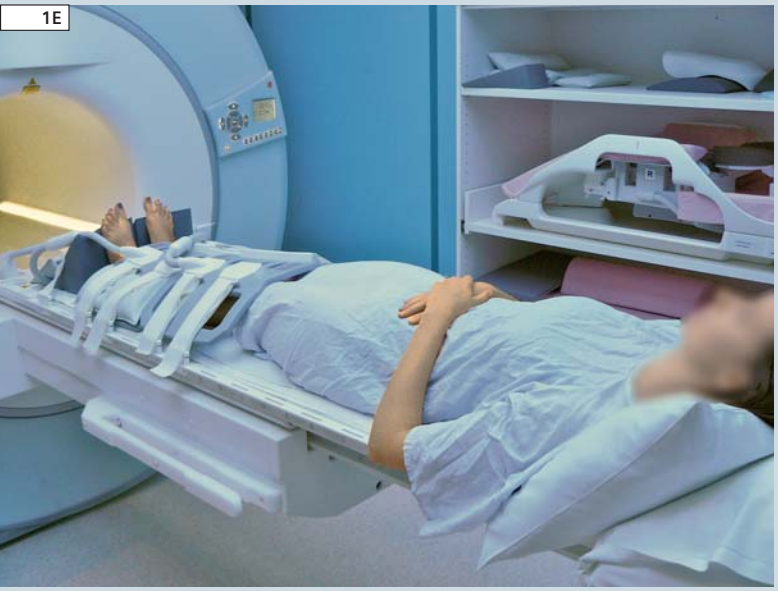

1F

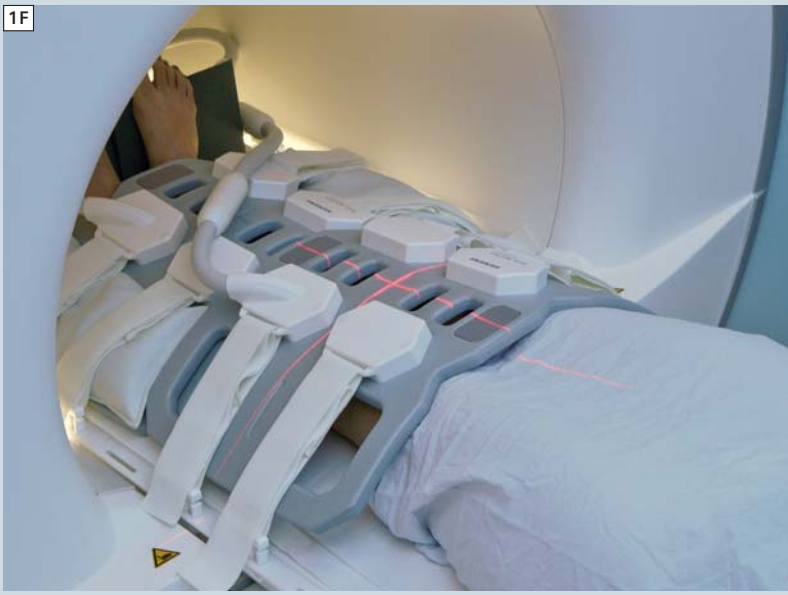

Tim planning

- When running a lower limb protocol it is useful to activate the Tim Planning Suite user interface.
- Figure 3 demonstrates the layout for the Tim User Interface. At our institution the protocol for lower limb MRI is saved under the MSK protocols within the Lower Extremity subsection.

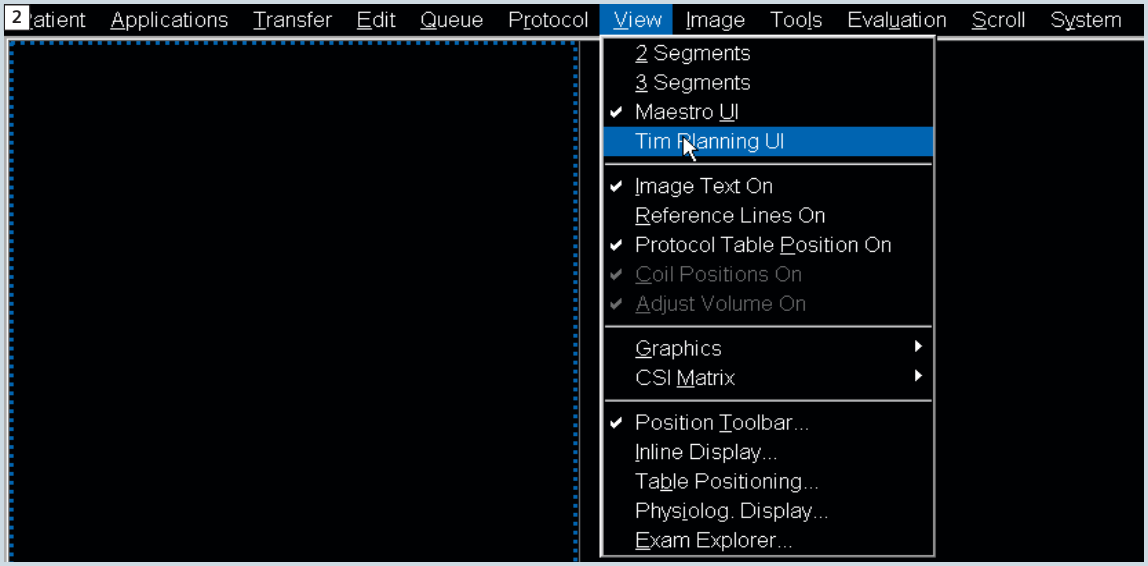

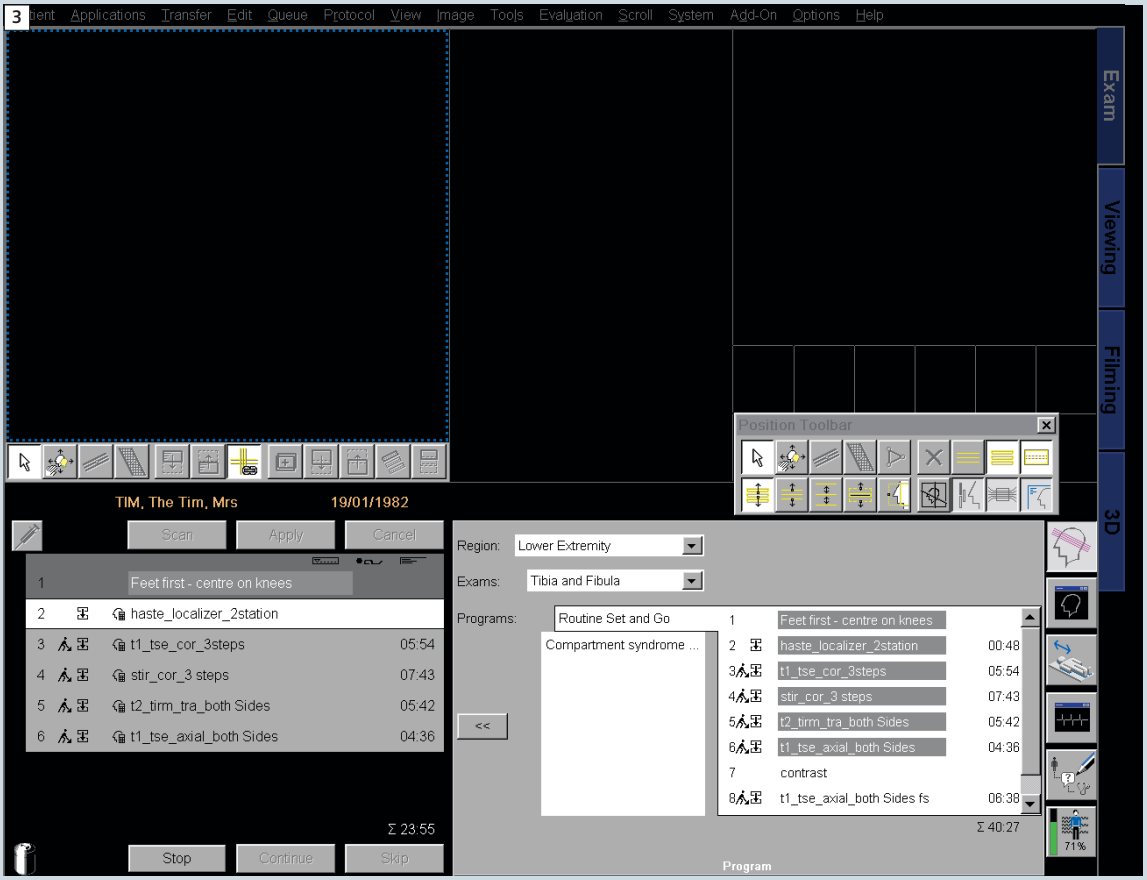

Running the localizers

- First step to planning is to run the localizers. Drag the appropriate HASTE localizer into the queue for running. You can bring the other sequences you will run over at the same time. This localizer begins running from the knee down to mid tibia/fibula then moves the table before running localizers from the mid tibia/fibula down to the ankle. We end up with two localizers in the running queue. Once complete the two stations are automatically composed Inline into one complete image for the entire lower limbs in both sagittal and coronal planes. These images allow us to plan the setup for the rest of the scans.

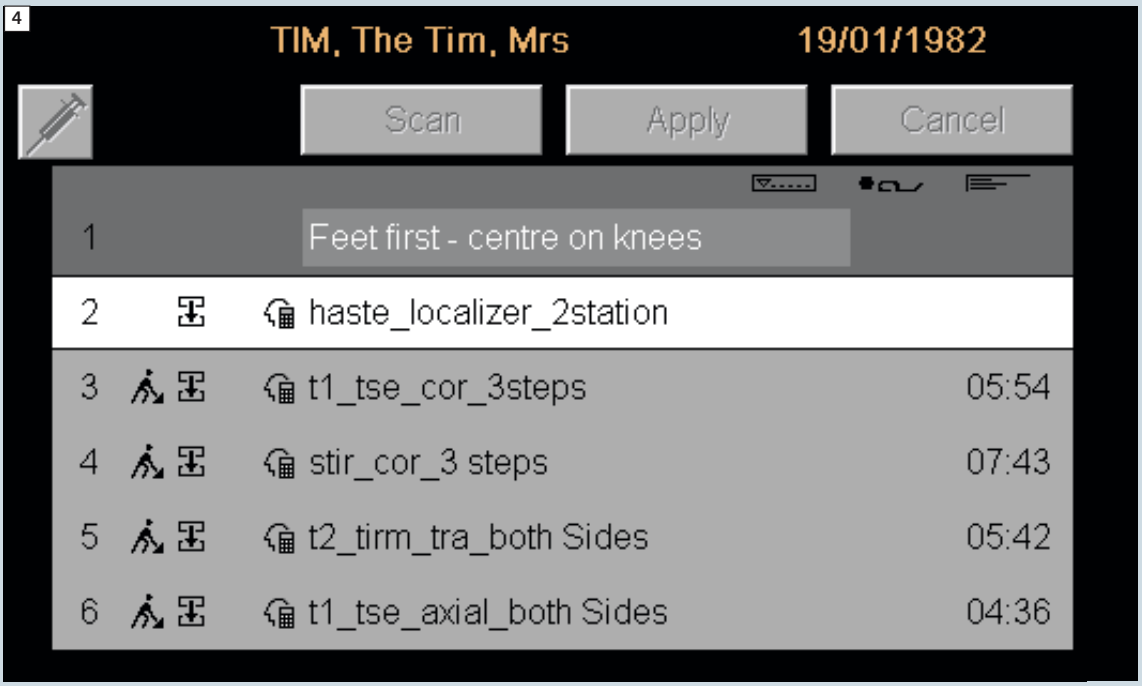

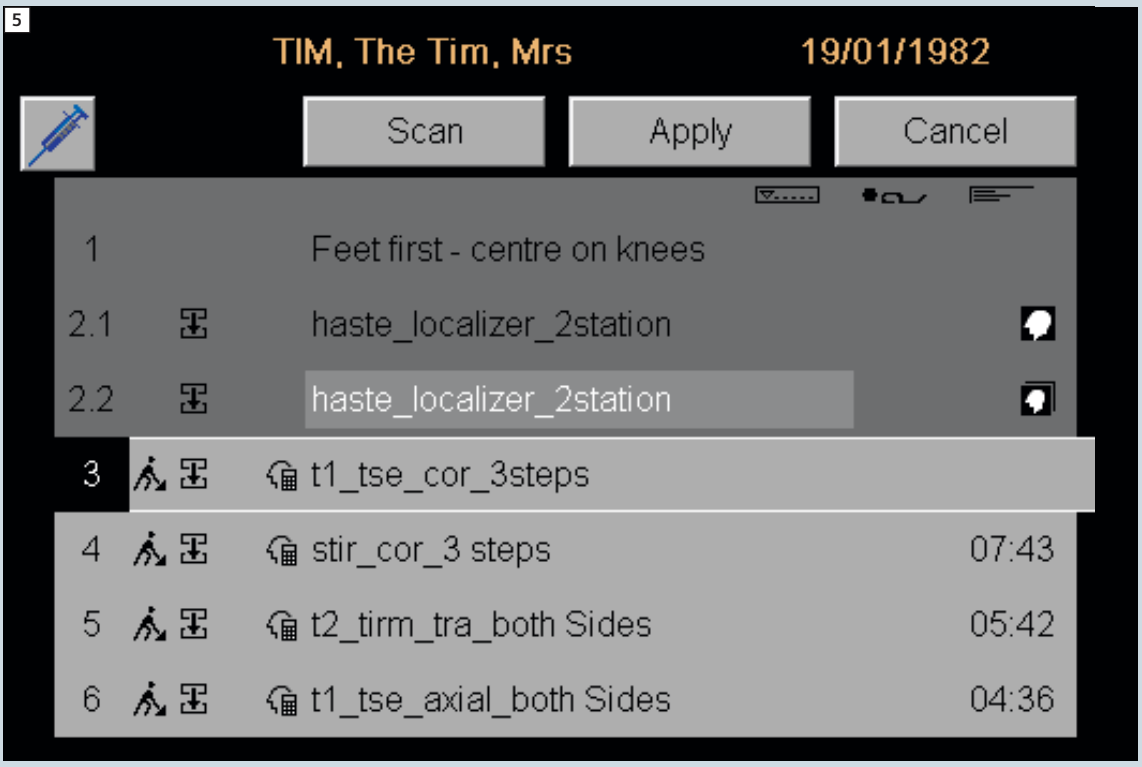

Coronal acquisitions

Setting up the correct fields-of-view

- Drag the T1 coronal sequences across into the queue and open it. This sequence displays three separate sub protocols. This ensures maximum coverage with minimal distortion.
- When setting up for any long bones it is best to take a systematic approach.
- Initially set up your FOV to ensure that you are going to cover the entire region. This involves placing a composed coronal image of the lower limbs into the middle rectangular window.
- When setting up your FOV coverage ensure **coupled graphics is on.** This can be achieved by right clicking in any of the three boxes and selecting the option.
- With coupled graphics on you can then move your FOV and position it appropriately for the correct coverage (Fig. 6).

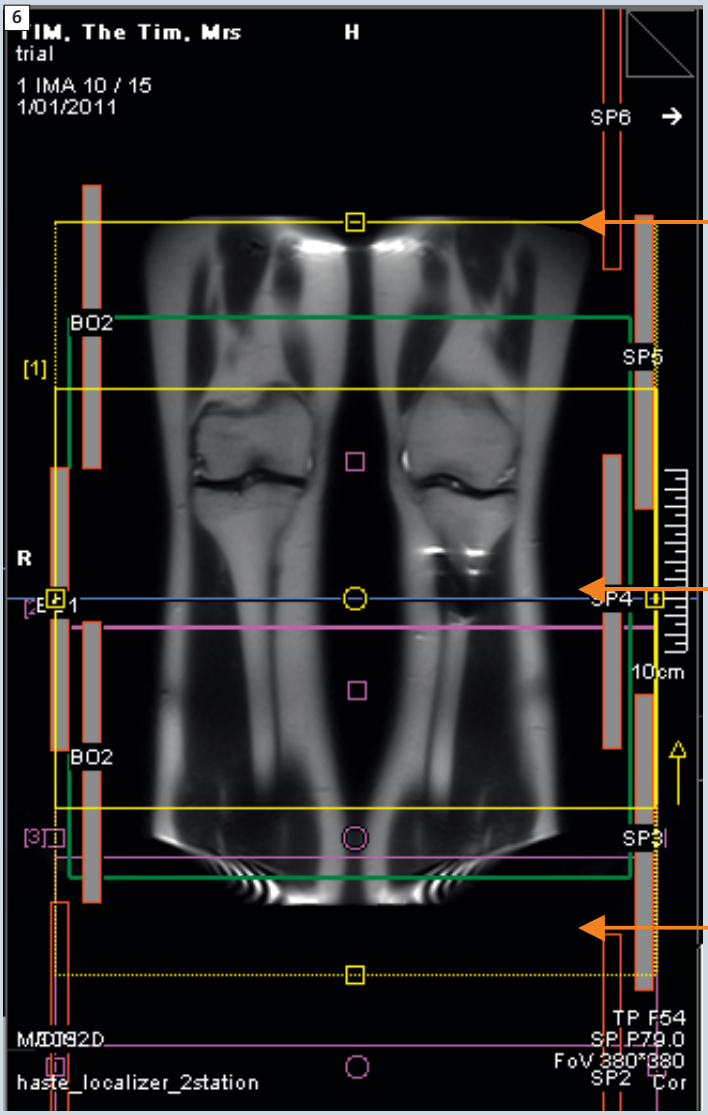

Note the three separate FOV boxes. The upper FOV is yellow and this indicates that it is currently active. By utilizing coupled graphics you can grab and drag all of the three and move them as one. This makes setting up your coverage very easy. Each FOV is also numbered and you can select them by clicking on the little numbers.

Setting up the slice positions

- Once the FOV has been set you need to set the slice group locations for each of the subgroups.
- The best way to do this is to load your individual axial station localizers into the two square windows. This helps you to visualize your coronal slices.
- In the rectangular window place a composed sagittal image. This gives you an indication of the relationship between each subgroup of slices.
- Unlike the spinal cord almost all patients' long bones are relatively straight. This makes setting the slice positions easy. You can leave coupled graphics on and move the slices as one. Our protocol is set up with plenty of slices to allow easy complete coverage in the coronal plane.

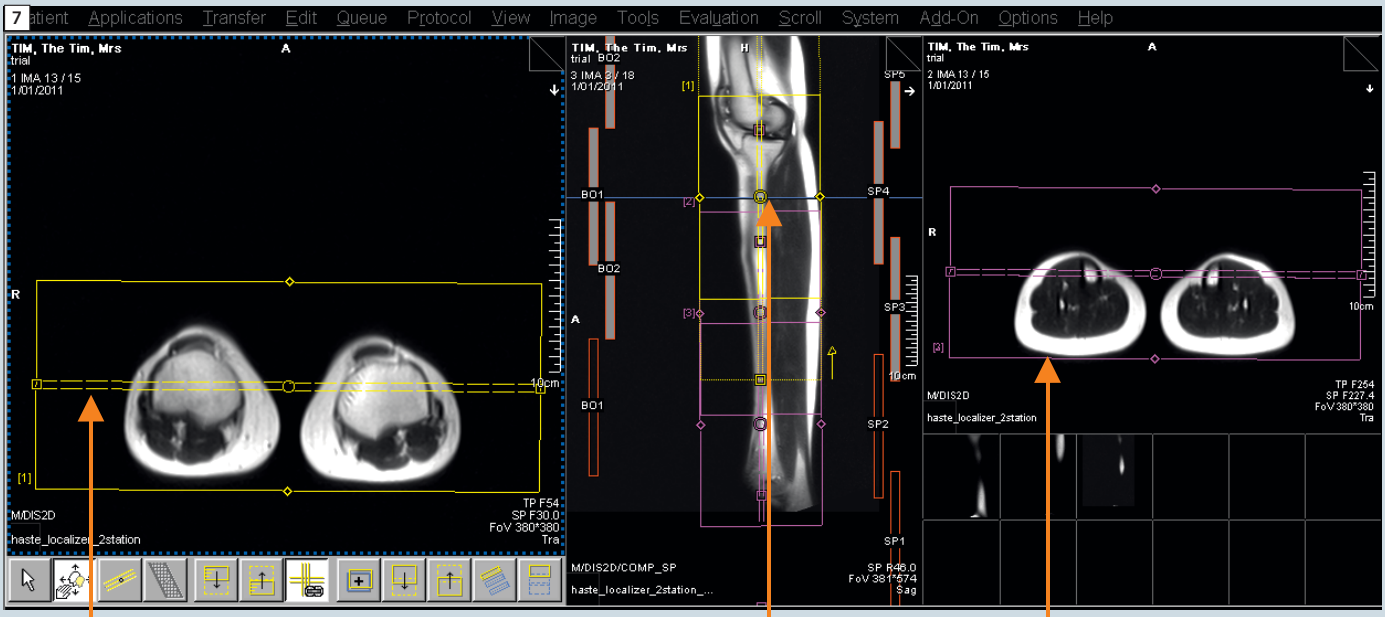

By having an axial localizer of the proximal tibia in this box you can keep an eye on your slice coverage for the proximal portion of the lower legs. Note that there is rotation of this sub-protocol about the H–F axis. This needs to be done with **coupled graphics on** so all sub-protocols match otherwise composition will fail.

A composed sagittal gives you an indication of both the position of your subgroup slice positions and also a good overview of your total FOV.

By having an axial localiser of the distal tibia in this box you can keep an eye on your slice coverage for the distal portion of the lower legs. Note that there is rotation of this sub-protocol about the H–F axis. This needs to be done with **coupled graphics on** so all sub-protocols match otherwise composition will fail.

Axial acquisitions

Setting up the correct fields-of-view

- Drag the T1 Axial sequences across into the queue and open it. This sequence displays two separate sub-protocols. This ensures we have maximum coverage with minimal distortion.
- To allow for the correct FOV you should again have a separate proximal and distal axial localizer in each of your square windows. This makes it easy to ensure your anatomy is in the middle of the FOV and that you will not cut off anatomical regions as your slices progress down the leg. When adjusting leave **coupled graphics on.**

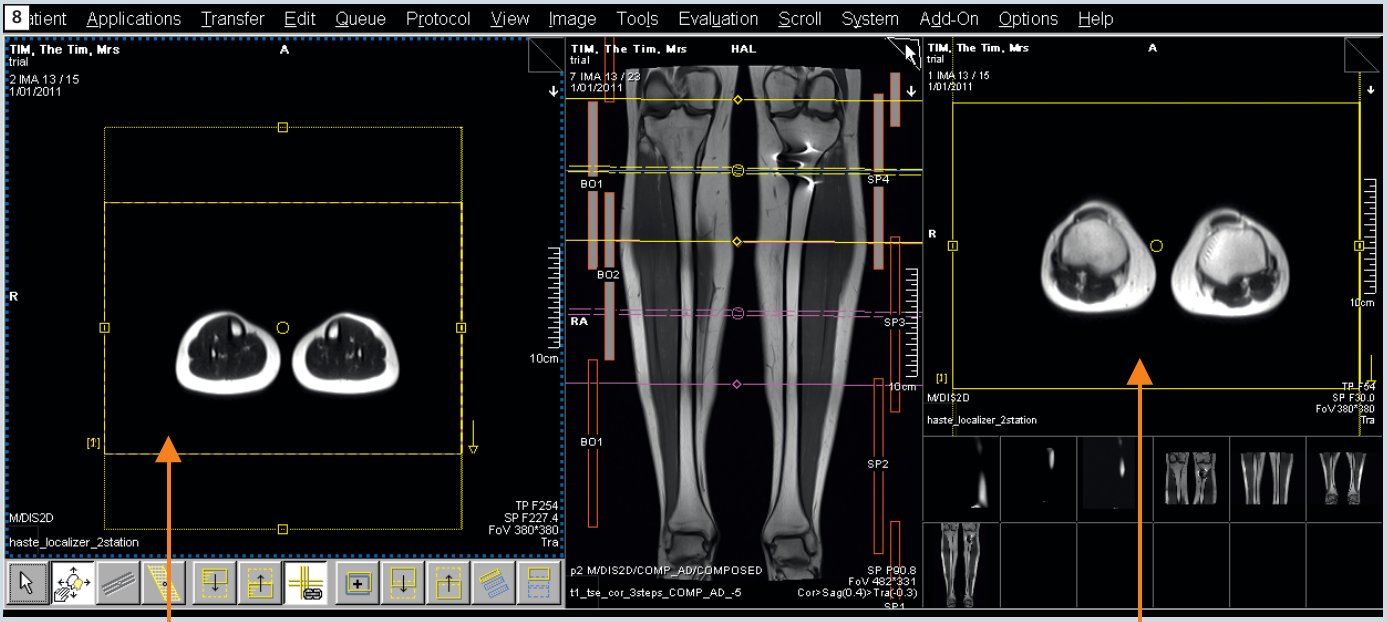

Distal axial localizer. This allows you to position the FOV to ensure you cover the entire distal portion.

Proximal axial localizer. This allows you to position your FOV to ensure you cover the entire proximal portion.

Setting up the slice positions

- Once the FOV has been set you need to set the slice group locations for your axials.
- In the rectangular window place a composed coronal image which you can use to position your slices. Position your slices to cover the area of interest and within this window switch between the coronal and sagittal composed images to ensure your slices are perpendicular and true axials.
- You do this with **coupled graphics on** as the two slice groups are linked and this ensures a contiguous run of axial slices.

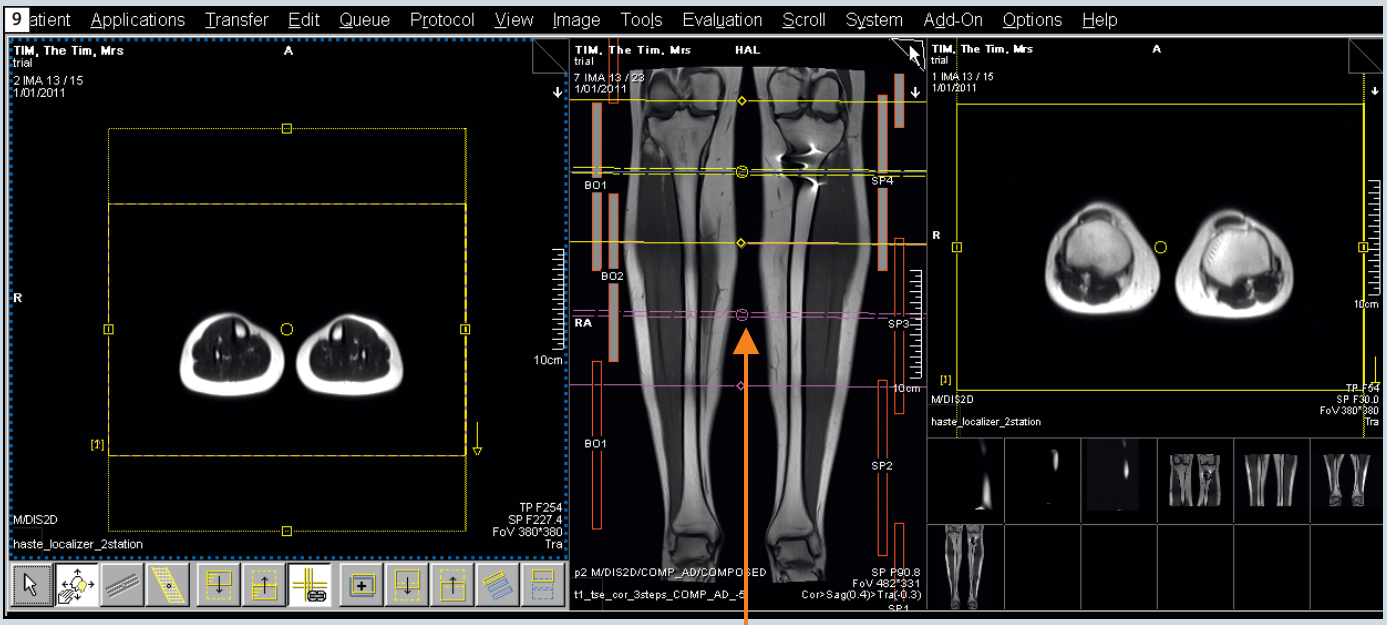

Switch between the coronal composed and sagittal composed images when setting up your slice groups. Obviously tailor your slice group to cover the region of interest.

10

You can see how each subgroup for the T1 coronals has its own number 3.1, 3.2, 3.3 etc. Thus if you need to rerun a region simply hold shift and click the one you need to repeat. Drag and drop that region back into the queue. A cross will run through the compose indicator, this shows that it is only going to run that one region again.

Important notes

- Any presets that you position will affect all three subgroups. As such if you use presets you must pay attention to their positioning.
- Changes made to one subgroup will not affect the other groups so never assume!
- Pay attention to the position of the patient on the table, they need to be close to the middle otherwise you are likely to encounter artifacts on your coronal images.
- Overlaps are built into the protocols, be careful when setting up your FOV. Keep these overlaps in place to ensure smooth composing of final images. Thus when setting up your FOV leave coupled graphics on.
- Avoid in-plane rotation when planning your sequences as this will affect the composing of the final images.
- For coronal and sagittal sequences you may angle your sub-protocols in either the A–P (coronal) or R–L (sagittal) planes when using these 2D protocols. However be aware of the previous point. Thus if setting up a coronal sequence you could angle in the sagittal plane to acquire well placed slices but obviously you need to avoid rotation in the coronal plane as this would correspond to in-plane rotation.
- Rotation of sub-protocols in the F–H (axial) plane should be avoided unless absolutely needed. A difference of just 1 degree between sub-protocols will cause composing to fail. If you do rotate in this plane make sure **coupled graphics is on** as this will ensure any changes you make in this plane apply to all sub-protocols.
- At our institution the axial sequences have been optimized to ensure the maximum coverage with minimal distortion. If you need more coverage consider adding a subgroup rather than increasing the number of slices.
- If you need to repeat a subgroup due to patient movement you only need select the region affected by the movement and rerun that particular subgroup. See the example in figure 10.

Contact
James Hancock
Benson Radiology MRI Department
Ground Floor, 57-59 Anzac Highway
Ashford 5035
South Australia
James.Hancock@bensonradiology.com.au

Siemens Healthcare Publications

Our publications offer the latest information and background for every healthcare field. From the hospital director to the radiological assistant – here, you can quickly find information relevant to your needs.

Medical Solutions
Innovations and trends in healthcare. The magazine is designed especially for members of hospital management, administration personnel, and heads of medical departments.

eNews
Register for the global Siemens Healthcare Newsletter at www.siemens.com/healthcare-eNews to receive monthly updates on topics that interest you.

AXIOM Innovations
Everything from the worlds of interventional radiology, cardiology, fluoroscopy, and radiography. This semiannual magazine is primarily designed for physicians, physicists, researchers, and medical technical personnel.

MAGNETOM Flash
Everything from the world of magnetic resonance imaging. The magazine presents case reports, technology, product news, and how-to articles. It is primarily designed for physicians, physicists, and medical technical personnel.

SOMATOM Sessions
Everything from the world of computed tomography. With its innovations, clinical applications, and visions, this semiannual magazine is primarily designed for physicians, physicists, researchers, and medical technical personnel.

Imaging Life
Everything from the world of molecular imaging innovations. This bi-annual magazine presents clinical case reports, customer experiences, and product news and is primarily designed for physicians, hospital management and researches.

For current and past issues and to order the magazines, please visit **www.siemens.com/healthcare-magazine.**

Global Siemens Headquarters

Siemens AG
Wittelsbacherplatz 2
80333 Muenchen
Germany

Global Siemens Healthcare Headquarters

Siemens AG
Healthcare Sector
Henkestrasse 127
91052 Erlangen
Germany
Phone: +49 9131 84-0
www.siemens.com/healthcare

www.siemens.com/healthcare-magazine

Order No. A91MR-1100-47X-7600 | Printed in Germany | CC 94 0212X. | © 02.12, Siemens AG

Global Business Unit

Siemens AG
Medical Solutions
Magnetic Resonance
Henkestr. 127
DE-91052 Erlangen
Germany
Phone: +49 9131 84-0
www.siemens.com/healthcare

Local Contact Information

Asia
Siemens Pte Ltd
The Siemens Center
60 MacPherson Road
Singapore 348615
Phone: +65 6490-8096

Canada
Siemens Canada Limited
Medical Solutions
2185 Derry Road West
Mississauga ON L5N 7A6
Canada
Phone: +1 905 819-5800

Europe/Africa/Middle East
Siemens AG
Medical Solutions
Henkestr. 127
91052 Erlangen
Germany
Phone: +49 9131 84-0

Latin America
Siemens S.A.
Medical Solutions
Avenida de Pte. Julio A. Roca No 516,
Piso 7
C1067ABN Buenos Aires
Argentina
Phone: +54 11 4340-8400

USA
Siemens Medical Solutions U.S.A., Inc.
51 Valley Stream Parkway
Malvern, PA 19355-1406
USA
Phone: +1-888-826-9702

Global Siemens Headquarters

Siemens AG
Wittelsbacherplatz 2
80333 Muenchen
Germany

Global Siemens Healthcare Headquarters

Siemens AG
Healthcare Sector
Henkestrasse 127
91052 Erlangen
Germany
Phone: +49 9131 84-0
www.siemens.com/healthcare

www.siemens.com/healthcare-magazine

Order No. A91MR-1100-47X-7600 | Printed in Germany | CC 94 0212X. | © 02.12, Siemens AG

Global Business Unit

Siemens AG
Medical Solutions
Magnetic Resonance
Henkestr. 127
DE-91052 Erlangen
Germany
Phone: +49 9131 84-0
www.siemens.com/healthcare

Local Contact Information

Asia
Siemens Pte Ltd
The Siemens Center
60 MacPherson Road
Singapore 348615
Phone: +65 6490-8096

Canada
Siemens Canada Limited
Medical Solutions
2185 Derry Road West
Mississauga ON L5N 7A6
Canada
Phone: +1 905 819-5800

Europe/Africa/Middle East
Siemens AG
Medical Solutions
Henkestr. 127
91052 Erlangen
Germany
Phone: +49 9131 84-0

Latin America
Siemens S.A.
Medical Solutions
Avenida de Pte. Julio A. Roca No 516,
Piso 7
C1067ABN Buenos Aires
Argentina
Phone: +54 11 4340-8400

USA
Siemens Medical Solutions U.S.A., Inc.
51 Valley Stream Parkway
Malvern, PA 19355-1406
USA
Phone: +1-888-826-9702